Functional Nanocarriers as Compartments for Artificial Cells
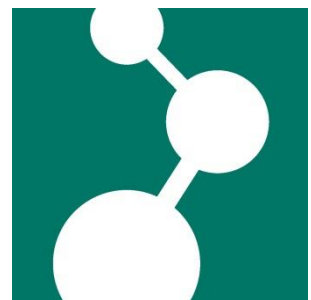
Dissertation
zur Erlangung des Grades
„Doktor der Naturwissenschaften"
im Promotionsfach Chemie

am Fachbereich Chemie, Pharmazie und Geowissenschaften
Johannes Gutenberg-Universität in Mainz

Laura Thomi
Geboren in Frankfurt am Main

Mainz, 2016

Diese Arbeit wurde in der Zeit von September 2013 bis September 2016 am Max-Planck-Institut für Polymerforschung in Mainz unter der Betreuung Dr. Frederik Wurm und Frau Prof. Dr. Katharina Landfester durchgeführt. Ich versichere, die vorliegende Arbeit selbstständig angefertigt zu haben. Alle verwendeten Hilfsmittel und Quellen habe ich eindeutig als solche kenntlich gemacht.

Dekan: ████████████████

1. Berichterstatterin: ████████████████████████

2. Berichterstatter: ████████████████

Table of Content

1. Motivation

"What I cannot create I do not understand." – Richard Feynman

These words by Richard Feynman were found on his blackboard at the time of his death in February 1988. What Feynman meant by these words, is that only if you can recreate an answer on a blank piece of paper, you have truly understood it. But it certainly holds true in a different sense as well – what I do not understand, I cannot create. Only by truly understanding something, one can reassemble all the parts into a working system. Throughout the centuries, mankind has delved deeper and deeper into its understanding of nature and has used these insights to create inventions inspired by nature. This school of thought has coined the term *biomimetics*, the study and imitation of mechanisms, shapes, materials and processes found in nature. Since nature has worked on its designs for billions of years of evolution, it has come up with ingenious solutions that have been a well of inspiration for scientists throughout the ages. The hydrophobicity of the lotus leaf, the reflectivity of a butterfly's wings and the strength of a spider's silk thread are only a few examples that come to mind.[1-3]

The field of synthetic biology is closely related to the fundamental principle, which resonates through Feynman's quote and the field of biomimicry - the idea that we can look at something and once we have understood it, can improve upon it. There is no single definition of synthetic biology that captures every one of its aspects. It is the rational design of biological molecules and processes. It is the repurposing of existing biological systems to new ends. It is an engineering approach to biology. It is the next step after the purely observational and descriptive phase of biochemistry – the tinkering with biochemical circuits. The motivation for synthetic biology is twofold: on the one hand, the design of new biological processes from well-defined building blocks enables scientists to precisely tailor them for their respective purpose. On the other hand, the process of designing and reconstituting simplified biological systems serves as a model for existing biological processes, which tend to be rather complex in nature. The hope is that the systematic approach will reveal new insights into form and function of existing processes. Therefore, creation and functionality go hand in hand with understanding in the field of synthetic biology, as they do in Feynman's quote.

One of the main goals in synthetic biology is the design of an artificial cell. An artificial (or minimal) cell is an engineered system which exhibits one or more characteristics of life. Rasmussen has formulated three key aspects for a synthetic minimal cell – container, metabolism and genes.[4] Again, both motivations fuel this goal. On the one hand, there is the

functionality. A minimal cell can be specifically tailored to certain functions, rendering it a more efficient machinery than conventional cells. On the other hand lies the understanding. In composing a minimal machinery, new insights will be gained on what is strictly necessary for a running system. There are two different approaches to minimal cells. The top-down approach takes an existing cell and systematically knocks down function after function. This elucidates the difference between vital cell functions and dispensable ones and shows how much of the genome can be removed until the cell is no longer 'alive', i.e. until essential functions, such as metabolic pathways, no longer work. The amount may be startlingly high, since all living organisms carry around a lot of genetic information that was required at some point along their evolutionary path. The bottom-up approach starts not from a living cell, but from wholly artificial building blocks. These are assembled to form systems of increasing complexity, which mimic certain aspects of life, e.g. compartmentalisation, metabolism or reproduction. The building blocks may be of biological, organic or inorganic origin.

This work is an exploration of the container aspect. In natural cells, the container is the cell membrane, a lipid bilayer mixed with proteins and cholesterol. Here, different approaches to synthetic containers are presented. They may be used as an enclosure for functional parts (like a cell membrane) on the inside or as enclosures for smaller compartments within a larger system (like mitochondria or endosomes). The goal was to not simply supply a container as a building block for more elaborate systems, but rather to use the science of chemistry to imbue the material with additional properties, i.e. to devise responsive or functional containers. These functional nanocarriers will be presented in the main part of this thesis and are categorised in four different projects (Figure 1). Project 1 deals with nanocapsules made from ferrocene-based materials, which lends its redox-responsive properties to the corresponding nanocarriers. Project 2 presents vesicles made from poly(butadiene)-*block*-poly(ethylene oxide) (PB-*b*-PEO). These block copolymers were functionalised with different end groups and used to form polymeric vesicles, or polymersomes, with addressable functional groups on their surface. Project 3 introduces a hybrid vesicle system made from the aforementioned PB-*b*-PEO polymers and lipids. From this, a platform for a permeable polymersome is devised. Lastly, project 4 presents polymersomes made from amphiphilic poly(phosphoester)s, an emerging class of biodegradable polymers.
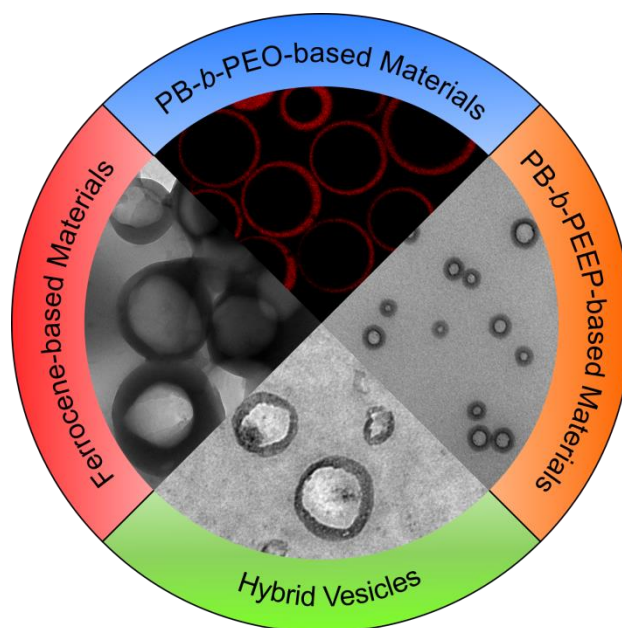
Figure 1. Main topics of this thesis.

This thesis is divided into five chapters, which will be briefly summarised in the following paragraph. The first chapter presents an introduction and motivation for this thesis. The second chapter will give the background information required for this work, as well as an overview of state-of-the-art examples from recent literature. The focus lies on a selection of nanocarrier systems relevant to this thesis and as compartments for synthetic biology in general, namely nanocapsules, liposomes, polymersomes and hybrid structures of the latter two. Other nanocarriers will only be mentioned briefly. The third chapter summarises the scientific results and is subdivided into four chapters, which correspond to the projects outlined above. Each chapter is preceded by a brief introduction and concludes with a summary and outlook. The fourth chapter gives the experimental and instrumental details. In the fifth chapter, a final summary is given.

In summary, several functional nanocarriers, which may be used as building blocks for artificial cells, are presented. Each nanocarrier has different properties, e.g. regarding rigidity, responsiveness or functionality, in order to cover a broad spectrum of requirements.

2. Theoretical Background[1]

2.1. The Importance of Compartments

According to Rasmussen, there are three essential components for a minimal cell: container, metabolism and genes.[4] The necessity of genes stems from the idea that an artificial cell needs to have the ability to replicate – a fundamental characteristic of life as we know it. Metabolism refers to its ability to conduct reactions and exist out of stasis – life is a process and shows itself in change. Both are fairly obvious properties of a living organism. The necessity of a container, however, is less intuitive. Yet, when one looks to nature, barriers that separate a living organism from the outside can be found everywhere. Just looking at animals, there is skin and fur, scales and exosceletons. On a microscopic level there are even more barriers - cell membranes in a myriad of different compositions. Why is that the case? What is the evolutionary advantage of compartmentalisation? This ties back to life being a non-equilibrium state. Organisms rely on concentration gradients to sustain reaction kinetics or fuel other responses. For example, a proton gradient is used to activate the enzyme ATP synthase, which supplies the cell with energy. Neuronal signaling relies on the release of ions in the postsynaptic cell. Compartmentalisation allows a cell to run thousands of different reactions at once – spatial concentration is the key to achieving this. Not only can a cell control local concentration to enhance reaction kinetics, it also reduces cross-talk between different metabolic pathways and ensures optimal reaction conditions for different enzymes. Furthermore, compartmentalisation protects living organisms from harmful influences, e.g. toxins or bacteria. Separate 'trash compartments', the lysosomes, enable cells to degrade and neutralise harmful materials and their most precious cargo, the DNA, is protected by an extra barrier, the cell core membrane. On a larger scale, compartmentalisation leads to specialisation, i.e. agglomerates of different cells take specific tasks and form our organs, which each serve a special function. Therefore, compartmentalisation is one of the key aspects of life. Synthetically, there are different strategies to realise compartmentalisation. In the following, different nanocarriers, which are suitable for such compartments, will be presented. Synthetic compartments presented herein can either be in the range of nanometers or micrometers.

2.2. Nanocarriers

A nanocarrier has a size between 1 and 1000 nm and is used to transport and/or protect its cargo. A number of different nanocarriers have been reported and their categorisation is at

---

[1] A review based on this chapter is in preparation.

least to some degree arbitrary and in instances overlapping, since they may be sorted by size, material, shape, preparation method or other characteristics. There are nanoparticles, nanocapsules, hydrogels, dendrimers, micelles, coacervates and vesicular structures.[5-10] Most of these can be composed of different classes of building blocks, e.g. inorganic materials or polymers. In case of the vesicular structures, specific names have emerged depending on the material. Lipid vesicles are commonly known as liposomes, while polymeric vesicles are called polymersomes.[11, 12] There are also less prominent representatives, such as the proteinosomes (made of proteins) or colloidosomes (from inorganic compounds).[13, 14] This chapter will highlight the properties of nanocapsules, liposomes, polymersomes and hybrid materials out of the latter two, always with special focus on the chemical functionality of the material.

Material functionality can be obtained by mixing functional components into the main building block, or the functionality is an inherent part of the nanocarrier's building block.[15, 16] Furthermore, there are chemically functional materials, bearing certain chemical groups that can interact with other components – either in a chemical reaction or through adhesion, as well as responsive materials that can react to a specific trigger, such as temperature, light or pH.[15, 17] Degradability can be viewed as an additional kind of responsiveness, in this case the response to the degrading trigger, e.g. an enzyme or pH.

2.2.1. Nanocapsules

In the following, the production of nanocapsules, as well as examples for their functionalisation will be presented. Nanocapsules are interfacially generated, polymeric shells that encapsulate a liquid core. Typically, they require surfactants to be stable.

2.2.1.1.   Production

Miniemulsion

A commonly used way to nanocapsules is the miniemulsion approach. Droplets are dispersed in a continuous phase and depending on the nature of the droplets, either nanocapsules with a hydrophilic or a hydrophobic core are obtained. Surfactants are needed to avoid coalescence of the droplets. This can be achieved either by ionic surfactants, which exhibit an electrostatic repulsion, or by non-ionic surfactants, that use a mechanism of steric repulsion. The nanocapsules can be formed by different mechanisms. One of them is the solvent evaporation process. Details on it can be found in section 3.1.1.2, as well as further details on the stability of miniemulsions, and will not be discussed in this chapter. Alternatively, nanocapsules can be formed by polymerisation. Different constellations concerning the location of the monomer are possible. It can either be dissolved in the

continuous phase, in that case the polymerisation has to take place at the droplet interface.[18] Alternatively, the monomer can be located in the dispersed phase, in this case the emerging polymer has to precipitate at the interface to form the shell material.[18] Lastly, two different monomers can be used, one situated in the dispersed phase and one in the continuous phase. Polymerisation can then exclusively take place at the interface. Diisocyanate chemistry is popular in this field, owing to its high reactivity.[6] This can, of course, be a drawback for the encapsulation of cargos, as isocyanates readily react with hydroxyl groups, carboxylic acids, as well as primary and secondary amines.[19]

Self-assembly

This route to nanocapsules starts from a vesicular precursor. The self-assembly approach uses a vesicle (either a lipo- or a polymersome), whose molecules bear polymerisable groups. In lipids, these are usually acrylate, methacrylate, sorbyl or dienoyl groups, which are polymerised by a radical mechanism. Both mono- and bis-substituted lipid have been investigated. Polymerising mono-substituted lipids results in a linear polymer, while bis-substituted ones introduce crosslinking.[20] Examples of polymerisable polymersomes are rare, though one will be introduced in this work in chapter 3.3.2. Examples from literature include vesicles from poly(isoprene)-*block*-poly(2-cinnamoyl methacrylate) (PI-*b*-PCEMA). The vesicles are formed in hexane-tetrahydrofuran mixtures and converted to nanocapsules dispersed in water using the following procedure: The PCEMA blocks were crosslinked using a photoinduced cycloaddition. In a second step, the PI blocks were hydroxylated to form a water-soluble corona.[21] In a different work, poly(2-methyl-oxazoline)-*block*-poly(dimethylsiloxane)-*block*-poly(2-methyl-oxazoline) (PMOXA-*b*-PDMS-*b*-PMOXA) was end-capped with methacrylate groups. Vesicles from this triblock copolymer were crosslinked using the methacrylate.[22] Synthesising nanocapsules using this self-assembly approach stabilises non-covalently linked vesicles, resulting in enhanced morphological integrity in different solvents and a higher resistance against osmotic shocks.

Template

Though ideationally similar, the template approach can be distinguished from the self-assembly one in a distinct way. Both start from a spherical template, but where the self-assembly approach uses a vesicle as a starting point, the template approach uses a solid particle, which is to be extracted later, leaving the hollow core of the nanocapsule. One of the most well-known procedures of the template approach is the layer-by-layer assembly of polyelectrolytes. A charged colloidal particle is used as a template for the deposition of an oppositely charged polyelectrolyte. During this, the original charge is overcompensated,

which means in the next step a polyelectrolyte of yet again the opposite charge can adsorb. Following this procedure, polyelectrolyte multilayers are obtained. Extraction of the original template results in hollow nanocarriers. Layer-by-layer assembly requires thorough purification to remove any amount of non-adsorbed polyelectrolyte between each step. In addition to that, capsules have to be prepared at low concentrations to avoid flocculation.[23]

Each preparation technique has its own advantages and disadvantages. Miniemulsion has a high encapsulation efficiency, but surfactants are required to keep the nanocapsules in dispersion. Furthermore, due to the difference in droplet size, the resulting nanocapsules are polydisperse. The use of templates, either vesicles or particles, results in well-defined nanocapsules in terms of size, however, loading is difficult.

2.2.1.2.   *Functionalisation of Nanocapsules*

The functionalisation of nanocapsules can either use the chemical groups that are inherently present on the nanocapsules' surface after their preparation or specific functional groups can be attached prior to the preparation by using a modified starting material. Alternatively, additional functional components can be mixed with the nanocapsule material and provide the functionality. However, this chapter will focus on functionality as an inherent part of the nanocarrier's building block.

Crosslinking of polyfunctional polymers at the droplet interface by diisocyanate chemistry is widely used to generate nanocapsules (see section 2.2.1.1). It can also be applied for post-preparation modification reactions. Diisocyanate poly(ethylene oxide) (PEO) was used as a linker between hydroxyethyl starch nanocapsules (with hydroxyl groups on the surface) and the hydroxyl groups of mannose.[24] Similarly, isophorone diisocyanate was used as a linker between nanocapsules made out of poly(*N*-[7-(*α*-D-mannopyranosyloxy)-heptyl]methacrylamide) and different amines, using the hydroxyl groups of the carbohydrate.[25] Diisocyanate chemistry, while highly useful, suffers from the limitation that reactions can hardly take place in water, because the isocyanate group will hydrolyse in aqueous environments. A more elaborate route, circumventing isocyanate chemistry, used 1-ethyl-3-(3-dimethylaminopropyl)carbodiimide (EDC)-coupling to form an amide bond between amine-functionalised folic acid and carboxylic acid-functionalised hydroxyethylstarch nanocapsules.[26] Moving on to examples of pre-functionalised nanocapsules, the literature is sparse. It is certainly the more difficult route compared to using the groups abundantly available on the nanocapsule, though it offers a precision and selectiveness unmatched by the first. To give one example, nanocapsules were prepared from *α*-azido-*ω*-2-chloroisobutyrate-poly(oligo(ethylene oxide) monomethyl ether methacrylate)-*block*-poly(*n*-

butyl methacrylate) by ATRP. The azide group, which remained undisturbed by this, was used to link a fluorescent marker bearing an alkyne via a cycloaddition.[27]

Responsiveness is usually introduced using the capsule material itself, e.g. redox-, pH- or temperature-responsive polymers.[28]

In summary, nanocapsules can be prepared by miniemulsion, self-assembly, template or dendrimers. Functionalisation is usually achieved by modification of the chemical groups that are present on the nanocapsule's surface rather than pre-preparation modification.

2.2.2. Liposomes and Polymersomes

The name liposome is derived from two words from ancient Greek– *lipos* (fat) and *soma* (body), ergo a structure made entirely out of fat. Liposomes are vesicular structures of an aqueous core delineated by one or more lipid bilayers. The lipid's nature can either be natural or synthetic. Depending on their size and structure, several types of liposomes are differentiated (Figure 2). With increasing size, there are small unilamellar vesicles (SUVs) ranging from 0.02 μm to 0.2 μm, large unilamellar vesicles (LUVs) from 0.2 μm to 1 μm and giant unilamellar vesicles (GUVs) above 1 μm. Liposomes with several bilayers are classified as multilamellar vesicles, liposomes with several subcompartments are called multivesicular or vesosomes.[11] What size of liposomes is formed depends on its composition and the preparation method. Lipid self-assembly takes place spontaneously in water. It is driven by the hydrophobic effect, the desire to minimise entropically unfavourable interactions between the hydrophobic alkyl chains and the surrounding aqueous medium.
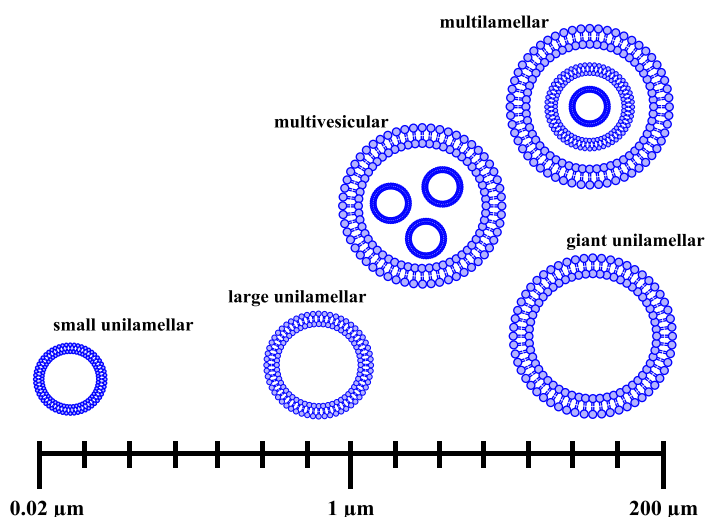

Figure 2. Schematic illustration of different liposome classes. Structures are not to scale.

The term polymersomes was coined by Discher *et al.* in 1999 as a reference to liposomes.[12] They are vesicular structures prepared from amphiphilic copolymers, usually in an aqueous

medium. The architecture of the polymer can vary – polymersomes have been reported from diblocks, triblocks, branched and comb-like structures.[12, 29-31] As for liposomes, their size can range from tens of nanometers to tens of micrometers, depending on the preparation method. However, there are a few key differences regarding the properties of polymer- and liposomes. The average lipid has a molecular weight below 1000 g/mol, while polymers can easily possess an order of magnitude more than that. Consequently, a polymersome membrane is larger than a lipid bilayer and will further increase in thickness and toughness with the molecular weight of the polymer.[12, 32] Polymersome membrane thicknesses typically range from 8-21 nm (depending on the molecular weight and the entanglement of the hydrophobic block), while liposomes fall within 3-5 nm.[33, 34] Accordingly, polymersomes have a lower permeability and higher mechanical stability (Figure 3). Furthermore, due to the slow diffusion and low critical micelle concentration of polymers compared to lipids, polymersomes can be regarded as kinetically trapped and therefore highly stable.[35] And lastly, and perhaps from a chemist's point of view most importantly, the properties of polymersomes can be tuned by altering their molecular composition.[36]
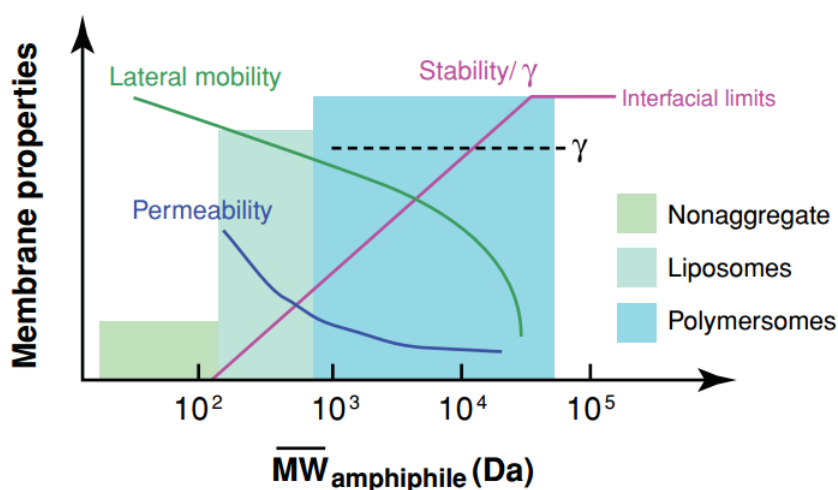
Figure 3. Properties of liposomes and polymersomes. Reproduced with permission from [35].

2.2.2.1.   Production

Small amphiphiles such as lipids can self-assemble in a number of different morphologies. Ninham *et al.* introduced the critical packing parameter P_c as a theoretical value to predict the morphology of a given amphiphile:

$$P_c = \frac{v}{a_0 * l_c} \qquad (1)$$

With v, the volume of the hydrophobic chain, a_0, the area of the hydrophilic head group and l_c, the length of the amphiphile.[37] As illustrated in Figure 4 , molecules with a P_c below 0.3 will

form highly curved aggregates, such as micelles. A P_c between 0.3 and 0.5 will result in cylindrical micelles, while amphiphiles with a P_c larger than 0.5 will form bilayers, i.e. vesicles. A P_c larger than 1 will result in inverted structures, e.g. inverse micelles. For this reason, not all small amphiphiles can be expected to form liposomes.
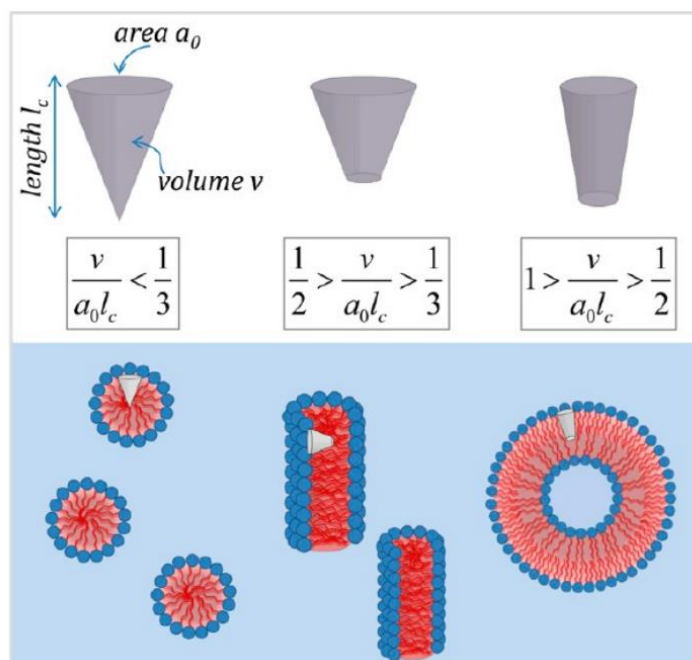
Figure 4. Aggregation morphologies of small amphiphiles with regard to the critical packing parameter P_c. Reprinted with permission from [38]. Copyright 2015 American Chemical Society.

For amphiphilic polymers, the driving force for self-assembly is to minimise the exposure of one of the block to the selective solvent, e.g. water. What structure is formed depends mostly on the amphiphilic proportions of the polymer and polymersomes are obtained only within a certain range (Figure 5). Bates *et al.* studied the influence of block length on self-assembly for a poly(butadiene)-*block*-poly(ethylene oxide) (PB-*b*-PEO) system.[39] Often associated with this phenomenon is the hydrophilic fraction $f_{hydrophilic}$, an empirical marker to predict the self-assembly behaviour. For many systems, it has been shown that polymers with a $f_{hydrophilic}$ of 25-45% are most likely to form polymersomes.[40] It should, however, be noted that those value are based on polymers that mostly consist of carbon, hydrogen and oxygen. It is less well-known how other elements influence this behaviour.

Figure 5. Influences on polymer self-assembly. Transmission electron micrographs of poly(styrene)-*block*-poly(acrylic acid) (PS-*b*-PAA) copolymers with varying amphiphilic proportions. HHHs are hexagonally packed hollow hoops, LCMs are large compound micelles. Reproduced from [41] with permission of The Royal Society of Chemistry.

In the following, the most commonly used preparation techniques for liposomes and polymersomes will be briefly explained. The typically obtained sizes are indicated for each method.
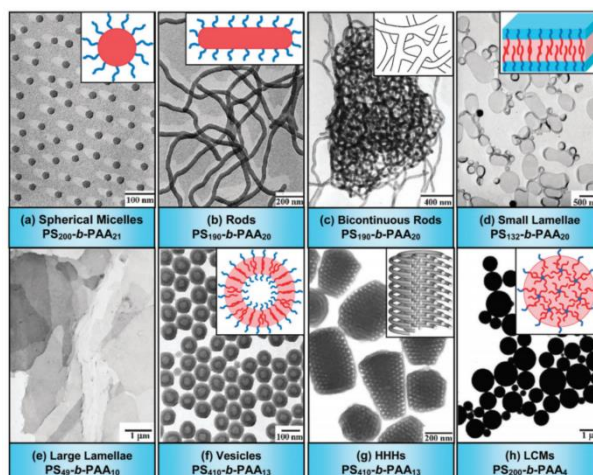
Film Hydration

The film hydration technique typically results in uni- and multilamellar vesicles in the nm-range, multilamellar structures can be broken down by mechanical agitation. The lipid or polymer is dried from an organic solution, either by evaporation, spray- or freeze-drying. The thereby generated thin film is agitated in an aqueous solution, which can be either pure water, buffer, or a solution of the cargo (Figure 6). Agitation is brought about by shaking, stirring or ultrasonication, higher agitation resulting in fewer multilamellar structures.[42-44] Multilamellar vesicles can be extruded to generate unilamellar vesicles. As multilamellar structures are forced under pressure through well-defined pores, the membranes rupture and reseal to form unilamellar vesicles of sizes corresponding to the pore size. A drawback of this is that during the extrusion, loaded cargo can spill out of the core as the membrane ruptures. To circumvent this, extrusion has to be carried out before free cargo on the outside of the vesicle is removed. For liposome formation, typically mixtures of different lipids and/or addition of cholesterol are used to achieve stable structures.[45, 46] Polymersomes can also be obtained from bulk hydration, rather than from film. Then, the process of hydration is usually longer. Detergent-aided variants of this technique have also been reported, to circumvent strong agitation for the singular case in which a polymer requires such force to form polymersomes, which could interfere with sensitive cargo molecules.[47]
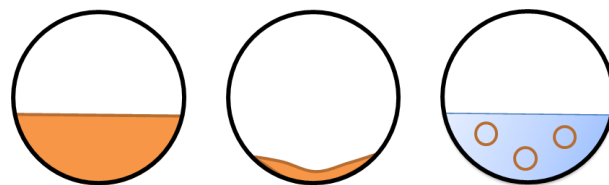
Figure 6. Illustration of film hydration. A thin film is obtained by evaporation from an organic solution and hydrated in water.

Solvent Displacement

In this method, the polymer or lipid is dissolved in a suitable organic solvent and subjected to an excess of the selective solvent, typically water (Figure 7). This can either be done by addition to water (solvent injection) or by dialysis against a larger volume of water.[48, 49] This method produces vesicles of a broad size distribution and is therefore usually followed by an extrusion step.[22] Ideally, the organic solvent is volatile and can be removed after vesicle formation.
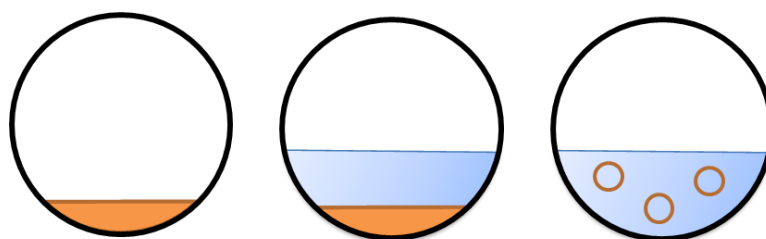
Figure 7. Illustration of solvent displacement. A concentrated polymer or lipid solution is diluted with a surplus of selective solvent.

Microfluidics

A number of different microfluidic platforms have been successfully used to generate liposomes – usually GUVs. Due to the dimensions of the microfluidic setup, those are the most easily obtained. Liposomes are often produced on a PDSM-chip from a lithographic template.[50] The lipids are dissolved in an organic solvent that is immiscible with water. Through two cross-junctions, a double emulsion of water in oil in water is obtained. Extraction or evaporation of the organic solvent leads to liposome assembly. Microfluidic setups have also been combined with electroformation.[51] Liposomes in the nm-range are accessible by microfluidics through the so-called microfluidic hydrodynamic focusing (Figure 8). Here, the lipid is dissolved in a water-miscible solvent (typically ethanol), which flows through the central channel. It is intersected by two water channels, which lead to a hydrodynamic focussing of the central ethanol jet. The size of this jet can be adjusted by tuning the flow rates. Further along the main channel, the ethanol jet begins to mix with the surrounding water. This decreases the alcohol concentration, until at a critical level the lipid

is no longer soluble. This triggers the spontaneous self-assembly and formation of liposomes. Liposomes ranging from 50 to 150 nm in diameter have been achieved using this technique.[52]
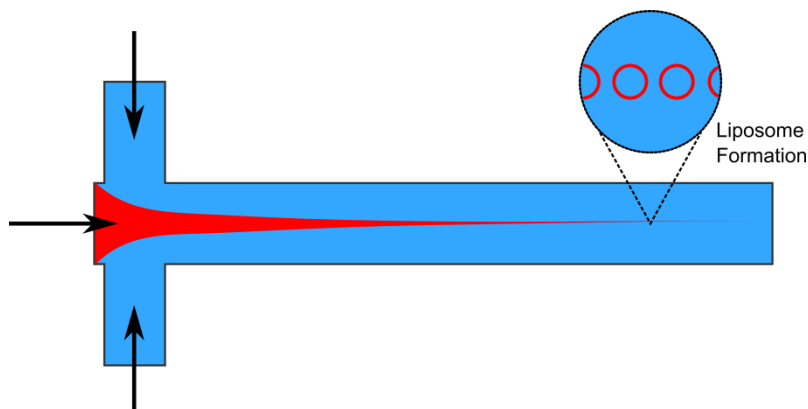
Figure 8. Illustration of microfluidic hydrodynamic focusing. The cross junction is shown. The central channel is filled with a lipid solution in alcohol (red). At the junction, two water channels (blue) focus the central stream.

In 2005, Weitz *et al.* published the first microfluidic approach to polymersomes.[53] They used a microfluidic setup to generate a double emulsion of water in tetrahydrofuran/toluene in water. The amphiphile, poly(butyl acrylate)-*block*-poly(acrylic acid) (PBA-*b*-PAA) was dissolved in the organic phase and after evaporation of the solvent, polymersomes were obtained. Cargo may be added to the inner water phase and thereby loaded onto the polymersomes.[54] Since then, the technique has been developed to produce multicompartment polymersomes.[55]
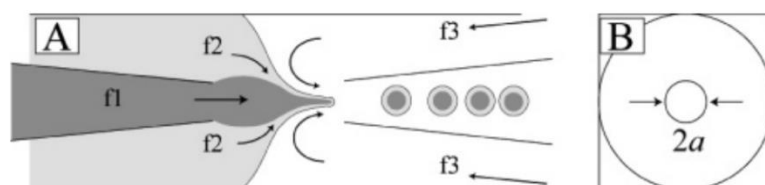
Figure 9. Microfluidic setup for polymersome preparation. Side view (a) and front view (b) of the device. Two tapered glass tubes rest inside a square tube. Three fluids (f1, f2 and f3) flow through the device. Reproduced with permission from [53]. Copyright (2005) American Chemical Society.

As for liposomes, due to the dimensions of the setup, typically polymersomes in the µm-range are produced. However, formation of polymersomes in the nm-range has been reported as well using hydrodynamic focusing.[56] Microfluidics is a high-output platform for the production of polymersomes or liposomes with a low dispersity. The size can be tuned by altering the flow rates, though the dispersity increases with increasing vesicle size. Disadvantageous is the necessity for additional components, such as surfactants, channel

treatment or osmolarity adjusting agents, as well as the necessity to remove the organic solvent.

Electroformation

During electroformation, lipid or polymer coated electrodes are subjected to an alternating electric field (Figure 10). This causes swelling of the film, single lamellae are detached and form vesicles. This method typically yields GUVs for lipids or unilamellar giant polymersomes with a diameter above 1 μm for polymers.[44]. Electrodes are usually platinum wires, gold wires or conductive glass (e.g. ITO).[12, 57] Lipids which are comparatively difficult to get into liposomes, tend to shape up during the electroformation process. Parameters influencing the vesicle generation are the thickness of the film (typically 25-50 μm are ideal), the frequency and the voltage. Often, lipid mixtures are used for this technique. Cholesterol is less commonly used.[51, 58] For polymersomes, no further additives are required.[44] Spin coating has been reported to successfully generate well-defined lipid films for this technique.[59] While electroformation allows easy production of vesicles in the μm-range with low dispersity, the total volume producible and the yield are suffer compared to other techniques.[44]
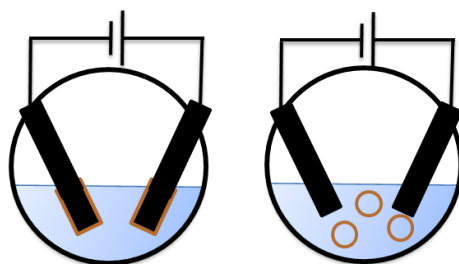
Figure 10. Illustration of electroformation. Vesicles are formed by applying an alternating electric field to two coated electrodes.

Others

Other techniques for liposome preparation include detergent removal, French pressure cells, inkjets and independent assembly.[60-63] The latter is especially useful for the preparation of asymmetric liposomes, because each layer is assembled in a separate step. Other reported techniques for polymersome preparation include templated formation, inkjets, micromixers and emulsion-centrifugation for the preparation of vesosomes (polymersomes in polymersomes).[62, 64-66]

2.2.2.2. *Functionalisation of Liposomes*

For functional liposomes, either natural lipids, which can be chemically modified to bear certain properties or synthetic lipids, which are tailored to the specific need, are used.

Modified lipids

The motivation to develop functional lipids arises mostly from the field of nanomedicine. Liposomes are of interest as drug carriers due to their biocompatibility, low toxicity and ability to protect their cargo from harmful influences such as changes in pH and enzymatic degradation.[67] Furthermore, they can carry hydrophilic cargo in their core and hydrophobic cargo can be embedded in the bilayer.[68] Functional liposomes aim to overcome the weaknesses of conventional liposomes, i.e. they aim for enhanced stability and blood circulation time, as well as introduction of specific targeting moieties.

Perhaps the most prominent class of functional liposomes are the stealth liposomes, or PEGylated liposomes, i.e. lipids functionalised with poly(ethylene glycol) (PEG). For liposomes, it is known to enhance the stability in blood by reducing adsorption of plasma proteins and degradation by macrophages.[68] Due to its popularity, PEGylated lipids have been commercially available for a while, earlier works coupled the amine group of a lipid to PEG, whose hydroxyl group had been activated using cyanuric chloride (Scheme 1).[69, 70]

Scheme 1. PEGylation of lipids using cyanuric chloride.

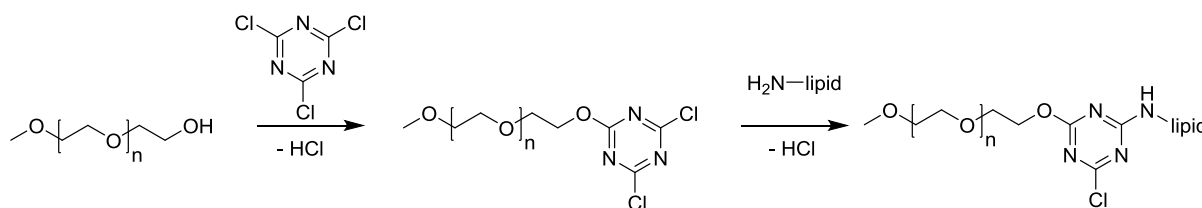The stability of PEGylated liposomes in blood was further enhanced by functionalising them with albumin. This was achieved by the hetero-bifunctional crosslinker *N*-succinimidyl 3-(2-pyridyldithio) propionate, which serves as a linker between the lipid and the albumin protein.[71] Due to its high water-binding capacities, PEG destabilises liposomes, most notably by reducing the hydration of the polar lipid head group. To counterbalance that, usually cholesterol is added to increase the stability and fluidity of the bilayer. An alternative to PEGylation to obtain liposomes with enhanced blood circulation time is the use of superhydrophilic zwitterionic polymers, though that is by far less common than PEGylation. They circumvent the membrane-destabilisation of PEG while supplying the same positive properties. Synthetically, this was realised by using an ATRP initiator with an *N*-hydroxysuccinimid (NHS) ester group. After polymerisation, the resulting poly(carboxybetaine) was coupled to the amine group of 1,2-distearoyl-*sn*-glycero-3-phosphoethanolamine (DSPE) using the NHS ester.[72]

The second major motivation for functional liposomes, besides enhanced stability, is a targeting ability for medical or diagnostic purposes. c(RGDyK), a peptide that targets the $\alpha_v\beta_3$

integrin receptor was coupled to DSPE using NHS and EDC chemistry. The modified liposomes were able to target cancer cells.[73] In a similar study, maleimide functionalised DSPE was coupled to cys-TAT, a cationic cell-penetrating peptide, using the reaction between maleimide and thiols. In the same study, T7, a targeting peptide for the transferrin receptor, was linked to DSPE-PEG$_{2000}$-BTC via a carbamate bond. BTC, or benzotriazole carbonate, serves as an activating group. The resulting dual-functional liposomes showed increased targeting ability and uptake for transferrin receptor enriched cells.[74] Jian *et al.* recently developed dual-functional liposomes with mitochondria-targeting ability and additional pH-responsiveness. Maleimide-thiol chemistry was used to link DSPE and cys-KLA, a mitochondria-targeting peptide. KLA bears positively charged lysine units, which facilitate endocytosis. However, during blood circulation this can lead to unspecific protein adsorption. To circumvent this, the liposomes were further functionalised with 2, 3-dimethylmaleic anhydride. Under basic conditions, the anhydride forms an amide bond with amine residues of the KLA peptide. This coats the surface with negative charges, thereby reducing protein adsorption. Under acidic conditions, as present in lysosomes, the amide bonds are cleaved and the mitochondria targeting KLA peptide is accessible again.[75] Vabbilisetty *et al.* used the Staudinger ligation to functionalise liposomes with lactose.[76] Like for the related Staudinger reaction, the reactants are an azide (here the lactose was modified accordingly) and a triarylphosphine (here DSPE was modified accordingly). The differences of the Staudinger reaction and ligation are shown in Scheme 2. In the conventional Staudinger reaction, the azide is attacked by the nucleophilic phosphine. A cyclic, four-membered transition state is formed and after nitrogen elimination, an aza-ylide is obtained. The ylide is hydrolysed to form an amine and phosphine oxide. The Staudinger reaction is a mild way to obtain amines from azides. In the Staudinger ligation, however, a trick is employed to prevent the hydrolysis. Up until the cyclic transition state, the reaction proceeds in the same way. However, the Staudinger ligation uses a modified phosphine, bearing an ester group in the ortho position. This introduces a new reaction, which competes with the hydrolysis and is favoured because of the proximity of the reactants. The ylide reacts with the 'electrophilic ester trap' to form an intramolecular cycle. This is then hydrolysed to an amide bond. The Staudinger ligation is a famous example for biorthogonal reactions, i.e. reactions that do not interfere with biological processes, since neither reactants is found in living systems.[77] The glyco-functionalised liposomes obtained by this method showed enhanced stability, interactions with lectin and sustained release.
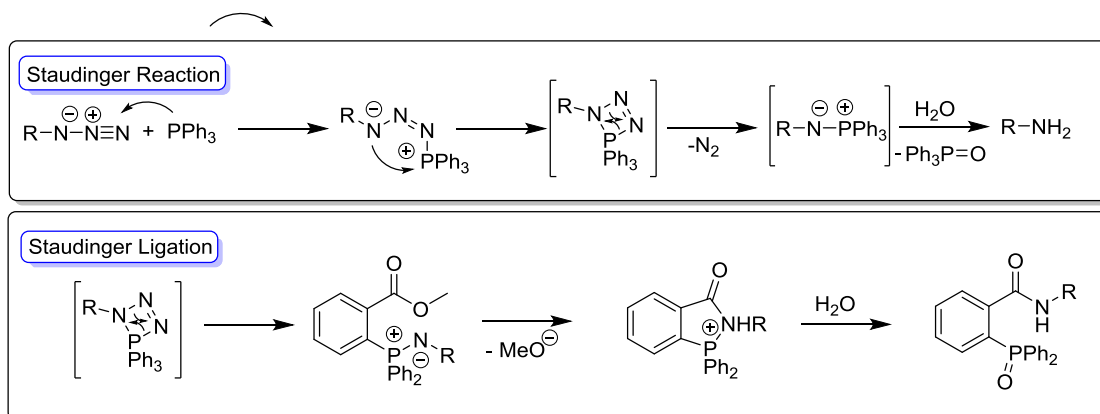
Scheme 2. Mechanisms of the Staudinger Reaction and the Staudinger Ligation.

Synthetic lipids

Best *et al.* devised photo-liable liposomes.[78] They synthesised a derivative of phosphatidylcholine (PC) with a photo-cleavable 2-nitrobenzyl group in one of its acyl chains (see Scheme 3 top and middle). The liposomes showed light triggered release of their cargo.
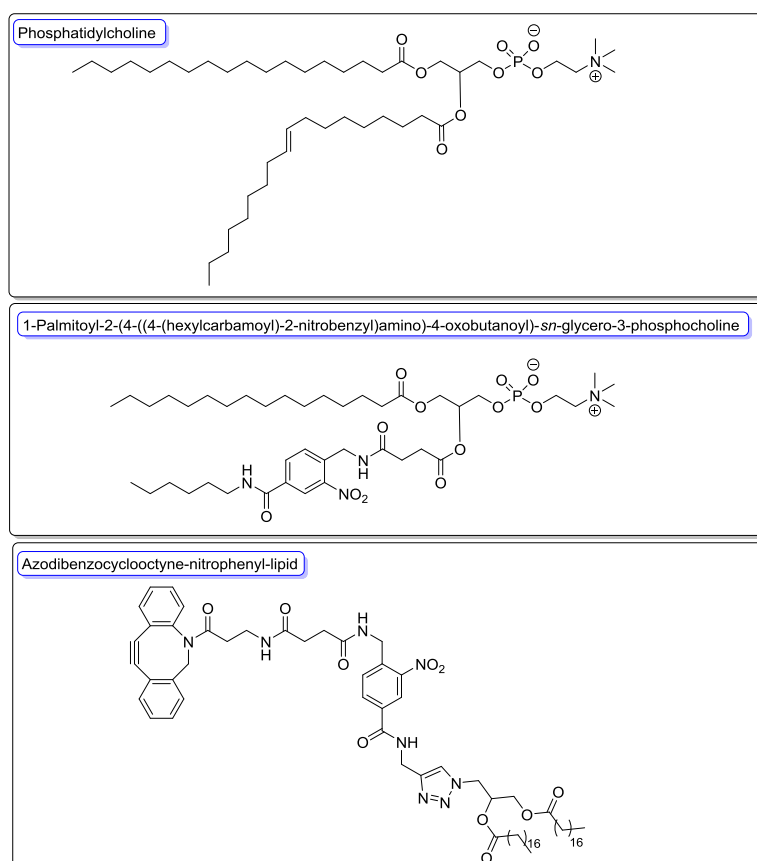
Scheme 3. Structure of phosphatidylcholine (top), its synthetic analogue 1-palmitoyl-2-(4-((4-(hexylcarbamoyl)-2-nitrobenzyl)amino)-4-oxobutanoyl)-*sn*-glycero-3-phosphocholine (middle) and the synthetic lipid azodibenzocyclooctyne-nitrophenyl-lipid (bottom).

Best *et al* presented a similar artificial lipid – azodibenzocyclooctyne-nitrophenyl-lipid (Scheme 3 bottom).[79] In addition to the photo-cleavable 2-nitrobeznyl group, this artificial lipid has a reactive alkyne group.

An important group of synthetic lipids are cationic lipids. Due to their ability to form charged complexes with DNA, so called lipoplexes, they are of considerable interest for the safe delivery of DNA based drugs.[80] The hydrophilic head group usually consists of a quaternary ammonium group, a polyamine or guanidinium salts. Charged heterocycles, such as imidazole or pyridinium have been reported as well, the hydrophilic part can also be based on an amino acid.[81] The hydrophobic part is most often a linear aliphatic chain.

Hanks *et al.* presented pH-responsive liposomes based on polydiacetylenes (PDA), which are artificial lipid-analogues. They exhibit a reversible colour and fluorescence switching, depending on the pH.[82] PDAs were combined with the redox-responsiveness of ferrocene in a molecule devised by Stevens *et al.* - *N*-(10,12-pentacosadiynoyl)acetylferrocene, which were used to form redox-responsive vesicles.[83]

In summary, the morphology of lipid assemblies depends on the critical packing parameter P_c. Given the appropriate P_c, liposomes are commonly prepared using film hydration, electroformation or microfluidics. The latter two techniques typically result in GUV formation, while film hydration produces SUVs or LUVs. Functional liposomes are accessible either by chemical modification of natural lipids or by synthetic lipids. Table 1 gives a summary of all modified lipids presented in this chapter. The lipid and the linked ligand are specified, as well as the chemistry used. With only a few exceptions, the functionalisation is commonly carried out before liposome formation, resulting in a distribution of the functional group on the inner and outer surface of the liposome. Notably, all liposome formulations include additional components, such as PC or cholesterol. This is required to stabilise the liposomes and illustrates where liposomes fall short: Many components are required to create a stable, functional liposome. The following chapter presents functionalisations on polymersomes, vesicular structures with an innately higher stability than liposomes. Furthermore, they are chemically more versatile, since the polymeric building block can be precisely tuned in regard to the monomer, block length and functionality.

Table 1. Summary of modified lipids presented in this chapter. The column modification denotes whether the functionalisation took place before or after liposome preparation. DSPE is 1,2-distearoyl-*sn*-glycero-3-phosphoethanolamine, PEG is poly(ethylene glycol). DSPC is 1,2-distearoyl-*sn*-glycero-3-phosphocholine, DOPE is 1,2-Dioleoyl-*sn*-glycero-3-phosphoethanolamine, NHS is *N*-hydroxysuccinimide, PC is phosphatidylcholine, c(RGDyK) is a targeting peptide, DSPG is 1,2-distearoyl-*sn*-glycero-3-phosphorylglycerol, TAT is a cell-penetrating peptide, BTC is benzotriazole carbonate, T7 is a targeting peptide, KLA is a targeting peptide, DPPC is 1,2-dipalmitoyl-*sn*-glycero-3-phosphocholine.

Lipid	Ligand	Chemistry	Modification	Other components	Reference
DSPE	PEG	Cyanuric chloride	pre	DSPC	[70]
DOPE	Albumin	NHS	both	Egg PC Cholesterol PEG-DSPE	[71]
DSPE	Polycarboxybetaine	NHS	pre	DSPC	[72]
DSPE-PEG$_{2000}$-COOH	c(RGDyK)	NHS	pre	DSPC DSPG MPEG$_{2000}$-DSPE	[73]
DPSE-PEG$_{2000}$-Mal	TAT	Maleimide/thiol	pre	PC Cholesterol DSPE-PEG$_{2000}$	[74]
DSPE-PEG$_{2000}$-BTC	T7	Benzotriazole carbonate	pre	PC Cholesterol DSPE-PEG$_{2000}$	[74]
DSPE	KLA	Maleimide/thiol	pre	PC Cholesterol	[75]
DSPE	Lactose	Staudinger ligation	post	DPPC	[76]

2.2.2.3. *Functionalisation of Polymersomes*

The functionalisation can be performed on preformed vesicles (Figure 11a), which results in a surface functionalisation. This is a way to produce asymmetric polymersomes. The polymer chain can also be functionalised before vesicle formation (Figure 11b) and polymersomes are formed by mixing functionalised and non-functionalised polymer. In this case, the functional groups will be distributed both on the in- and outside of the polymersome. The advantage here lies in the control over the functionalisation density. Lastly, the polymer can have an inherent functionality in one of its blocks (Figure 11c). Neither functionalisation can alter the amphiphilic proportions of the polymer too much, otherwise the self-assembly can

be disturbed.

Functionalisation of polymersomes is usually carried out to introduce a targeting moiety for drug delivery purposes or immobilisation on surfaces. Especially for the former, the requirements for the functionalisation are an aqueous environment. In the following, examples for such reactions will be given.
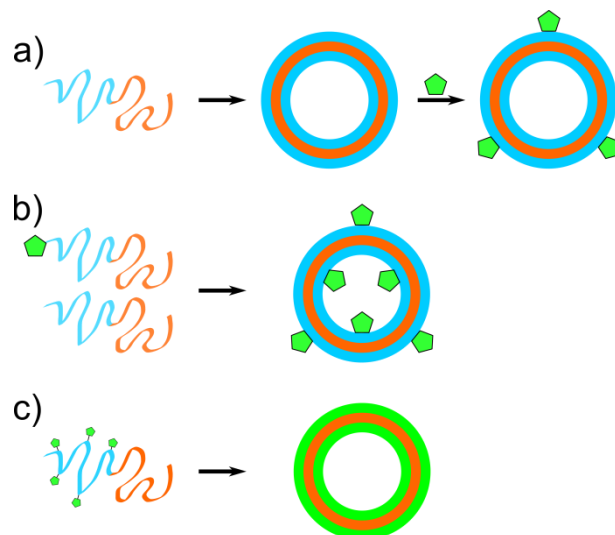
Figure 11. Strategies for functional polymersomes. Functionalisation can take place after polymersome formation (a) or before (b). The functionality can be part of the hydrophilic block (c).

Non-covalent functionalisations

A popular strategy is the biotin-streptavidin pair. Biotin was coupled to PMOXA-*b*-PDMS-*b*-PMOXA triblock copolymers using and esterification reaction catalysed by *N,N'*-dicyclohexylcarbodiimide (DCC) and 4-(dimethylamino)-pyridine (DMAP). Streptavidin was used to achieve a conjugation to biotinylated polyguanylic acid, a ligand for the macrophage SRA1 receptor.[84] Alternatively, tresyl chloride was used to transform a hydroxyl terminus into a good leaving group for subsequent substitution of biocytin.[85] The interaction between biotin and streptavidin is one of the strongest non-covalent interactions known. But it remains a non-covalent interaction, therefore a dynamic ligand exchange can take place in a system that contains multiple biotinylated compounds. Furthermore, care has to be taken to prevent crosslinking between polymersomes. The non-covalent interaction between lysine-nitrilotriacetic acid (NTA)-metal complexes and oligohistidin sequences has also been successfully utilised on polymersomes. NHS chemistry was used to couple NTA to a carboxy terminus of PB-*b*-PEO. The interaction with oligohistidin was shown on his-tagged model proteins, namely enhanced green fluorescent protein (EGFP) and red fluorescent protein (RFP).[86] The last non-covalent interaction which shall be presented here is the host-guest interaction between β-cyclodextrin and adamantane groups. Polymersomes from PS

terminated with methylated β-cyclodextrin were coupled to adamantane-labeled horse radish peroxidase. Self-assembly takes places because the cyclodextrin serves as a hydrophilic moiety of the polymer.[87]

Covalent functionalisations

Moving on to covalent functionalisations, the most popular strategy is certainly the 1, 3-dipolar cycloaddition between azides and alkynes. Van Hest *et al.* presented clickable polymersomes. PS-*b*-PAA was prepared using ATRP. The terminal bromides were substituted for azides using azidotrimethylsilane. The resulting azide-coated polymersomes were brought to reaction with several alkyne bearing molecules, e.g. biotin and EGFP. The required Cu(I) was generated *in situ* from sodium ascorbate and copper sulfate.[88]
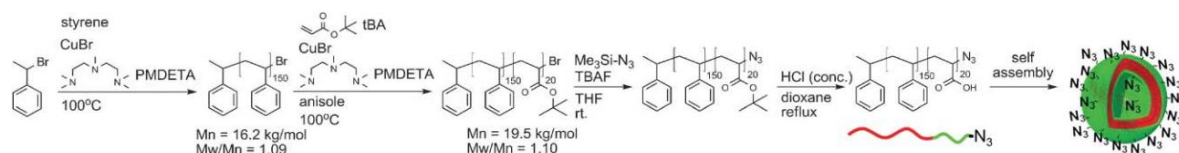
Scheme 4. Strategy for azide-functionalised polymersomes. Reproduced from [88] with permission of The Royal Society of Chemistry.

Shortly thereafter, van Hest and coworkers presented reversely oriented polymersomes. Azide-functionalised PS (accessible through the bromine leftover from ATRP) was linked to a,ω-diacetylene-functionalised PEO using the Cu(I) catalysed click reaction. The second alkyne group was left unreacted and remained available on the surface of the polymersomes. Those were coated with azido-functionalised Candida antarctica Lipase B.[89] Van Hest and coworkers have expanded their portfolio of functionalisation reactions even further. In an attempt to increase cellular uptake, they coated polymersomes with the cell penetrating peptide TAT.[90] This was achieved by using a cycloaddition/retro Diels Alder reaction between azide-functionalised TAT and oxanorbornadiene-functionalised PS-*b*-PEO block copolymers (Figure 12).
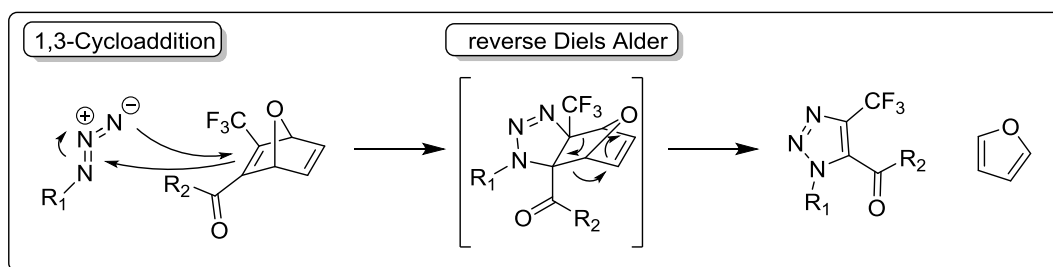

Figure 12. Mechanism of the cycloaddition/retro Diels Alder reaction.

The chemistry between thiols and maleimides has been employed on polymersomes as well. Cysteine residues of the antibody OX26 were reacted with maleimide end groups of poly(caprolactone)-*block*-poly(ethylene oxide) (PCL-*b*-PEO). OX26 is thought to initiate transcytosis of the polymersomes across the blood-brain barrier.[91] In addition, polymersomes were prepared from folate-PEO_{114}-*block*-(γ-benzyl-L-glutamate). The folate moiety was introduced by reacting maleimide-PEO_{114}-*block*-(γ-benzyl-L-glutamate) and thiol-functionalised folate. The folate is used to target cancer cells. To supplement this, the anticancer drug doxorubicin was coupled to the hydrophobic block by substituting some benzyl groups with hydrazides. Doxorubicin was then linked to the polymer backbone by an ester-amide exchange aminolysis reaction.[92] The mild coupling reaction of thiol groups to vinyl sulfones was used by Hillmyer *et al.* to link cysteine residues of peptides to poly(ethylene oxide)-*block*-poly(γ-methyl-ε-caprolactone) (PEO-*b*-PMCL), which was functionalised with a vinyl sulfone.[93] NHS esters were used to functionalise amino-terminated PDMS-*b*-PMOXA block copolymers with a fluorescent probe and aldehyde end groups of poly(lactide)-*block*-poly(ethylene oxide) (PLA-*b*-PEO) were used to immobilise polymersomes on an aminated glass surfaces via an imine bond (Figure 13).[94, 95]
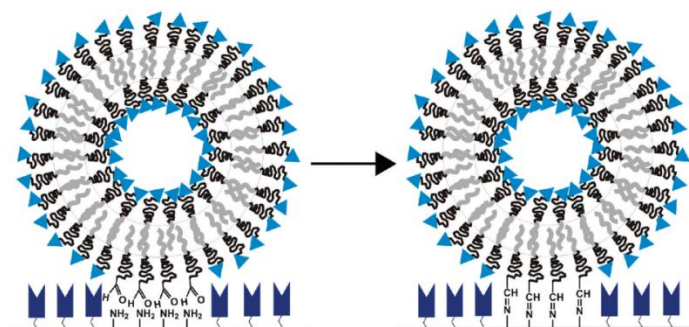
Figure 13. Immobilisation of vesicles on an aminated glass surface by imine bonds. Reproduced with permission from [95]. Copyright 2010 American Chemical Society.

Similarly, PB-*b*-PEO polymersomes were conjugated with PR_b, a targeting peptide for the $α_5β_1$ integrin receptor, using a NHS end group and the peptide's *N*-terminus.[96] Finally, 4-formylbenzoate modified PDMS-*b*-PMOXA has been reacted with 6-hydrazinonicotate acetone hydrazine modified ligands to form a stable hydrazone bond. This was used to functionalise polymersomes with either IgG or trastuzumab, the former as a patterning device, the latter for cancer cell targeting.[94] An interesting approach to polymersome functionalisation was presented by Kros and coworkers. They synthesised polypeptides consisting of a poly(γ-benzyl-L-glutamate) (PBLG) block and a hydrophilic block of a coiled-coil forming peptide. Coiled-coil peptides are able to form noncovalent complexes with complementary partners, allowing attachment of different ligands, as long as they possess

the complementary peptide sequence.[97]

These examples represent the most commonly used synthetic strategies for functionalised polymersomes. They can be either carried out before or after vesicle formation (Figure 11a or b).

Functional materials

Polymersomes, in which the functionality is not introduced by a chemical modification, but is a part of the polymer from the beginning will be addressed in the following (Figure 11c). Prominent representatives of this class are bio-inspired block copolymers, in which the hydrophilic block consists of a biological polymer. Typical building blocks are sugars, peptides, proteins and oligonucleotides.[98-101] Since in this case there are no different functionalisation strategies, but rather simply different polymerisation techniques, no specific example will be given and the reader is referred to the given references.

Another type of polymersomes with an inherent functionality are responsive materials, made from a polymer that is able to sense changes in the environment, such as light or temperature, and changes its physical or chemical structure as a response. In the following, examples for stimulus-responsive polymersomes will be given in order of the stimulus.

Responsiveness to pH is commonly used to adjust the morphology and the permeability of polymersomes. One of the earliest examples for pH-sensitive polymersomes was presented by Eisenberg *et al.* in 2003.[102] They studied the self-assembly morphologies of the triblock copolymer poly(acrylic acid)-*block*-poly(styrene)-*block*-poly(4-vinyl pyridine) (PAA-*b*-PS-*b*-P4VP) in dependence of the pH value. At a pH of 1, the polymer forms vesicles, which transition to solid aggregates in a pH range from 3-11. At pH 14, the morphology changes again to vesicles. Interestingly, vesicles at low pH carry P4VP on the outside, while at pH14 the PAA block is on the surface. This is caused by repulsive interactions within the different blocks. At low pH, the P4VP block is charged. In an attempt to minimise the repulsion between the charges, the system form polymersomes with the P4VP block on the outside. At pH 14, the PAA block is negatively charged, leading to a reversed structure (Figure 14).
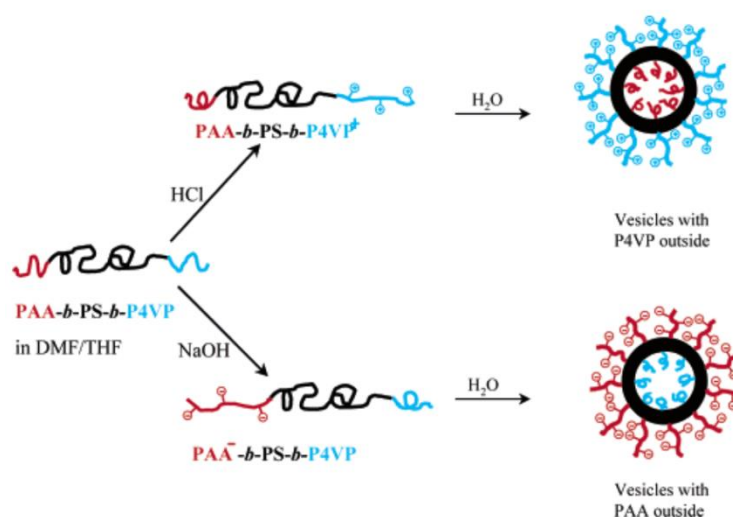
Figure 14. Illustration of possible vesicle morphologies for PAA-*b*-PS-*b*-P4VP copolymers. Reproduced with permission from [102]. Copyright 2003 American Chemical Society.

In a later work, Eisenberg and coworkers presented 'breathing' polymersomes. This effect is also caused by pH responsiveness. The polymersomes were assembled from the triblock copolymer poly(ethylene oxide)-*block*-poly(styrene)-*block*-poly(2-diethylamino ethyl methacrylate) (PEO-*b*-PS-*b*-PDEAEMA) at a high pH, at which the PDEAEMA block is hydrophobic and forms the inner part of the vesicle together with the PS block. Decreasing the pH leads to protonation of the PDEAEMA block, thereby increasing its hydrophilicity. This causes swelling and cracking of the vesicle shell, which in its turn increases its size and permeability to water.[103] Other examples for pH responsive polymers, whose pH selective assembly into polymersomes have been shown, include poly(*N*,*N*-dimethylacrylamide)-*block*-poly(styrene)-*block*-poly[*N*-(4-vinylbenzyl)-*N*,*N*-dibutylamine] (PDMA-*b*-PS-*b*-PVBA) and poly[2-(diisopropylamino)ethyl methacrylate](PDPA).[104, 105]

Temperature-responsive polymersomes use polymer blocks that exhibit a lower or an upper critical solution temperature (LCST or UCST). The most commonly used polymer in this field is poly(*N*-isopropylacrylamide) (PNIPAM), which has a LCST around 32 °C. Temperature dependent self-assembly of PEO-*b*-PNIPAM has been shown by Discher and Coworkers.[106] Above the LCST, PNIPAM is not soluble and vesicles are formed. Those disassemble once the temperature drops below the LCST to release hydrophobic molecules loaded in their shell. Alternatively, poly(*N*-vinylcaprolactam) (PVCL) has been used as a temperature responsive block. PVCL-*b*-PDMS-*b*-PVCL copolymers were used to assemble polymersomes. PVCL has a LCST of 37-42 °C, above which the polymersomes became porous, leading to an enhanced drug release.[107] Recently, polymersomes with both a LCST and UCST were reported. The LCST is due to 2-methoxyethyl side chains and the UCST is

caused by imidazolium salt side-chains. The self-assembly morphology of this system was strongly temperature dependent (Figure 15).[108]
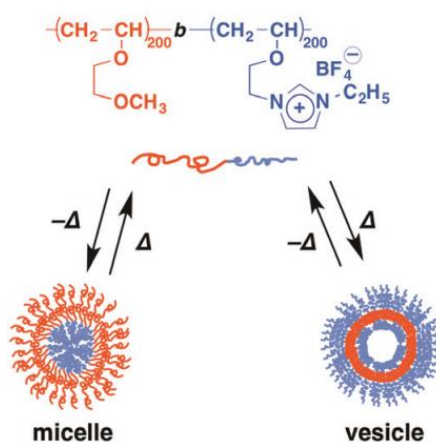
Figure 15. Illustration of self-assembly into micelles or polymersomes of MOVE$_{200}$-*b*-([EtIm][BF4])$_{200}$ in water. Reproduced from [108] with permission of The Royal Society of Chemistry.

Temperature- and pH-responsive polymersomes were reported by Li and coworkers. They studied the block copolymer poly(ethylene oxide)-*block*-poly[*trans-N*-(2-ethoxyl-1,3-dioxan-5yl) acrylamide] (PEO-*b*-PtNEA). At higher temperatures, this system will form polymersomes. Under acidic conditions, the ortho ester group of the PtNEA block is hydrolysed, increasing the hydrophilicity of the PtNEA block and destabilising the vesicles.[109] Huang *et al.* reported temperature- and photo-responsive polymersomes. They used an azobenzene-modified PS, which was decorated with a water-soluble pillar[7]arene by a host-guest interaction with the azobenzene side chain. Below the LCST of the pillar[7]arene, polymersome formation took place. The photoresponsive azobenze group was used to release the cargo calcein in a controlled manner.[110]

Next, redox-responsive polymersomes will be discussed. Several polymersomes have been assembled from block copolymers bearing an intermittent disulfide bond, which can be cleaved in a reductive environment.[111-113] This leads to disassembly of the vesicles. Hubbell and coworkers presented polymersomes, whose hydrophobic blocks were oxidisable. The triblock copolymer poly(ethylene oxide)-*block*-poly(propylene sulfide)-*block*-poly(ethylene oxide) (PEO-*b*-PPS-*b*-PEO) was used to form polymersomes. Hydrogen peroxide oxidises the hydrophobic block to poly(sulfoxide)s and poly(sulfone)s, which increases its hydrophilicity, destabilising the vesicles.[114] Yin *et al.* developed voltage-responsive polymersomes. Two independent homopolymers, poly(styrene)-cyclodextrin (PS-CD) and poly(ethylene oxide)-ferrocene (PEO-Fc) self-assembled into polymersomes through the host-guest interaction between ferrocene and cyclodextrin. By applying a voltage above

1.5 V, this host-guest interaction is disturbed by the oxidation of ferrocene to ferrocenium, which destroys the vesicles.[115]

Light-responsive polymersomes usually consist of a photo-sensitive polymer, which will undergo a conformational change or be cleaved when irradiated with light. As mentioned above, the light dependent host-guest interaction of azobenzene and pillar[7]arene was used to construct light-sensitive polymersomes. Oriol and coworkers reported polymersomes made from amphiphilic linear-dendritic block copolymers, in which a linear PEO segment was linked to a fourth generation 2,2-di(hydroxymethyl)propionic acid (bis-MPA)-based dendron, which contained 4-isobutyloxyazobenzene units in its periphery. Light-induced isomerisation of the azobenzene group deformed the vesicles and increased their permeability to cargo molecules.[116] Liu *et al.* presented polymersomes from poly(benzyl carbamate)-*block*-poly(*N*,*N*-dimethyl acrylamide) (PBC-*b*-PDMA). PBC is degradable and was triggered to depolymerise by various stimuli through endcapping with a responsive group. Either perylen-3-yl, 2-nitrobenzyl, or disulfide bonds were used. The trigger was visible light (420 nm), UV light (365 nm) or reductive milieu respectively (Figure 16).[117]
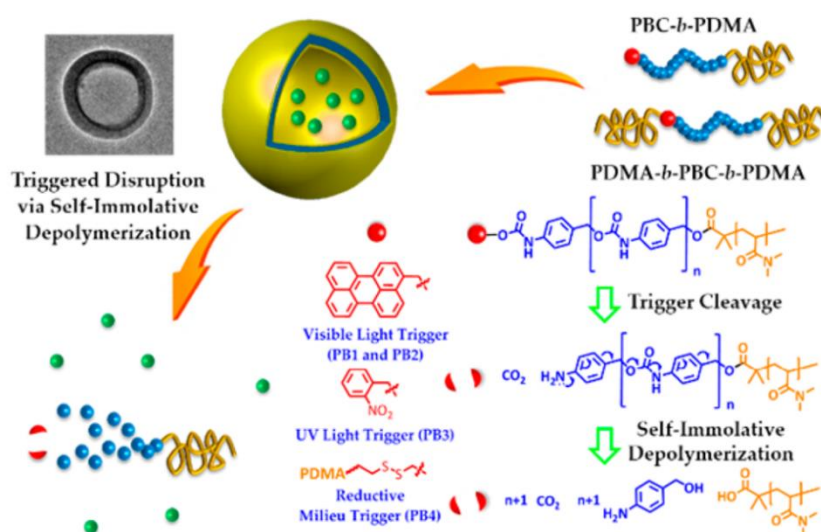
Figure 16. Illustration of polymersomes made from PBC-*b*-PDMA with different responsive groups, i.e. perylen-3-yl, 2-nitrobenzyl and disulfide groups leading to degradation triggered by visible light, UV light and reduction respectively. Reproduced with permission from [117]. Copyright 2014 American Chemical Society.

Light-responsiveness has also been used to crosslink polymersomes, rather than disassemble them. Polymersomes made from poly(ethylene oxide)-*block*-poly(2-nitrobenzyloxycarbonylaminoethylmethacrylate) (PEO-*b*-PNBOC) were prepared and irradiated with UV light, leading to cleavage of the carbamate group, leaving amine moieties. This led to amidation reactions with ester groups, crosslinking the vesicles as a result.[118]

The responsiveness to gas is certainly less well-known. However, since a number of biologically relevant molecules are gases (O_2, CO_2, NO), such systems are of interest for biomedical applications, such as drug delivery and bioimaging. Yuan *et al.* developed 'breathing' polymersomes from the CO_2 responsive block copolymer poly(ethylene oxide)-*block*-poly[(*N*-amidino)dodecyl acrylamide] (PEO-*b*-PAD). The amidine groups transform to charged amidinium groups in the presence of CO_2. This process is reversible after exposure to argon. Consequently, treatment with CO_2 led to an increase in size and volume of the polymersomes, which could be reversed under argon atmosphere.[119] CO_2 responsive vesicles, formed through a host-guest interaction, which is gas-dependent, have been reported by Zhao and coworkers. β-Cyclodextrin capped dextran was assembled with poly(L-valine), which was functionalised with benzimidazole. The host-guest interaction between cyclodextrin and benzimidazole is disturbed in the presence of CO_2, which protonates benzimidazole.[120] Recently, polymersomes which disassemble in the presence of H_2S were presented. They were made from poly(ethylene oxide)-*block*-poly(azidomethyl benzoyl glycerol methacrylate) (PEO-*b*-PAGMA) block copolymers. Exposure to H_2S reduces the azide to an amine, which leads to an intramolecular cyclisation and elimination of the side chain, which renders the formerly hydrophobic block hydrophilic.[121]

In summary, amphiphilic copolymers can form polymersomes, given the right amphiphilic proportions. Polymersomes are commonly prepared using film hydration, solvent displacement, electroformation, or microfluidics. The latter two techniques typically yied polymersomes in the µm-range, while the first two form polymersomes in the nm-range. Functionalisation can take place either before or after polymersome formation. Alternatively, the functionality can be an inherent part of the polymer, such as a LCST or degradability. Table 2 summarises the chemical functionalisations on polymersomes, that were presented in this chapter. In contrast to Table 1, the modification in lipids, the column with additional components is omitted, since polymersomes do not require a mixture of several components to be stable. Typically, functionalised polymer is mixed with non-functionalised polymer for vesicle formation. Functional polymersomes have been prepare using a variety of different reactions. Some, but not all, have also been used on liposomes, illustrating the versatility of functionalisations on polymersomes. Furthermore, while most functional liposomes are prepared using DSPE, functional polymersomes can be prepared from a number of different blocks, which in turn allows tuning their properties even further. Table 3 summarises the responsive polymersomes, that were presented in this chapter. Examples for polymersomes responsive to pH, temperature, redox processes, light and gas were selected. Evidently, there are many possibilities to precisely equip polymersomes with desired properties.

Table 2. Summary of functionalised polymersomes. The column modification denotes whether the functionalisation took place before or after liposome preparation. PMOXA-*b*-PDMS-*b*-PMOXA is (poly(2-methyl-oxazoline)–*block*-poly(dimethylsiloxane)–*block*-poly(2-methyl-oxazoline, DCC is dicyclohexylcarbodiimide, DMAP is 4-(dimethylamino)pyridine, PB-*b*-PEO is poly(butadiene)-*block*-poly(ethylene oxide), NTA is lysine-nitriloacetic acid, NHS is *N*-hydroxysuccinimide, PS is poly(styrene), PAA is poly(acrylic acid), CalB is candida Antarctica lipase B, PIAT is poly[L-isocyanoalanine(2-thiophen-3-yl-e thyl)amide, TAT is a cell-penetrating peptide, PBLG is poly(γ-benzyl-L-glutamate), PMCL is poly(γ-methyl-ε-caprolactone, PLA is poly(lactide), PR_b is a targeting peptide.

Polymer	Ligand	Chemistry	Modification	Reference
PMOXA-*b*-PDMS-*b*-PMOXA	Biotin	Esterification (DCC/DMAP)	pre	[84]
PB-*b*-PEO	Biocytin	Tresyl chloride	pre	[85]
PB-*b*-PEO	NTA metal complex	NHS	pre	[86]
PS	β-Cyclodextrin	Azide/alkye	pre	[87]
PS-*b*-PAA	Biotin	Azide/alkyne	post	[88]
PS-*b*-PEO	CalB	Azide/alkyne	post	[89]
PS-*b*-PEO	TAT	Retro Diels Alder	pre	[90]
PCL-*b*-PEO	OX26	Maleimide/thiol	post	[91]
PEO-*b*-PBLG-*b*-PEO	Folate	Maleimide/thiol	pre	[92]
PEO-*b*-PBLG-*b*-PEO	Doxorubicin	Ester-amide exchange	pre	[92]
PEO-*b*-PMCL	Peptides	Thiol/vinyl sulfone	post	[93]
PDMS-*b*-PMOXA	Dye	NHS	post	[94]
PLA-*b*-PEO	Aminated glass	Amine/aldehyde	post	[95]
PB-*b*-PEO	PR_b	NHS	post	[96]
PDMS-*b*-PMOXA	IgG or trastuzumab	Hydrazone	post	[94]
PBLG-*b*-peptide	Peptide	Complexation	during	[97]

[a] not specifically given in the literature

Table 3. Summary of responsive polymersomes. PAA-*b*-PS-*b*-P4VP is poly(acrylic acid)-*block*-poly(styrene)-*block*-poly(4-vinyl pyridine), PEO is poly(ethylene oxide), PDEAEMA is poly(2-diethylamino ethyl methacrylate), PDMA is poly(*N,N*-dimethylacrylamide), PVBA is poly[*N*-(4-vinylbenzyl)-*N,N*-dibutylamine], PMPC-*b*-PDPA is poly(2-(methacryloyloxy)ethyl phosphorylcholine)-*block*-poly(2-(diisopropylamino)ethylmethacrylate), PNIPAM is poly(*N*-isopropylacrylamide, PVCL-*b*-PDMS-*b*-PVCL is poly(*N*-vinylcaprolacatam)-*block*-poly(dimethylsiloxane)-*block*-poly(*N*-caprolactam), MOVE is 2-methoxyethyl vinyl ether, ([EtIm][BF4]) is 1-(2-vinyloxyethyl)-3-ethylimidazolium tetrafluoroborate, PtNEA is poly[*trans-N*-(2-ethoxyl,1,3-dioxan-5-yl) acrylamide], PPS is poly(propylene sulfide), pPEGMA-PCL-SS-PCL-pPEGMA is poly(polyethylene glycol methacrylate)-poly(caprolactone)-SS-poly(caprolactone)-poly(polyethylene glycol methacrylate), CD is cyclodextrin, Fc is ferrocene, MPA is 2,2-di(hydroxymethyl)propionic acid, PBC is poly(benzyl carbamate), PNBOC is poly(2-nitrobenzyloxycarbonylaminoethylmethacrylate), PVal is poly(L-valine), PAGMA is poly(azidomethyl benzoyl glycerol methacrylate).

Polymer	Responsive moiety	Responsiveness	Reference
PAA-*b*-PS-*b*-P4VP	PAA, P4VP	pH	[102]
PEO-*b*-PS-*b*-PDEAEMA	PDEAEMA	pH	[103]
PDMA-*b*-PS-*b*-PVBA	PVBA	pH	[104]
PMPC-*b*-PDPA	PDPA	pH	[105]
PEO-*b*-PNIPAM	PNIPAM	Temperature	[106]
PVCL-*b*-PDMS-*b*-PVCL	PVCL	Temperature	[107]
MOVE-*b*-([EtIm][BF4])	MOVE, ([EtIm][BF4]	Temperature	[108]
PEO-*b*-PtNEA	PtNEA	Temperature, pH	[109]
Azobenzene-modified PS and water-soluble pillar[7]arene	Azobenzene, pillar[7]rene	Temperature, light	[110]
PEO-SS-PPS	disulfide	Redox	[111]
pPEGMA-PCL-SS-PCL-pPEGMA	disulfide	Redox	[112]
PEO-*SS*-polyions	disulfide	Redox	[113]
PEO-*b*-PPS-*b*-PEO	PPS	Redox	[114]
PS-CD and PEO-Fc	Fc	Redox	[115]
PEO-*b*-bisMPA dendron	azobenzene	Light	[116]
PBC-*b*-PDMA	PBC (end group)	Light, Redox	[117]
PEO-*b*-PNBOC	PNBOC	Light	[118]
PEO-*b*-PAD	PAD	gas	[119]
Dextran and PVal	benzimidazole	gas	[120]
PEO-*b*-PAGMA	PAGMA	gas	[121]

[a] not specifically given in the literature

2.2.3. Hybrid Vesicles

Hybrid vesicles, composed of lipids and polymers, offer a more elaborate platform to engineer vesicles with customised properties. Many of the functional liposomes presented in chapter 2.2.2.2, aim to increase the stability of liposomes. At the same time, functional polymersomes are often designed to destabilise the polymer membrane in order to decrease mechanical stability and increase permeability. Both of those aims can certainly be achieved by careful chemical synthesis, however, hybrid vesicles may offer an easier route to the same end. By tuning the ratio of lipid to polymer, the physical properties of the resulting vesicle are altered as well, because lipid membranes are inherently less stable, as explained in section 2.2.2, without requiring additional chemical reactions. It seems surprising that molecules with such a sharp difference in molecular weight such as a polymer and a lipid are able to form hybrid structures at all, yet they have been reported for polymers with a molecular weight of up to 9000 g/mol.[122] Depending on the properties of polymer and lipid, as well as their interactions, the components will form a homogeneous membrane or subdomains. The transition temperature T_m of the lipid from fluid to gel is essential. Lipids with a T_m above room temperature tend to phase separate into domains, if the lipid content is high enough.[123] Conversely, homogenous membranes are favoured when a lipid is above its T_m.[124] Furthermore, the size difference of polymer and lipid plays a crucial role. As mentioned in previous chapters, a typical lipid bilayer is 3-5 nm thick, while a polymer bilayer can range from 8-21 nm, depending on the length of the hydrophobic block. Given a certain size difference between lipid and polymer, domain formation will result in exposure of hydrophobic blocks to water at the edge of those domains. To counterbalance this, smaller chains, present due to the dispersity of the polymer, will segregate to the border of lipid domains. Additionally, the polymers next to the lipid domains will be deformed and compressed, as shown in Figure 17. This decreases their conformational freedom and therefore comes at an entropic cost. And finally, in an attempt to minimise the surface area, the lipid domains can become larger. Consequently, the molecular weight and rigidity of the hydrophobic block has an impact on whether or not domain formation takes place. If it cannot facilitate those processes, domain formation is unlikely.[125]
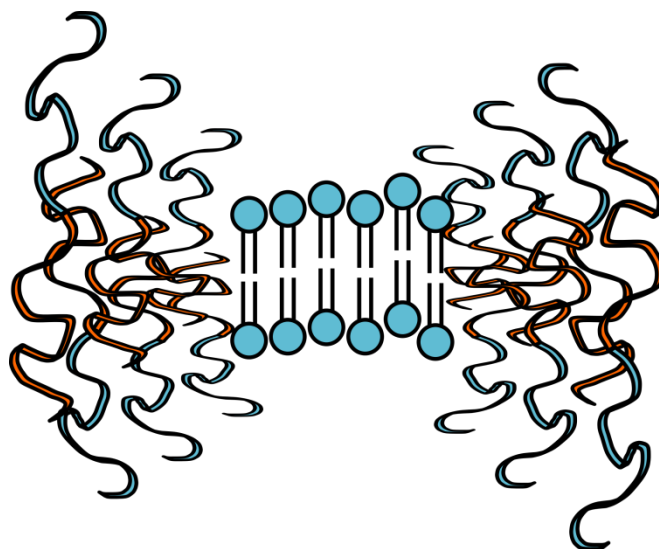
Figure 17. Illustration of the deformation of polymer chains next to lipid domains in hybrid vesicles.

In the following, a few hybrid vesicle systems from literature will be discussed. Recently, Chen *et al.* presented hybrid vesicles from DSPC and glycopolymers, namely poly(methacrylate)s with pendant cholesterol, mannose or galactose groups. Cholesterol was used as a hydrophobic anchor for the glycopolymers, while the sugars served as targeting moieties.[126] Kono and coworkers developed dual-responsive hybrid vesicles from egg yolk phosphatidylcholine (EYPC) and hyperbranched poly(glycerols)s (hbPG) with decyl, NIPAM and carboxylic acid groups. The decyl rest served as an anchor in the lipid bilayer. A temperature-responsiveness was introduced by the NIPAM groups, pH-responsiveness by the acid groups. At elevated temperatures or low pH, the solubility of the hbPG in water decreased, destabilising the vesicles, which led to release of the cargo.[127] Tsourkas *et al.* presented paramagnetic porous polymersomes, which were manufactured via hybrid vesicles. By mixing PEO-*b*-PB block copolymers with 1-palmitoyl-2-oleoyl-*sn*-glycero-3-phosphocholine (POPC), hybrid vesicles were obtained. The polymer chains were radically crosslinked using sodium metabisulfite and ferrous sulfate. After surfactant-mediated extraction of the lipid, porous polymersomes were obtained, which allowed an exchange of water across the membrane, while retaining encapsulated Gd chelate complex.[128]

3. Results and Discussion

Herein, the different nanocarriers, that were developed for this thesis, are presented and discussed. In chapter 3.1, ferrocene-based nanocontainers are investigated. Here, the focus lies on the redox-responsive properties of the nanocarriers, that are imbued by the ferrocene group. Chapter 3.2 is based on poly(butadiene)-*block*-poly(ethylene oxide) (PB-*b*-PEO) block copolymers, that are self-assembled into polymersomes. Different vesicle sizes, from tens on nanometers to tens of micrometers, are investigated as functional nanocarriers. Chapter 3.3 presents a hybrid vesicle system from PB-*b*-PEO block copolymers and lipids, as a platform for permeable polymersomes. Finally, chapter 3.4 introduces polymersomes from poly(butadiene)-*block*-poly(ethyl ethylenephosphate) (PB-*b*-PEEP) block copolymers, a novel class of biocompatible and degradable polymers.

3.1. Ferrocene-based Materials

Redox-responsive nanocapsules from poly(ferrocenylsilane), which will be refered to as PFS nanocontainers in the following, were synthesised by a miniemulsion/solvent evaporation protocol. Their electrochemical behaviour was studied using cyclic voltammetry (CV), revealing that the oxidation and consequently the reversibility of the process was hindered in PFS nanocontainers compared to pure PFS. Complete oxidation was achieved electrolytically, the resulting morphology change of the nanocontainers was imaged using transmission electron microscopy (TEM). Chemical oxidation of the nanocontainers led to release of encapsulated cargo. Due to the miniemulsion/solvent evaporation protocol, the nanocontainers had an oily centre, allowing only loading with hydrophobic cargo. A double emulsion/solvent evaporation protocol was developed for the production of nanocontainers with an aqueous core. However, no stable nanocontainers could be produced as shown by fluorescence correlation spectroscopy (FCS).

3.1.1. Stimulus-responsive Release from Poly(ferrocenylsilane) Nanocontainers[2]

3.1.1.1. *Motivation*

Stimuli-responsive nanocontainers have the potential to be beneficial to a number of different fields, such as drug delivery, contrast agents, self-healing materials, the food sector and as containers for confined reactions.[129-133] Generally, the nanocontainer serves as protection for the cargo from external influences and can differ in size, shape, and composition. The next

---

[2] This chapter (with the exception of 3.1.1.5) is based on the publication 'Stimulus-Responsive Release from Poly(ferrocenyl silane) Nanocontainers' by Laura Thomi, Philipp Schaefer, Katharina Landfester, and Frederik R. Wurm, published 2016 in Macromolecules, volume 49 on page 105-109 (http://pubs.acs.org/doi/full/10.1021/acs.macromol.5b02367). Reprinted with permission.

level is the introduction of responsive behavior, enabling the nanocontainer to react to an external stimulus. This opens up a field of functional nanocarriers, able to interact with their environment in a predefined way. In most synthetic polymers, these stimuli are pH or temperature, sometimes light.[134-136] Some of the most common stimuli in nature, however, are oxidation and reduction processes, which occur for example in cellular signaling pathways and photosynthesis.[111, 114, 137, 138] Man-made examples for such materials include the field of disulfide or diselenide chemistry, conductive polymers (e.g. polyaniline), or metallocenes (especially the ferrocene group (fc)).[132, 139-145] Ferrocene itself is seldomly used, however it can be incorporated into polymeric materials either in the side or main chain.[146] Poly(ferrocenylsilane)s (PFS), whose structure consists of alternating ferrocene and organosilane units, belong to the main chain ferrocene containing polymers. Among others, PFS materials have been studied regarding the self-assembly of block copolymers and subsequent use for the fabrication of magnetic ceramics.[147] The Vancso group investigated the formation of microcapsules through layer-by-layer self-assembly of polyanoinic and polycationic PFS.[148] The Manners group presented PFS microparticles, which were prepared in situ by a precipitation polymerization; also the self-assembly in confinement of PFS-*b*-PS block copolymers was studied.[149, 150] Herein, we present the first preparation of stimulus-responsive PFS nanocontainers by a miniemulsion protocol that can be loaded with hydrophobic cargo, and their behavior upon chemical and electrochemical oxidation is studied. Oxidation of ferrocene (Fe^{2+}) to ferrocenium (Fe^{3+}) can be achieved by common oxidants, like H_2O_2, $KMnO_4$, or $FeCl_3$.[143, 148] Additionally to that, we show oxidation through the enzymatic oxidation of glucose by glucose oxidase. The oxidation process introduces a positive charge into the polymer backbone, and enhances the swelling of the shell in water and the repulsion between the polymer chains. This generates a more permeable shell, which leads to an exchange between the core and the external water phase. With regard to the importance of redox processes in nature, these synthetic nanocontainers are an ideal handle to mimic biological systems. These redox-responsive PFS nanocarriers may find useful application in future sensing devices or self-healing matrices, where the redox potential of ferrocene triggers the release.

3.1.1.2. *Preparation and Characterisation*

Redox-responsive nanocontainers based on a hydrophobic PFS block copolymer, namely poly(dimethyl ferrocenylsilane)$_{0.87}$-block-poly(methyl vinyl ferrocenylsilane)$_{0.13}$ (hence referred to as PFS), were prepared by a miniemulsion/solvent evaporation protocol (Figure 19).[143] PFS was kindly provided by Dr. Wurm and characterised using ^{1}H NMR spectroscopy (Figure 18) and SEC (Table 4). The ratio of dimethyl ferrocenylsilane to methyl vinyl

ferrocenylsilane was calculated from the NMR spectrum by comparing the signals of the vinyl group (marked in yellow) to the methyl groups (marked in blue).
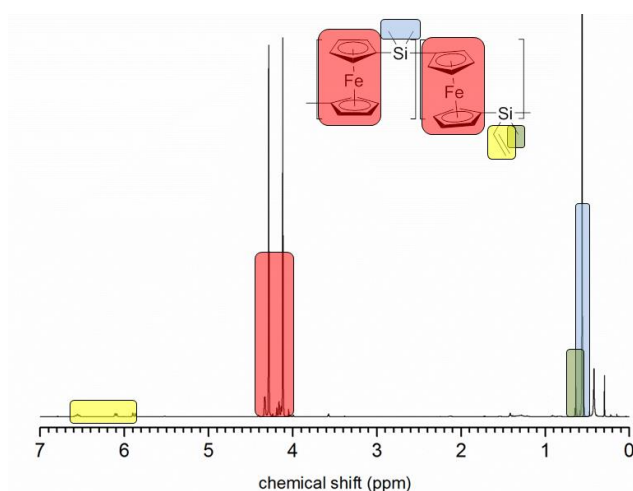
Figure 18. ^{1}H NMR spectrum (300 MHz, 298 K) of poly(dimethylferrocenylsilane)$_{0.87}$-block-poly(methyl vinyl ferrocenylsilane)$_{0.13}$ in CDCl$_3$.

Using this ratio and M_n obtained from SEC analysis, the degree of polymerisation for the two monomers can be calculated. However, since M_n was obtained vs. a PS standard, these values are not absolute.

Table 4. SEC data of poly(dimethyl ferrocenylsilane)$_{0.87}$-block-poly(methyl vinyl ferrocenylsilane)$_{0.13}$ in THF versus PS standard.

	Đ	M_n/ g/mol	DP_{PDMFS}[a]	DP_{PMVFS}[a]
poly(dimethyl ferrocenylsilane)$_{0.87}$-*block*-poly(methyl vinyl ferrocenylsilane)$_{0.13}$	1.09	37 900	136	19

[a] calculated from M_n obtained from SEC vs PS standard and ratio obtained from NMR.

For the nanocontainer formation, PFS was dissolved in dichloromethane (DCM) and dispersed in an aqueous solution of sodium dodecylsulfate (0.01 wt%) (SDS). The DCM droplets were further stabilized by the addition of hexadecane, which acts as an ultrahydrophobe to reduce Ostwald ripening (i.e. the growth of larger colloidal structures at the expense of smaller ones).[151] In addition, as a non-solvent for PFS, hexadecane serves as the oily core of the resulting nanocontainers. Stable DCM nanodroplets were achieved using ultrasonication. Subsequently, the DCM, a good solvent for PFS, is slowly evaporated. As the good solvent leaves the system, PFS is forced to precipitate at the interface between the continuous water phase and the hexadecane core, thereby forming a solid shell around

the liquid hexadecane core (Figure 19). This is possible because the interfacial tension between PFS and water is smaller than in a comparable hexadecane and water interface.[152] Therefore, a nanocontainer with PFS on the outside and hexadecane on the inside is energetically more favorable than vice versa. Afterwards, the excess of free surfactant was removed by centrifugation of the nanocontainers. The supernatant, containing free surfactant, was removed and the nanocontainers were redispersed in water. PFS nanocontainers with a mean hydrodynamic radius R_H of 233 ± 24 nm (determined by DLS) were generated by this protocol. Loading of these nanocontainers is possible with any hydrophobic cargo that does not interrupt the phase separation process.

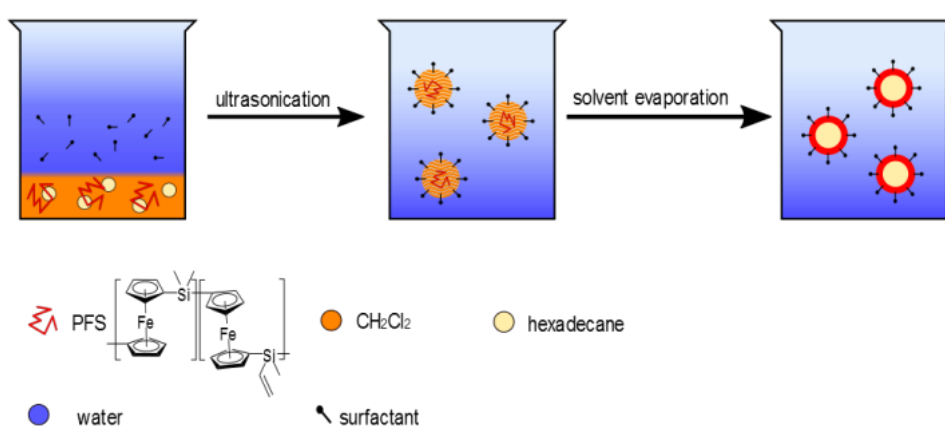**Figure 19. Preparation of core-shell PFS nanocontainers through a miniemulsion/solvent evaporation protocol.**

The PFS nanocontainers were visualized by TEM and SEM (Figure 20). They can be imaged without further staining due to the high electron density of the ferrocene group. The mean size from electron microscopy (506 nm) is in good accordance with the diameter obtained from DLS (466 nm).
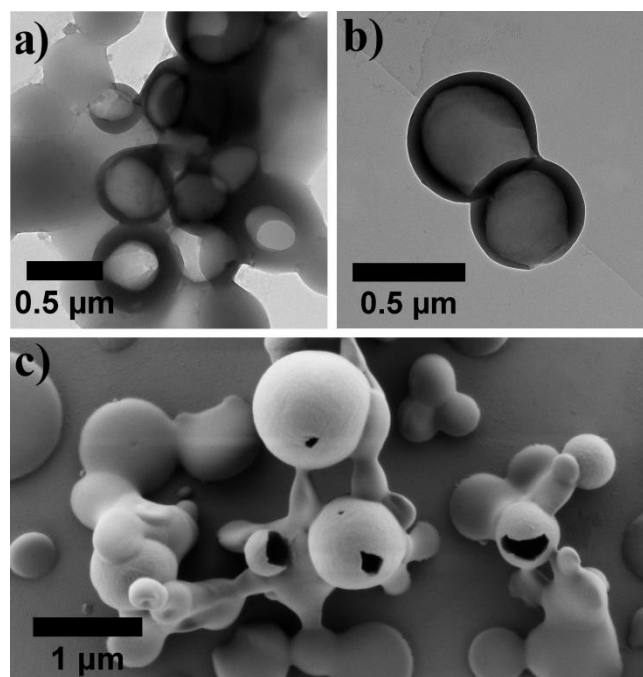
Figure 20. TEM micrographs of PFS nanocontainers (a and b) and SEM micrograph of PFS nanocontainers (c).

Their shell thickness can be estimated from TEM to be ca. 29 nm. The nanocontainers show an even surface morphology and high structural integrity, retaining their shape during the drying and imaging process. In SEM especially, the stability of the shell becomes apparent, as the morphology stays intact, i.e. does not deflate but small chips of the sphere break out during the drying process. The hexadecane core of the containers spills out as they break during drying and is visible in both SEM and TEM images as puddles next to the containers. Differential scanning calorimetry (DSC) was used to assess the thermal properties of the nanocontainers. They exhibit a melting temperature T_m of 132 °C and a glass transition temperature T_g of 18 °C. The polymeric starting material shows similar results, a T_m of 129 °C and a T_g of 29 °C. Differences can be attributed to the surfactant as well as the hexadecane which both may act as a softener in the nanocontainers. This is in accordance with the properties expected of mainly symmetrically substituted PFS as well as DSC data in literature.[153-155]

3.1.1.3. Electrolysis

The redox-responsiveness of PFS nanocontainers was investigated using cyclic voltammetry (CV) (Figure 21). The redox behavior of the aqueous dispersion was compared to the polymeric starting material. The measurement of the polymeric starting material required the deposition of a thin PFS film on the working electrode, because of the non-solubility of the

herein used PFS in water. The nanocontainers were measured either from drop-casting the dispersion on the electrode and obtaining a dried film or directly from dispersion (the numerical results are summarized in Table 5.

Table 5. CV peak data from Figure 3. E_{pa} and E_{pc} are the anodic and cathodic peak potential. I_{pa} and I_{pc} are the anodic and cathodic peak currents. Q_a and Q_c are the charges transferred during oxidation and reduction. Q_a and Q_c were calculated by integration of the measured currents. Γ, the surface coverage of the electrode, was determined from Q_a by $\Gamma = Q/nFA$ with n the number of transferred electrons, F the Faraday constant and A the surface of the electrode. For determination of E_{pc}, E_{pa}, I_{pc} and I_{pa} see Figure 22.

Sample	E_{pa} [V]	E_{pc} [V]	ΔE_p [V]	I_{pa} [μA cm^{-2}]	I_{pc} [μA cm^{-2}]	Q_a [C cm^{-2}]	Q_c [C cm^{-2}]	Γ [mol cm^{-2}]
PFS ads.	0.65	0.50	0.15	204	-208	1.42E-3	9.564E-4	1.48E-8
PFS containers ads.	0.55	0.52	0.03	42	-20	4.07E-4	2.27E-4	4.22E-9
PFS containers	0.58	0.50	0.08	-	-	-	-	-

The cyclic voltammogram of the adsorbed polymeric starting material film (PFS ads. in Figure 21) shows a single pair of oxidation and reduction peaks with an anodic peak potential E_{pa} of 0.65 V and a cathodic peak potential E_{pc} of 0.50 V (see Figure 22 at the end of this section for a definition of E_p and I_p). It is known in literature, that cyclic voltammograms of PFS generally show two sets of oxidation and reduction peaks, which is attributed to the stepwise reversible oxidation of the ferrocene units along polymer chain. The first set of peaks is caused by oxidation of the chain at every other ferrocene unit. Subsequent oxidation of the remaining units is energetically less favorable and therefore shifted to a higher potential giving rise to a second set of peaks.[156] However, this effect has been shown to be dependent on the solvent. In a solvent that does not facilitate swelling of the polymer film, interaction between the ferrocene centers and diffusion of counterions needed to balance the oxidation is hindered. Therefore, in solvents such as water the double peaks are rarely observable for hydrophobic PFS.[157] The peak separation ΔE_p and peak current I_p are indicators for the reversibility of a redox process. With ΔE_p of 0.15 V and almost identical I_{pc}

and I_{pa}, the process is partly reversible.

The adsorbed PFS nanocontainers show an E_{pa} of 0.55 V and a E_{pc} of 0.52 V. The ΔE_p of 0.03 V is indicative of a reversible process. It is clear, that the nanocontainer film differs in its electrochemical behavior from the polymer film. The adsorbed PFS film displays a large ΔE_p (0.15 V) as well as broad oxidation and reduction peaks, indicative of materials in which the charge transfer is hindered by diffusion. On the other hand, the adsorbed PFS nanocontainers show a small ΔE_p (0.03 V) and sharp oxidation and reduction peaks, typical for thin polymer films under non-diffusion limited conditions.[158] We believe the explanation for this lies in the difference of chain mobility in the two species. The presence of softeners (i.e. SDS and hexadecane) in the adsorbed PFS nanocontainers lowers the T_g under room temperature (18 °C), while the adsorbed PFS film remains at a T_g above room temperature (29 °C). That means under the experimental conditions (ca. 20 °C), the PFS film is in a glassy state, while the PFS nanocontainers remain flexible, removing the diffusion barrier. We were also able to measure the redox behavior of the nanocontainers in dispersion. It was noticeable that the peak current of the dispersion was significantly smaller. This is caused by the reduced concentration near the electrode. The dispersion did not show a clear reduction peak, which could be caused by too little oxidized material being available near the electrode and the slow diffusion of the containers compared to lower molecular weight material. The dispersion exhibited an E_{pa} of 0.58 V and a E_{pc} of 0.50 V (as determined after electrolysis), similar values as obtained for the deposited nanocontainers.

In a next step the effect on electrochemical oxidation on the morphology of the nanocontainers was investigated. The oxidation of ferrocene is a one electron process; therefore the amount of ferrocene (n_{fc}) multiplied with the Faraday constant (F), i.e. the electric charge per mole electrons, equals the charge necessary for complete oxidation. A constant potential of 0.75 V – well above the oxidation potential of the nanocontainers – was applied until the electrolysis was complete. The CV measurements of the sample after electrolysis (Figure 21b) show almost no oxidation and a pronounced reduction peak, proving that the vast majority of the material was oxidized. The morphology of the containers was assessed at theoretically 0%, 50% and 100% oxidation (Figure 21c, d and e) by TEM. At 0% oxidation the containers are intact, as to be expected. At 50% oxidation less intact core-shell structures can be detected. Instead sharper, fragmentation and high-contrast material next to the liquid hexadecane droplets appear. At 100% oxidation the hexadecane droplets are still visible (blue arrow in Figure 21e), with small high-contrast agglomerates next to them, presumably precipitated PFS (red arrow in Figure 21e) (drying effects during sample

preparation have to be taken into account). TEM images are not representative of containers in solution, but it can be observed that their integrity decreases during electrolysis.
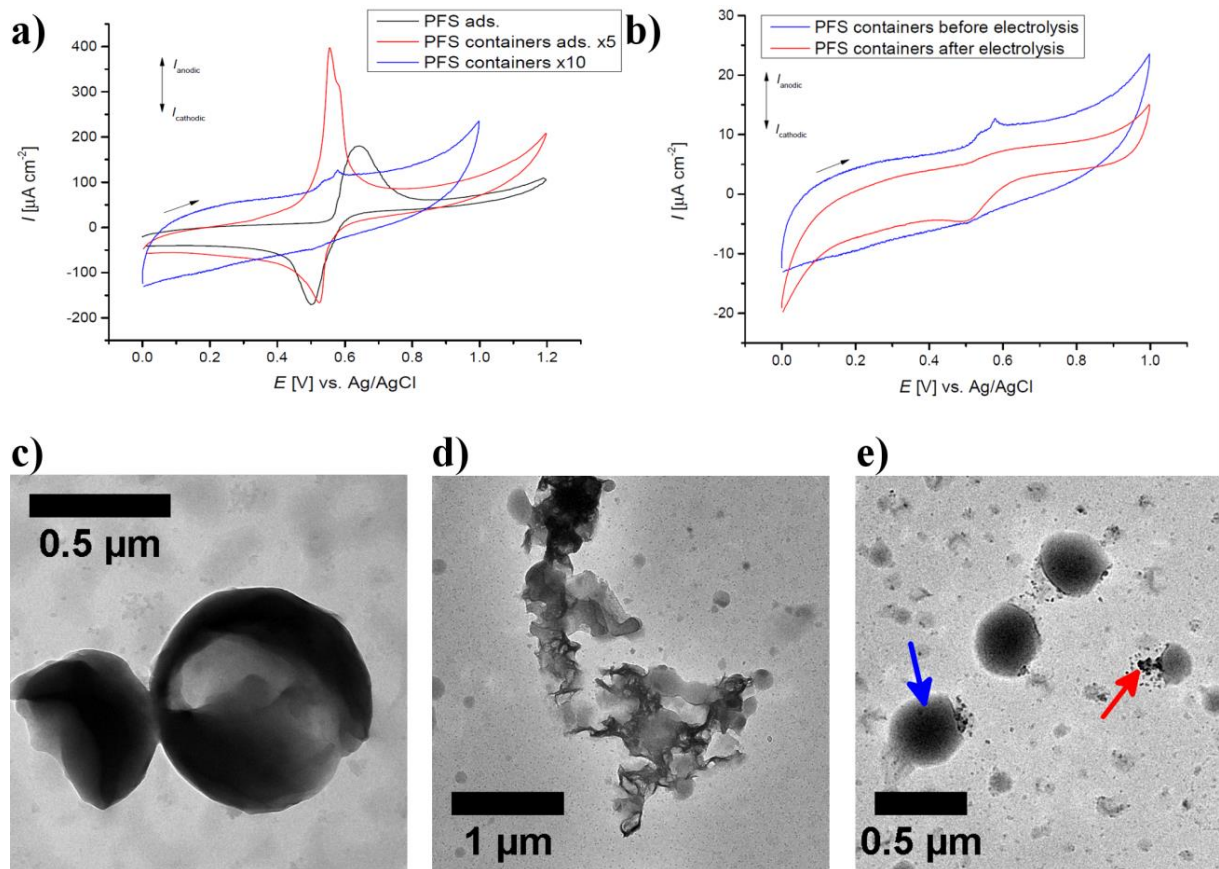
Figure 21. Electrolysis of PFS nanocontainers. a) Cyclic voltammograms of PFS adsorbed on the electrode (black), PFS nanocontainers adsorbed on the electrode (red) and PFS nanocontainers in dispersion (blue). The latter two were multiplied by 5 and 10 respectively for better visibility. Scan rates were 20 mV/s for PFS adsorbed and PFS nanocontainers adsorbed. PFS containers were measured at 10 mV/s. Measurements were carried out in PBS buffer. b) Cyclic voltammograms of PFS nanocontainers before (blue) and after (red) electrolysis. Scan rates were 10 mV/s. Measurements were carried out in PBS buffer. c) TEM image of PFS nanocontainers at 0% electrolysis. d) TEM image of PFS nanocontainers at 50% electrolysis. e) TEM image of PFS nanocontainers at 100% electrolysis.
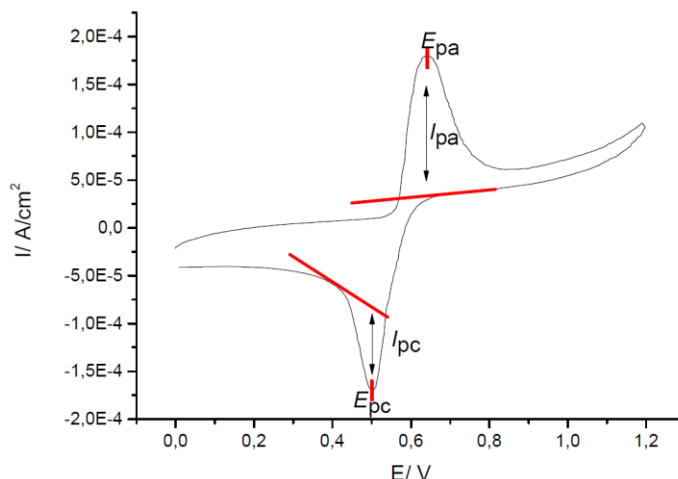
Figure 22. Cyclic voltammogram showing the definition of the anodic and cathodic peak potential (E_{pa} and E_{pc}) and the anodic and cathodic peak current (I_{pc} and I_{pc}).

3.1.1.4.   *Chemical Oxidation*

In a next step, the oxidation of PFS containers by chemical means was investigated regarding a) the change of the barrier properties of the PFS shell, visualized by confocal laser scanning microscopy (CLSM) and fluorescence intensity and b) the release of a hydrophobic cargo molecule measured by UV/Vis spectroscopy. Chemical oxidation of PFS nanocontainers was achieved by the addition of hydrogen peroxide to the dispersion under acidic conditions.[159] The nanocontainers were imaged using CLSM (Figure 23a and b). Fluorescin isothiocyanate-dextran (FITC-dextran) was added to the continuous water phase as a green fluorescent marker. Before oxidation, the nanocontainers are visible in the transmission image and appear as dark spots in the fluorescent channel (Figure 23a). The PFS shell acts as an efficient barrier, FITC-dextran cannot pass through it. After oxidation, the nanocontainers are still visible in the transmission channel; however, the fluorescence is now evenly distributed (Figure 23b). This shows that oxidation leads to opening of the shell, which is caused by the positive charges in the main chain, which are introduced through oxidation. They enhance swelling in water and lead to repulsion of the polymer chains, thus allowing the diffusion of the aqueous FITC-dextran solution into the interior of the nanocontainers.
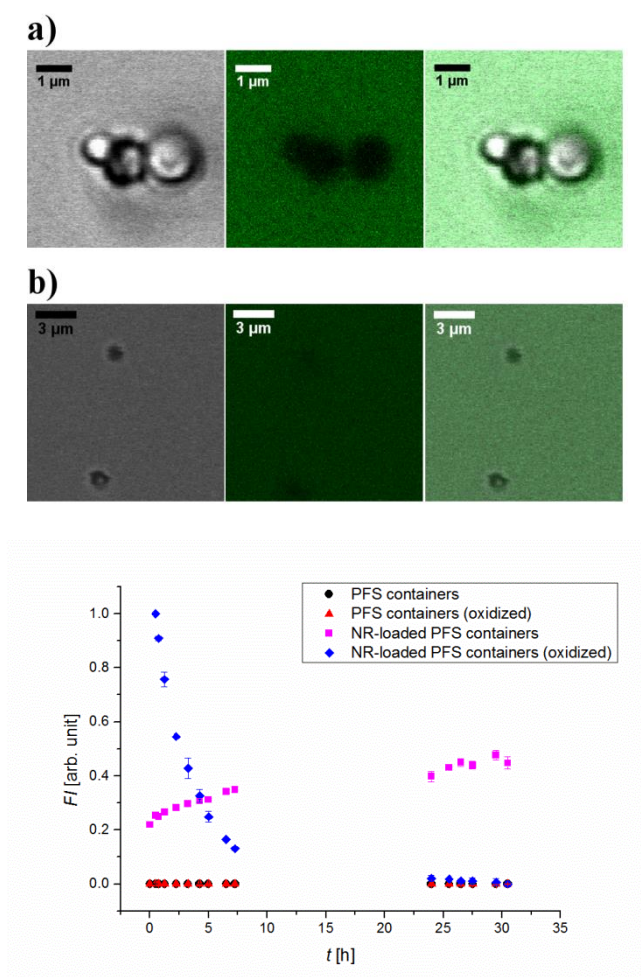
Figure 23. Confocal laser scanning microscopy (CLSM) images of PFS nanocontainers dispersed in FITC-dextran before (a) and after (b) oxidation with H_2O_2. Images show the transmission channel (left), fluorescent channel (middle) and the overlay (right). c) Fluorescence intensity over time of PFS nanocontainers (black spheres), PFS nanocontainers with H_2O_2 (red triangles), Nile Red-loaded PFS nanocontainers (pink squares) and Nile Red-loaded PFS nanocontainers with H_2O_2 (blue diamonds). Error bars represent the mean of two separate measurements.

In another experiment, nanocontainers loaded with Nile Red (NR) were subjected to chemical oxidation by hydrogen peroxide under acidic conditions (Figure 23c). NR is a well-known solvatochrome, which will hardly fluoresce at all in a hydrophilic environment and show good fluorescence in a hydrophobic environment.[160] Here, the hexadecane core of the nanocontainers will provide the hydrophobic environment for NR, while the aqueous, continuous phase will represent the hydrophilic environment. PFS nanocontainers with a hexadecane and NR core were prepared and the fluorescent intensity was measured. After addition of the oxidant to the dispersion the fluorescence intensity was monitored. PFS nanocontainers without NR were measured as a control to eliminate any influence of

scattering during the measurement. The empty nanocontainers showed no significant fluorescence over time, which remains unchanged in the presence of the oxidant. NR-loaded nanocontainers show a slight increase in fluorescence over time, which could be caused by evaporation of solvent, although steps were taken to keep this to a minimum. However, the NR-loaded sample showed an unexpectedly high fluorescence at the start of the experiment, which decreased significantly over time. In control experiments it was found that hydrogen peroxide does not increase NR fluorescence (data not shown). The initially high fluorescence is thought to be caused by an instantaneous increase in container size upon oxidation. This is followed by an expansion of the oily core, reducing the self-quenching of NR molecules. It has been shown in literature that the fluorescence of NR has a maximum at a certain concentration, once it is exceeded, quenching occurs.[161] After that, water can diffuse into the containers and thus the fluorescence of NR decreases as the hydrophilicity of the environment increases.

Besides the chemical oxidation by the direct addition of hydrogen peroxide, the enzyme-triggered release from the PFS nanocontainers was investigated. The enzyme glucose oxidase (GOx) oxidizes glucose to D-glucono-δ-lactone and generates hydrogen peroxide continuously over time, providing less harsh conditions than adding the entire amount of hydrogen peroxide at the beginning (Scheme 5).
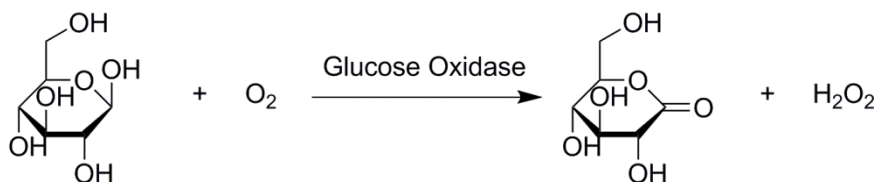
Scheme 5. Reaction of glucose to D-glucono-δ-lactone and hydrogen peroxide catalyzed by glucose oxidase.

In addition, release of a model compound was to be shown. 2-Propylpyridine was chosen for that, as it is soluble in hexadecane, shows partial solubility in water and is detectable using UV/Vis spectroscopy. The PFS nanocontainer dispersion as well as the enzyme was placed inside a dialysis tube, which is permeable to the model compound and was dialyzed against an aqueous solution of glucose (1.32 wt%) and additional surfactant (0.01 wt% SDS) to prevent aggregation. The experiment was conducted under acidic conditions (0.56 wt% 0.1 M HCl). When 2-propylpyridine is released from the nanocontainers, it can diffuse through the dialysis tube into the outer phase. Aliquots were taken at defined points over time, in which 2-propylpyridine was detected using UV/Vis spectroscopy. Figure 24 shows the release from PFS nanocontainers. The results clearly prove that the PFS nanocontainers

can be oxidized by the enzymatically generated hydrogen peroxide and thus exhibits an enhanced release compared to the unoxidized nanocontainers, which show excellent barrier properties, also for 2-propylpyridine.

Thus, cargo release from PFS nanocontainers can be triggered using an enzymatically coupled reaction making these structures also interesting for biological applications.
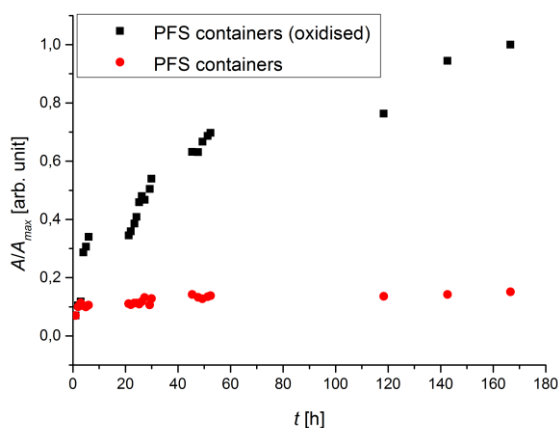
Figure 24. Release of 2-propylpyridine from PFS nanocontainers over time (red) and upon enzymatic oxidation with glucose oxidase in the presence of glucose (black).

3.1.1.5.   Attempts at Crosslinking

As evident from Figure 24, about 15% of the 2-vinylpyridine cargo released under oxidative conditions is also released from non-oxidative conditions. At t_0 about 6% 2-vinylpyridine is already released. This initial release burst can be attributed to residual 2-vinylpyridine, that ended up on the outside of the nanocontainer during the preparation, dissolving into the water phase. The remaining 9% are caused by leakage over time. The pendant vinyl group of the methyl vinyl ferrocenylsilane repeating unit offers the possibility to crosslink the nanocontainer shell using UV light, leading to a denser shell, thereby reducing unspecific leakage over time. For irradiation, the nanocontainer dispersion was placed in a quarz cuvette and stirred for 2 h while irradiating using a 10 W mercury short-arc lamp. Figure 25 shows a zoom in on the ^{1}H NMR spectra before and after irradiation. No change in the signals of the double bond was observed, therefore no crosslinking took place. This was attributed to the high concentration and scattering of the nanocontainer dispersion.
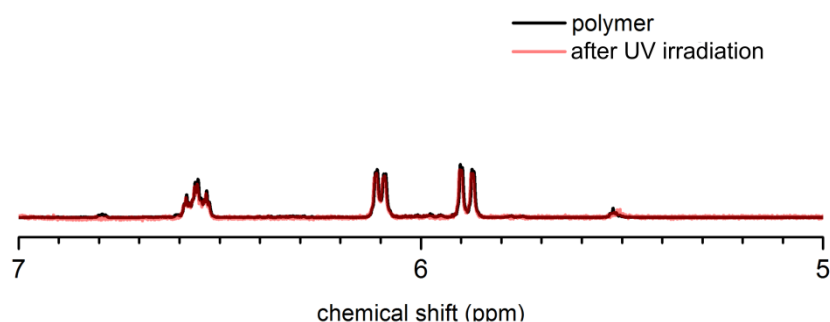
Figure 25. Zoom in on ^{1}H NMR spectra of nanocontainers before and after UV irradiation.

In a second attempt, an irradiation setup consisting of a tube spiraling around a UV lamp was used. The thinner tube allows for a better penetration of UV light into the sample. The nanocontainer dispersion was irradiated using a flow rate of 0.4 mL/min for 30 min. Figure 26 shows a zoom in on the ^{1}H NMR spectra before and after irradiation. No change in the signals of the double bond was observed, therefore no crosslinking took place.
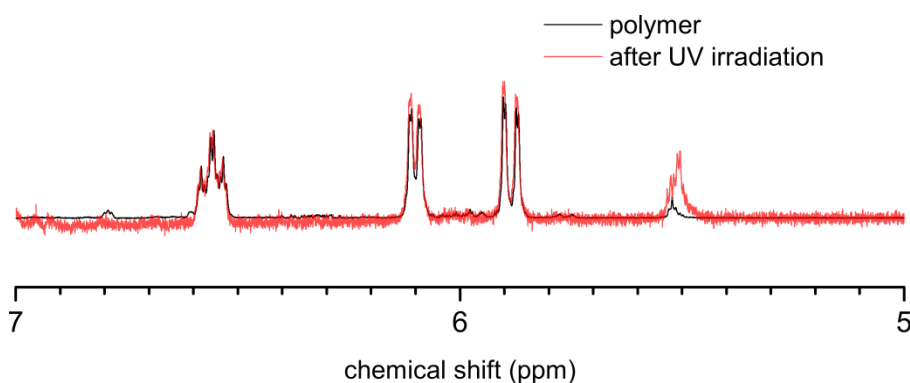
Figure 26. Zoom in on ^{1}H NMR spectra of nanocontainers before and after UV irradiation.

As no improvement could be made using another setup, it seems likely that the problem does not lie with scattering or concentration. Rather, the crystallinity of the shell might be the reason no crosslinking could be achieved. As evidenced by DSC and SEM data (see section 3.1.1.2 and Figure 20), PFS nanocontainers are a highly crystalline material. Given that the shell material is in a solid-like state, radical reactions needed to achieve crosslinking are likely hindered.

3.1.1.6. Conclusion

In conclusion, the first redox-responsive poly(ferrocenylsilane) nanocontainers were prepared in a miniemulsion approach through solvent evaporation. Previously reported, related materials include PFS microcontainers by layer-by-layer assembly of polycationic and

polyanionic PFS on colloidal templates and nanovesicles based on a hydrophilic PFS and a hydrophobic PDMS.[148, 162] The obtained core-shell structures with a solid PFS shell and a liquid hexadecane core can be loaded with hydrophobic cargo. The nanocontainers exhibited diameters of ca. 466 nm determined from DLS. Electron microscopy (TEM and SEM) visualizes the core-shell structures and an approximate shell thickness of 29 nm was determined. The preparation protocol allows loading the PFS nanocontainers with a great variety of hydrophobic molecules (Nile Red and 2-propylpyridine were used as examples). The electrochemical behavior of PFS containers was studied using CV, where it was observed that the oxidation was less pronounced in dispersion and the reversibility of the process was hindered. However, complete oxidation was achieved through electrolysis, during which nanocontainer morphology change was studied using TEM. It was found that the nanocontainers did not retain their shape during the electrolysis and may release the cargo after an electrochemical trigger. Both, the barrier properties of the PFS shell against leakage and permeation from outside were proven. However, after oxidation the permeation through the PFS barrier or the release from the core of the nanocontainers was proven. The release can also be coupled to the enzymatic oxidation of glucose with oxygen by the enzyme glucose oxidase. The pendant vinyl groups of the PFS block copolymer used in this work, offer possibilities for future modification of the nanocontainers. The herein presented PFS nanocontainers add a new tool to the kit of responsive nanocarriers, enriching the field of smart materials and their application in drug delivery, self-healing applications and synthetic biology.

3.1.2. PFS Nanocontainers via Double Emulsion

3.1.2.1. Motivation

In section 3.1.1, a redox-responsive nanocarrier system was established and investigated concerning its electrochemical properties. In this chapter we aim to overcome one condition this redox-responsive nanocarrier system is subjected to – the hydrophobic core. Loading the nanocarrier with hydrophilic cargo is not possible in such a system with an oily centre. A nanocarrier system with a hydrophilic core, however, would enable loading the carrier with active biomolecules, such as enzymes, the majority of which are water-soluble. This would create a closed compartment in which catalytic reaction could take place undisturbed by harmful influences on the outside, i.e. a system akin to a cell.

3.1.2.2. Double Emulsion Approach

The most obvious way to create such a system is an inverse miniemulsion approach, in which the aqueous phase is dispersed in a continuous oil phase. As in the solvent

evaporation in direct miniemulsion described in section 3.1.1.2, in inverse miniemulsion a volatile solvent for the carrier material is added to the dispersed phase. Upon evaporation, the carrier material precipitates at the oil-water interface, thereby forming the nanocarrier.[163] However, this approach is not feasible in the case of the herein used PFS, as it is too hydrophobic and will not dissolve in the dispersed phase of the inverse miniemulsion. Instead a double emulsion approach was used as illustrated in Figure 27. In a first step, a water-in-oil emulsion was prepared, using DCM as the continuous oil phase and water as the dispersed phase. FITC-dextran was added as a fluorophore to the water phase to assess whether the inner water phase w_i leaked into the outer water phase w_o. Furthermore, sodium chloride (1.2 wt%) was added as an osmotic agent to impede Ostwald ripening (see addition of hexadecane in section 3.1.1.2). The oil phase o contained oleic acid (OA) as a surfactant and PFS to form the nanocontainer shell. Emulsification was achieved by ultrasonication. The obtained primary emulsion was added at a controlled speed to the stirred w_o containing SDS as a surfactant. For producing a double emulsion two different surfactants with different HLB values are needed, since no surfactant is able to sufficiently stabilise both a w/o and an o/w emulsion. The stirring speed is crucial, it cannot be too low, else the double emulsion will agglomerate and it cannot be too high, else the double emulsion droplets will break. Nanocontainer formation was achieved by evaporation of the volatile solvent DCM. It should be noted that Figure 27 is an ideal depiction in which each droplet of the primary emulsion added to the outer water phase contains only one aqueous core. In reality, it is likely that the amount of aqueous cores is larger than one and varies from droplet to droplet.
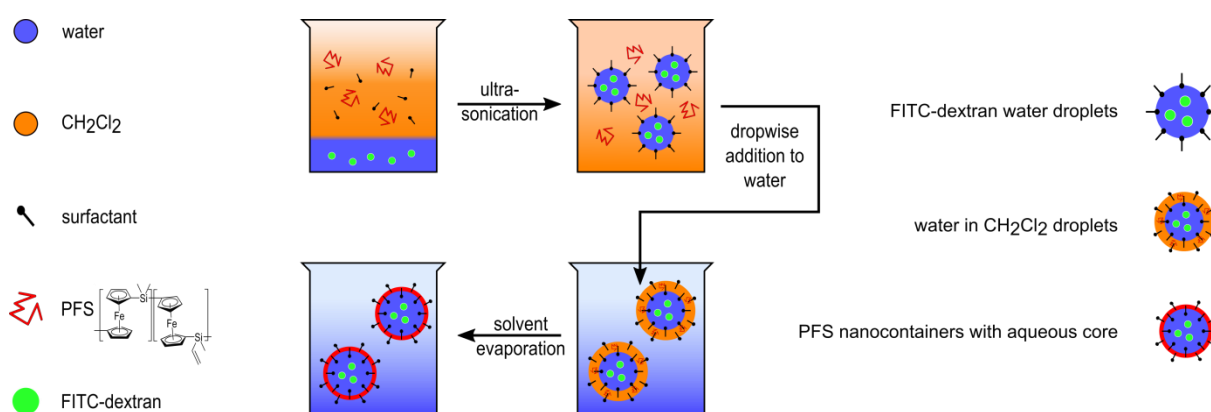
Figure 27. Preparation of core-shell PFS nanocontainers with an aqueous core through a double emulsion/solvent evaporation protocol.

Samples with varying amounts of surfactant were produced and investigated using DLS and fluorescence correlation spectroscopy (FCS). The results are summarised in Table 6. DLS measurements showed that the samples contained two different species of roughly the same

concentration, one with a R_H of about 270 nm and one significantly smaller with a R_H of about 45 nm. Due to the size it seems likely that the smaller species consists of PFS particles, formed when the preformed w/o droplets tear and w_i spills into w_o. The larger species might however be the desired nanocarrier with a hydrophilic core.

Table 6. Surfactant amounts and characterisation data for w/o/w samples and FITC-dextran as a reference.

Sample	OA	SDS	R_H/ nm^a	τ/ µs^b	D/ m^2*s$^{-1 b}$	R_H/ nm ^{b}
1	5 wt%	1 wt%	263 (46%) 57 (54%)	23 (64%) 198 (36%)	5.2E-11	4.4
2	7.5 wt%	3 wt%	282 (56%) 35 (44%)	22 (9%) 228 (91%)	4.1E-11	5.4
FITC-dextran	-	-	-	23 (26%) 203 (74%)	5.1E-11	4.5

^{a} obtained from DLS

^{b} obtained from FCS, R_H corresponds to the large species

FCS measurements were carried out for additional information. In FCS, the fluctuation of fluorescence intensity in the observation volume is measured over time and analysed autocorrelatively as illustrated in Figure 28.

Figure 28. FCS Setup. V_{obs} is the observation volume.

Since the observation volume is miniscule (about $1*10^{-15}$ L), the diffusion of single fluorescent species in and out of it can be observed if the sample is sufficiently low in concentration.[164]

From the fluctuation in fluorescence intensity over time, the probability that a signal at the time $t+\tau$ is caused by the same molecule as at the time t can be calculated using the autocorrelation function:
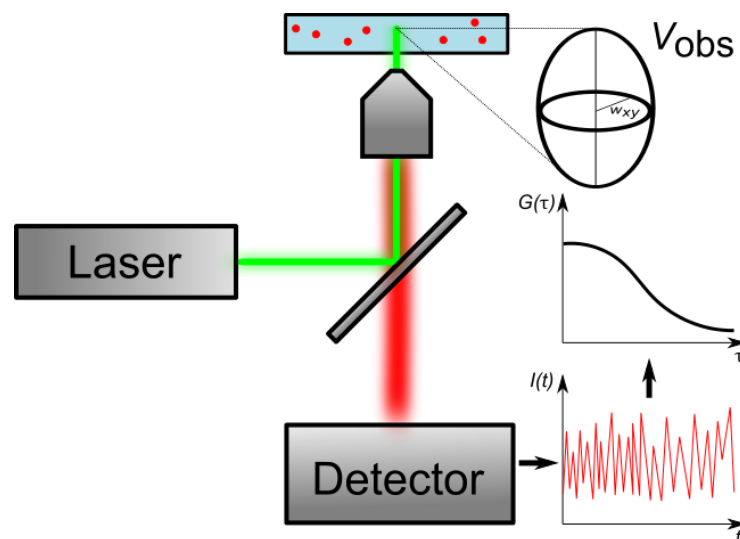
$$G_{(\tau)} = 1 + \frac{1}{N} * \left(1 + \frac{\tau}{\tau_D}\right)^{-1} * (1 + \frac{\tau}{S^2 \tau_D})^{-\frac{1}{2}} \qquad (2)$$

with N the average number of fluorescent species in the observation volume V_{obs}, τ_D the lateral diffusion through V_{obs} and S the ratio of axial to lateral dimension of V_{obs}. From this, the diffusion coefficient D and the hydrodynamic radius R_H can be calculated:

$$D = \frac{w_{xy}}{4\tau_D} \qquad (3)$$

with w_{xy} the lateral radius of the ellipsoidal V_{obs}.[165] R_H is calculated from the Stokes Einstein equation:

$$D = \frac{k_B T}{6\pi\eta R_H} \qquad (4)$$

with k_B the Boltzmann constant, T the temperature and η the viscosity of the solvent. Here, samples were investigated regarding their diffusion time τ, D and R_H. The results are summarised in Table 6. Should the sample contain FITC-dextran within the nanocarrier, the fluorophore should show a significantly slower diffusion time compared to free FITC-dextran, given that the nanocarrier is smaller than V_{obs} and single diffusion events can still be detected. FITC-dextran was measured as a reference. Unexpectedly, it showed two different species – one diffusing at 23 µs and one at 203 µs. It is likely that the smaller compound is free FITC, showing that FITC-dextran decomposes over time or that the dye was not sufficiently purified. Sample 1 and 2 showed two different fluorescent species as well with diffusion times almost identical to FITC-dextran. D and R_H were calculated from the diffusion time of FITC-dextran (ca. 200 µs). From FCS measurements, it is clear that – while optically stable – no sample contained a stable double emulsion. Leakage of FITC-dextran in the outer water phase occurred in all cases.

3.1.2.3. Conclusion

A double emulsion/solvent evaporation protocol was found to be an unsuitable method to produce PFS nanocontainers with a hydrophilic core. An optically stable double emulsion was obtained using sodium chloride as an osmotic agent and oleic acid and SDS as surfactants. DLS measurements revealed two different species, likely solid particles and hollow containers. FCS measurements showed that samples did not retain the fluorophore FITC-dextran in their inner water core. Further investigation is needed to assess at which

step leakage occurs. Intuitively, the initial addition of the primary emulsion to the outer water phase or the evaporation of DCM seems to be the most critical points in time. However, it should be noted that most samples produced by this protocol precipitated soon after addition of the primary emulsion and could not even be characterised further, elucidating the intrinsic fragility of this protocol. Further investigations into the flaws of this protocol therefore seem less promising than an entirely different strategy. An inverse miniemulsion approach was dismissed due to insufficient solubility of PFS in hydrophilic solvents. Yet several techniques remain to be tested, e.g. membrane emulsification. This method uses a preformed primary emulsion which is pushed through a membrane, thereby forming the double emulsion.[166] Shirasu Porous Glass (SPG) membranes are widely used for this technique due to their narrow size distribution.[167] Another promising candidate is a mixromixer setup.[168]

3.2. Poly(butadiene)-*block*-poly(ethylene oxide)-based Materials[3]

PB-*b*-PEO block copolymers of different molecular weights were synthesised via anionic polymerisation and functionalised at the hydroxyl end group with either an alkyne, acrylate or succinic acid end group. The self-assembly into polymersomes (100-200 nm diameter) was shown for all molecular weights and functionalities using dynamic and static light scattering measurements (DLS/SLS). cDICE, a technique to produce lipid GUVs was found to be unsuitable to produce polymersomes in the µm-range. However, large polymersomes were successfully produced on a microfluidic platform. Large polymersomes with acrylate and alkyne functionalities were prepared and labelled simultaneously with specific dyes, proving the orthogonal nature of the acrylate and alkyne group. Acrylate-containing vesicles were functionalised with biotin and their interactions with NeutrAvidin-coated surfaces was investigated using the micropipette force sensor technique.

3.2.1. Motivation

Synthetic biology has recently emerged as a new field of research for understanding natural systems from a fundamental point of view. The "bottom-up" approach aims to create an artificial organism, not from modifying a living cell, but from assembling synthetic components into a larger system. These systems, though still far from resembling a living organism, can be used as a simplified model for living cells. One key challenge lies in the fabrication of compartments, such as vesicles, that can be viewed as model membranes. Polymeric vesicles, or polymersomes, benefit from the vast variety of polymer synthesis. Their properties, such as membrane thickness, composition and fluidity can be tuned by changing the polymeric building block, e.g. in regard to monomer selection, molecular

---

[3] A publication based on this chapter is in preparation.

weight, functionality and crystallinity. In this chapter we establish a tool-kit for functional polymersomes based on a well-known polymer system for vesicular self-assembly – PB-*b*-PEO. Different functionalities, i.e. alkyne, acrylate and succinic acid, are introduced and addressed, resulting in a modularly composable system for functional vesicles. These block copolymers are brought to self-assembly through different techniques, i.e. solvent displacement, continuous droplet interface crossing encapsulation (cDICE) and microfluidics to yield polymersomes of different sizes.

3.2.2. PB-*b*-PEO Synthesis

PB-*b*-PEO block copolymers were accessible by anionic polymerisation following the reaction scheme shown in Scheme 6. Cumylpotassium was used as an initiator. Because both the anion polymerisation of 1,3-butadiene and ethylene oxide are compatible with potassium a counter ion, this excludes the necessity of purification between the two monomers, as would be the case if the polymerisation was initiated with *sec*-butyllithium. Polymerisation in THF resulted mostly in 1,2-addition (84% 1,2-addition, 16% 1,4-addition). Before addition of the second monomer, ethylene oxide, an aliquot of the PB precursor was characterised using SEC. The polymerisation was terminated using degassed methanol, resulting in a hydroxyl end group at the PB-*b*-PEO polymer.
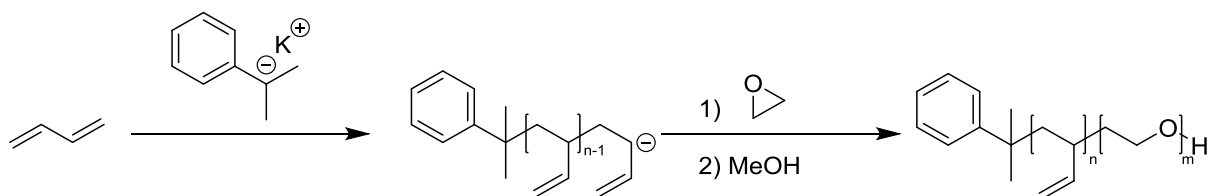
Scheme 6. Polymerisation procedure for PB-*b*-PEO block copolymers. For clarity, the 1,4-addition of 1,3-butadiene is not shown.

Three different block copolymers, ranging from 7 600 to 17 200 g/mol, were synthesised and characterised by NMR and SEC. An exemplary ^{1}H NMR spectrum is shown in Figure 31. The resonances of the aromatic initiator at 7.3-7.0 ppm are superimposed by the solvent $CDCl_3$. The resonances of the PB block are visible at 5.7-4.6 ppm (double bond) and 2.3-0.8 ppm (aliphatic backbone and methyl groups of the initiator). The PEO block appears as a singlet at 3.6 ppm.
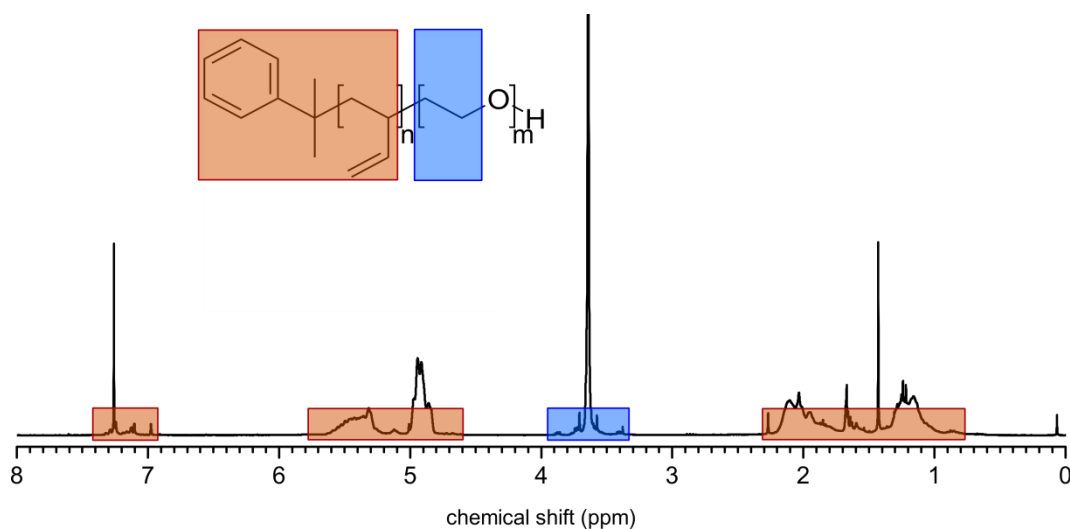
Figure 31. ^{1}H NMR (300 MHz, 298 K) spectrum of PB$_{85}$-*b*-PEO$_{68}$ in CDCl$_3$.

To prove that block copolymers, rather than two separate homopolymers, were formed, ^{1}H DOSY NMR spectra were recorded of all three PB-*b*-PEO block copolymers (Figure 32). All three polymers exhibit only one diffusion coefficient, which coincides well with the signals of the PB and the PEO backbone, proving block copolymer formation.
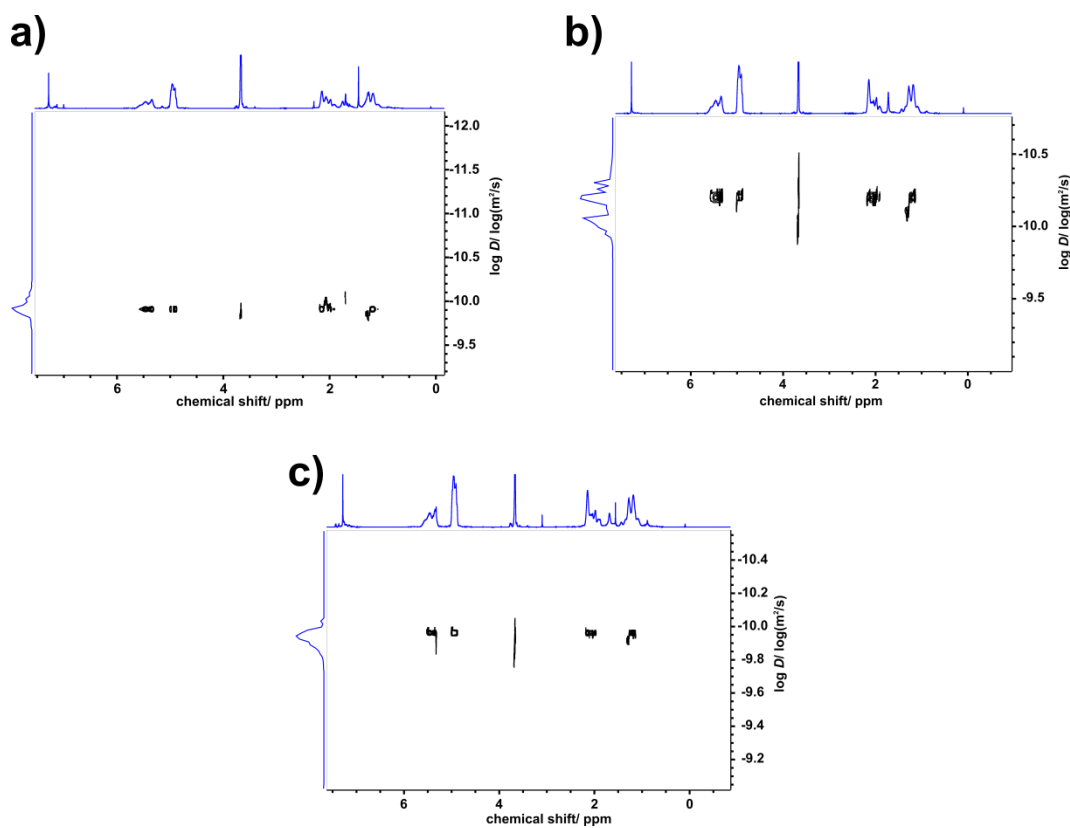
Figure 32. ^{1}H DOSY NMR (700 MHz, 298 K) spectrum of PB$_{85}$-*b*-PEO$_{68}$ (a), PB$_{237}$-*b*-PEO$_{101}$ (b) and PB$_{127}$-*b*-PEO$_{40}$ (c) in CDCl$_3$.

The characterisation results of all polymers are summarised in Table 7. The degree of polymerisation of the PB block DP_{PB} was determined by SEC from the precursor. DP_{PEO} was calculated from the ^{1}H NMR spectroscopy. With a polydispersity index $Đ$ below 1.24, all polymers show a narrow size distribution. The hydrophilic fraction $f_{hydrophilic}$ was calculated using the following equation:

$$f_{hydrophilic} = \frac{M_{EO} * DP_{PEO}}{(M_{EO} * DP_{PEO}) + (M_B * DP_{PB})} \tag{5}$$

$f_{hydrophilic}$ is an important marker for the self-assembly behaviour, albeit an empirical one. For a given polymer system, only a certain range of $f_{hydrophilic}$ will form polymersomes. While the exact values depend on the polymer, a certain degree of generalisation is possible. According to Discher and Eisenberg, polymers with $f_{hydrophilic}$ between 25 and 45% are likely to form polymersomes. Below 25%, inverted microstructures are predominant. Above 45%, the prevalent structures are micelles, while cylindrical micelles exist at a lower $f_{hydrophilic}$ than spherical micelles.[40] As evident from Table 7, all PB-*b*-PEO block copolymers are within (or close in case of PB$_{127}$-*b*-PEO$_{40}$) to the range in which one would theoretically expect polymersomes to form.

**Table 7. Characterisation data for PB-*b*-PEO block copolymers.**

Sample	M_n/ g/mol[a, b]	DP_{PB}[a]	DP_{PEO}[b]	$Đ$	$f_{hydrophilic}$
PB$_{85}$-*b*-PEO$_{68}$	7 600	85	68	1.24	0.40
PB$_{237}$-*b*-PEO$_{101}$	17 200	237	101	1.16	0.26
PB$_{127}$-*b*-PEO$_{40}$	8 600	127	40	1.23	0.20

[a] obtained from SEC

[b] obtained from NMR

3.2.3. PB-*b*-PEO Functionalisation

Vesicles from PB-*b*-PEO block copolymers in water would be covered with the hydroxyl end group on the in- and the outside. Consequently, by modifying the hydroxyl end group, one can easily obtain vesicles with different functionalities on their surface.

The first functionality to be introduced was an activated alkyne group, which allows for facile further modifications using the click reaction between azides and alkynes. The reaction is shown in Scheme 7. In a Steglich esterification, the PB-*b*-PEO is brought to reaction with propiolic acid, using DCC and DMAP as catalysts. It should be noted that a different approach was tested first – an esterification reaction under acidic conditions using sulfuric

acid. While the esterification worked, the reaction conditions proved too harsh for the double bond, a decrease of its signal was observed in the ^{1}H NMR spectrum. Presumably electrophilic additions took place at the double bond.
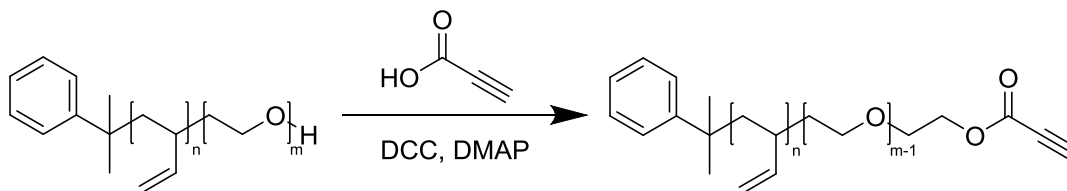
Scheme 7. Reaction scheme for the alkyne functionalisation.

Figure 33 shows the ^{1}H NMR spectra of the polymer before and after the reaction, as well as the other functionalisations, which shall be addressed shortly. The resonances of the polymer backbone remain unchanged and two additional resonances can be identified. At 4.3 ppm the methylene group adjacent to the ester bond appears as a triplet. At 2.9 ppm the single proton of the alkyne forms a singlet. The degree of functionalisation (see Table 8) was determined from the deviation of the methylene group's integral at 4.3 ppm from the maximum value of 2 protons at 100% functionalisation. The degree of functionalisation ranged from 28 to 70%.

The second functionality introduced was an acrylate. While this group does not undergo reactions quite as easily as an alkyne, the enone still enables mild reaction like a Michael addition, using nucleophiles as a reaction partner, such as amines and thiols. PB-*b*-PEO was brought to reaction with acryloyl chloride using triethylamine (NEt$_3$) as a basic catalyst as illustrated in Scheme 8.
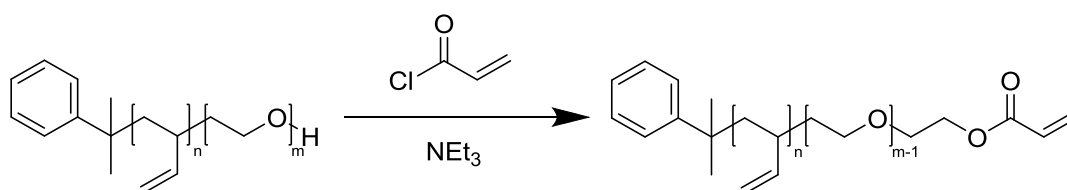
Scheme 8. Reaction scheme for the acrylate functionalisation.

Again, the resonances of the polymer backbone remain unchanged in the ^{1}H NMR spectrum (see Figure 33). The methylene group adjacent to the end group can be identified as a triplet at 4.3 ppm, while the resonances of the enone's double bond appear in the range of 6.5 to 5.8 ppm. The degree of functionalisation was determined from the methylene group (see Table 8).

The third functionality introduced was a succinic acid group. In this case it was not to be used

for undergoing further reactions, but rather to introduce a pH-responsive group. PB-*b*-PEO was esterified with succinic anhydride using DMAP as a basic catalyst (see Scheme 9). The degree of functionalisation ranged from 58 to 100%.
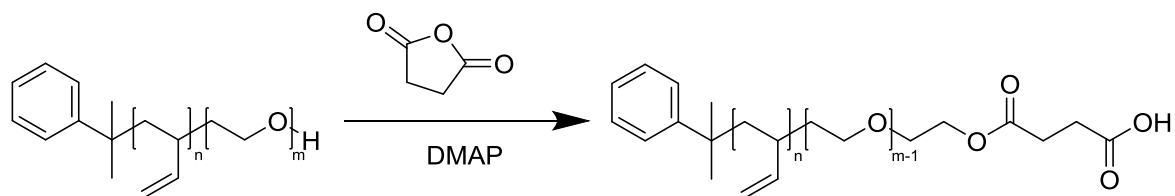
Scheme 9. Reaction scheme for the succinic acid functionalisation.

Again, the resonances of the polymer backbone remain unchanged in the ^{1}H NMR spectrum (see Figure 33). The methylene group adjacent to the end group can be identified as a triplet at 4.3 ppm, the methylene groups of succinic acid are visible as a triplet at 2.7 ppm. The degree of functionalisation was determined from the methylene group adjacent to the end group (see Table 8). The degree of functionalisation ranged from 74 to 79%.

Table 8. Summary of PB-*b*-PEO functionalities.

	Functionality	Degree of functionalisation
PB$_{85}$-*b*-PEO$_{68}$	alkyne	70%
	acrylate	100%
	succinic acid	79%
PB$_{237}$-*b*-PEO$_{101}$	alkyne	28%
	acrylate	62%
	succinic acid	74%
PB$_{127}$-*b*-PEO$_{40}$	alkyne	35%
	acrylate	58%
	succinic acid	75%
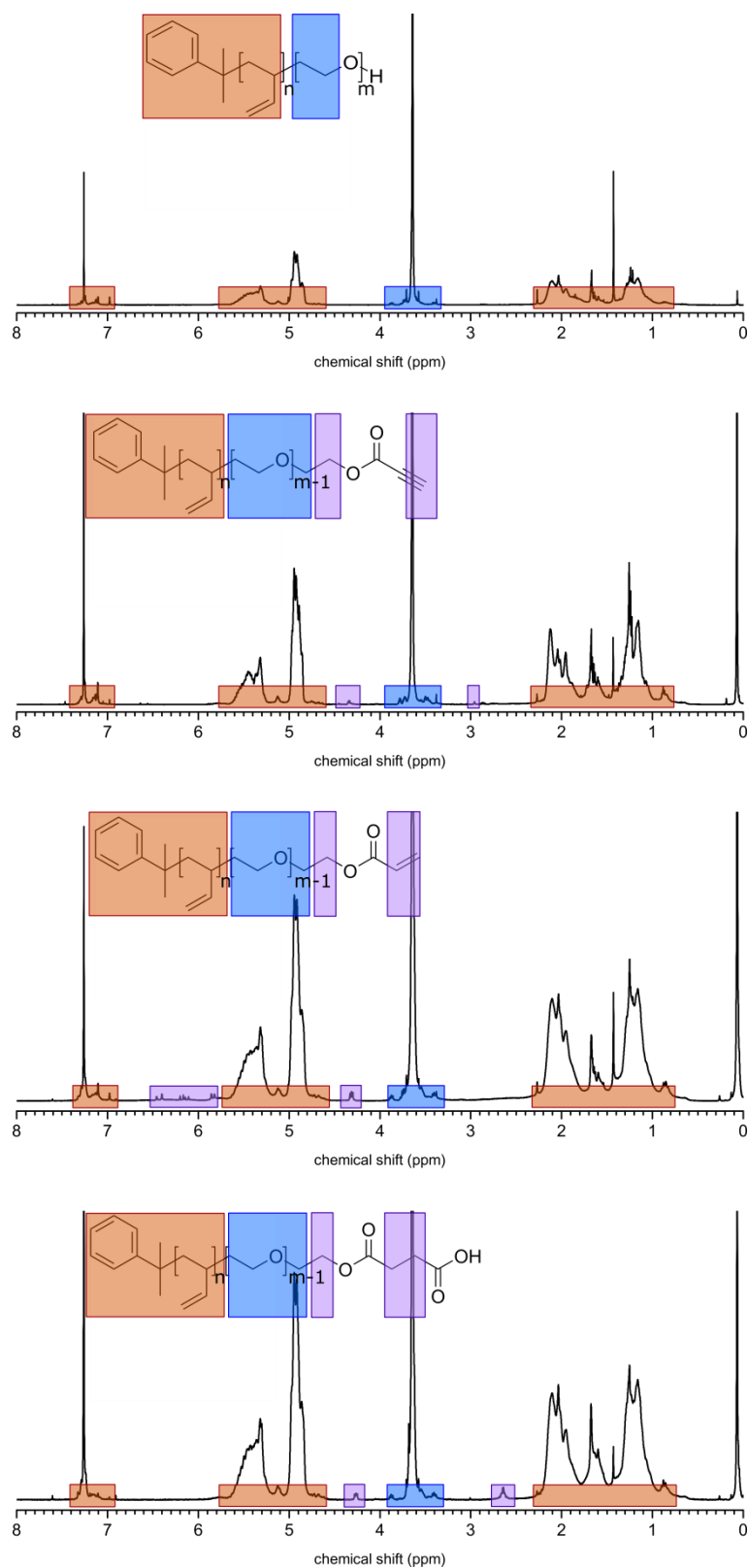
Figure 33. ^{1}H NMR (300 MHz, 298 K) spectrum of PB$_{85}$-*b*-PEO$_{68}$ (first), the alkyne functionalised PB$_{85}$-*b*-PEO$_{68}$ (second), the acrylate functionalised PB$_{85}$-*b*-PEO$_{68}$ (third) and the succinic acid functionalised PB$_{85}$-*b*-PEO$_{68}$ (last) in CDCl$_3$.

3.2.4. Giant Unilamellar Vesicles via cDICE

Continuous droplet interface crossing encapsulation (cDICE) is a technique for the production of giant unilamellar vesicles developed by Massiera et al.[169] Originally used for lipid GUVs, herein, we test the methods capability to form polymeric GUVs. A schematic representation of the setup used is shown in Figure 34 (for an experimental setup see Figure 66). GUV formation is achieved by water droplets travelling through different phases due to centrifugal force. A chamber, rotating at a speed ω is filled with the dispersing aqueous solution (DAS), the lipid in oil solution (LOS) and decane. Due to the difference in densities and the rotation of the chamber, perpendicular layers are formed. A capillary containing the encapsulated aqueous solution (EAS) is inserted into the decane phase. The decane serves as a barrier, if the capillary were to be inserted directly into the LOS, the lipid could easily clog the opening and prevent flow of the EAS. By applying a slight pressure to the capillary, aqueous droplets are formed in the decane phase. They are continuously sheared of by the rotation, this and their higher density causes them to travel through all layers until they have reached the DAS. As the EAS droplets enter the LOS layer, they are coated with the amphiphilic lipid (coating). When the coated droplet passes the second interface into the DAS layer, a second coat of lipid is added (zipping), forming a lipid bilayer. The size of the GUVs depends on the orifice of the capillary.
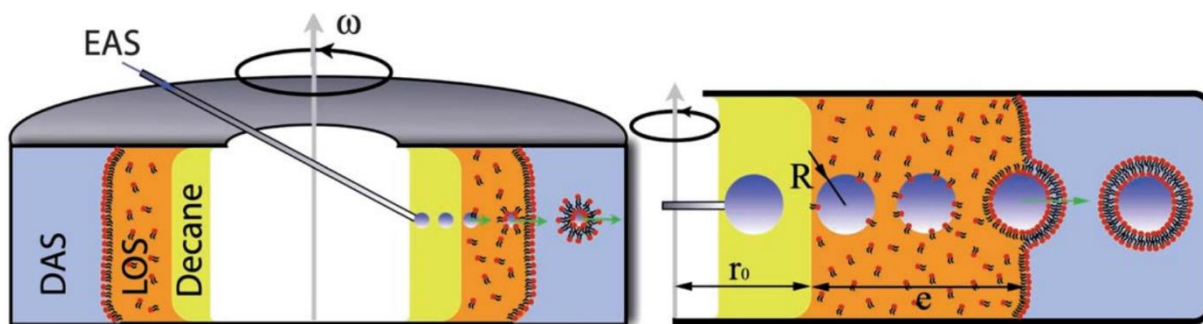
Figure 34. Schematic view of the cDICE setup. Reproduced with permission from [169] with permission of The Royal Society of Chemistry.

This chapter aims to test whether this technique can also be employed to form GUVs out of block copolymers, more specifically the PB-*b*-PEO block copolymers introduced in section 3.2.2. Therefore, instead of a lipid in oil (LOS) solution, a polymer in oil (POS) solution is used. Massiera et al. used mineral oil to dissolve the lipids.[169] However, PB-*b*-PEO block copolymers proved to be insoluble in that. Therefore, the first task was to find an appropriate solvent for the POS. The requirements are the ability to dissolve PB-*b*-PEO, a density between that of water and decane and immiscibility with both water and decane over the

experimental timeframe (about 30 min). The tested solvents and the results are summarised in Table 9. As mentioned before, mineral oil does not dissolve PB-*b*-PEO. While toluene, benzene, and ethylbenzene are good solvents for the block copolymer, neither of them showed sufficient stability during the rotation. The phases collapsed before 30 min had passed. Therefore, a mixture of ethylbenzene and mineral oil was tested. A 14:1 mixture showed no enhanced stability compared to pure ethylbenzene. A 2:1 mixture had a sufficiently high ethylbenzene content to dissolve the block copolymer (though its cloudiness hints at aggregates invisible to the naked eye) and enough mineral oil to push the stability beyond the 30 min mark.

Table 9. Tested polymer in oil compositions.

POS	Dissolves PB-*b*-PEO	Stable (15 min)	Stable (30 min)
Mineral oil	no	yes	yes
Toluene	yes	no	no
Benzene	yes	no	no
Ethylbenzene	yes	yes	no
Ethylbenzene/mineral oil (14:1)	n.a.	yes	no
Ethylbenzene/mineral oil (2:1)	yes*	yes	yes

*cloudy solution, hints at aggregates

GUV production was started using a 2:1 mixture of ethylbenzene and mineral oil as a POS. Several experimental parameters can be tuned to result in successful production of GUVs – the rotation speed, the pressure at the capillary and the volumes of decane, POS and DAS. The experimental settings of run 1-6 are summarised in section 4.2.4, Table 17. After a production run, an aliquot of the DAS was collected and stained using CellMask Deep Red, a hydrophobic dye, which should insert into the hydrophobic part of the GUV membrane. Aliquots of all runs were imaged using CLSM. Only run 2 showed visible structures, in the transmission channel as well as the fluorescent channel (Figure 35). However, the structures observed are evenly fluorescent. Therefore, they are oil droplets, not GUVs, whose aqueous core should not fluoresce. Apparently, the conditions of run 2 led to a microscopically instable phase system, resulting in small POS droplets in the DAS. It is unknown whether those are pure POS droplets or whether the EAS droplets mix with POS during their flight through the layer. This miscibility problem could be solved by addition of salt to the DAS, thereby lowering the miscibility of the two phases.
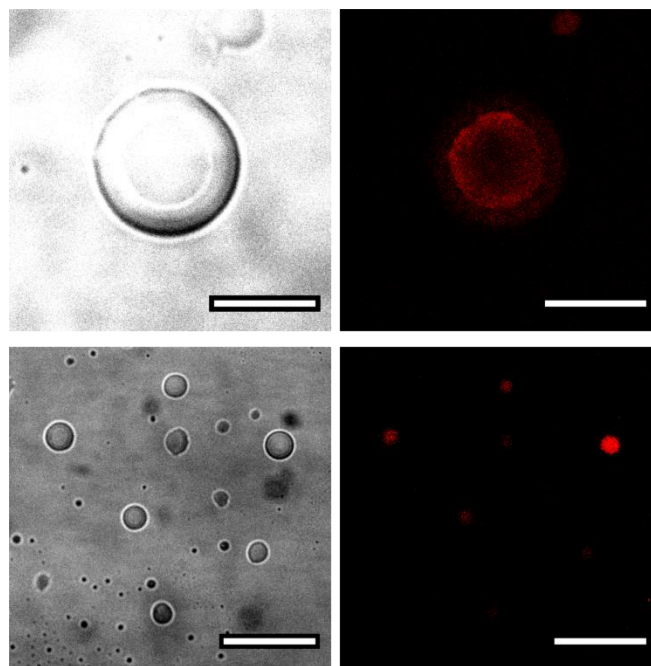
Figure 35. CLSM images of run 2. Scales are 10 μm (top) and 40 μm (bottom). The transmission channel is on the right hand side, the fluorescence channel on the left.

Under the conditions tested, no polymeric GUVs could be produced using the cDICE technique. The reason for this lies in the mechanism of cDICE. For a successful GUV production, the droplet flight time through the oil phase has to be longer than the adsorption time of the lipid/polymer. Since lipids diffuse much faster than a polymer chain of thousands of grams per mole, this technique is better suited for lipid systems.

3.2.5. Polymersomes via Solvent Displacement

In this chapter the self-assembly behaviour of PB-*b*-PEO block copolymers is tested using the solvent displacement technique. For this, a solution of the polymer in a good solvent is prepared. Here, THF is used (though chloroform is possible as well). This is dialysed against a large surplus of water in a dialysis tube which is too small to allow the block copolymer to pass. As the water continually mixes with the good solvent, at some point the block copolymer cannot stay in solution. It self-assembles with the hydrophobic PB blocks sticking together. Depending on the $f_{hydrophilic}$, different structures are the most stable (see section 2.2.2). With the PB-*b*-PEO polymers introduced in section 3.2.2 we aimed for the formation of polymersomes.

3.2.5.1.   Self-assembly Behaviour

After the solvent displacement procedure, the obtained solutions were opaque, indicating that self-assembly took place. This technique usually yields small, disperse structures, which

are hard to characterise further. Therefore, samples were extruded using a LiposoFast setup, i.e. they were pushed repeatedly through polycarbonate membranes of different sizes, starting form 1000 nm pore size down to 200 nm. This process reduces the dispersity and breaks down multilamellar structures. Samples were then characterised by dynamic light scattering for their hydrodynamic radius R_H and by static light scattering for their radius of gyration R_g. The results are summarised in Table 10. From R_H and R_g the so called ρ-ratio can be determined:

$$\rho = \frac{\sqrt{\langle R_g \rangle^2}}{\left(\langle \frac{1}{R_H} \rangle \right)^{-1}} \tag{6}$$

This empirical value provides information on the morphology of the sample by comparing the experimentally obtained ρ-ratio to theoretically calculated ones. A ρ-ratio of 1 is common for a hollow sphere with an infinitesimally thin membrane, i.e. a polymersome. A decrease in the ρ-ratio translates to a hollow sphere with an increasingly thicker membrane. At a ρ-ratio of 0.775 a solid sphere is reached.[170] All samples show a R_H in the range or below 100 nm, as is expected because all samples were extruded through a 200 nm pore size membrane. Since smaller structures can easily pass through and are not affected by the extrusion process, pore sizes smaller than 200 nm would be needed to reduce the dispersity even further. Beyond that it is treacherous to discuss the size differences between the different samples, as the size depends partly on the pressure and its continuity during extrusion. Since this was a manual process, there is no guarantee that it was comparable from sample to sample, as would be the case for an automated system. But it can be noted that PB$_{85}$-b-PEO$_{68}$, the smallest block copolymer, also shows a tendency to form smaller structures (R_H between 43.7 and 51.7 nm) than the two larger polymers (R_H between 64.5 and 112.0 nm). The ρ-ratio of all samples is close to the ideal value of 1.00. A slight deviation is to be expected, due to the margin of error from the light scattering data and the thickness of the polymer membrane. The end group functionalisation does not seem to have an impact on the self-assembly.

Table 10. Light scattering results for PB-*b*-PEO block copolymers.

Polymer	End group	R_g/ nm	R_H/ nm	ρ-ratio
PB$_{85}$-*b*-PEO$_{68}$	hydroxyl	48.5	51.7	0.94
	alkyne	39.3	43.7	0.90
	acrylate	43.5	49.9	0.87
	succinic acid	51.2	50.8	1.01
PB$_{237}$-*b*-PEO$_{101}$	hydroxyl	71.0	75.6	0.94
	alkyne	116.7	112.0	1.04
	acrylate	64.9	78.9	0.82
	succinic acid	88.5	95.9	0.92
PB$_{127}$-*b*-PEO$_{40}$	hydroxyl	66.2	64.5	1.03
	alkyne	116.7	91.1	1.28
	acrylate	120.8	109.2	1.10
	succinic acid	117.7	104.5	1.13

3.2.5.2.   Dye Functionalisation

The functional polymersomes prepared from PB$_{237}$-*b*-PEO$_{101}$ in the previous section 3.2.5.1, were further modified with fluorescent dyes. The alkyne end group was reacted with a dye bearing an azide group (Chromeo azide), while the acrylate underwent a Michael addition with an amine-functionalised dye (BODIPY amine) (Figure 36).
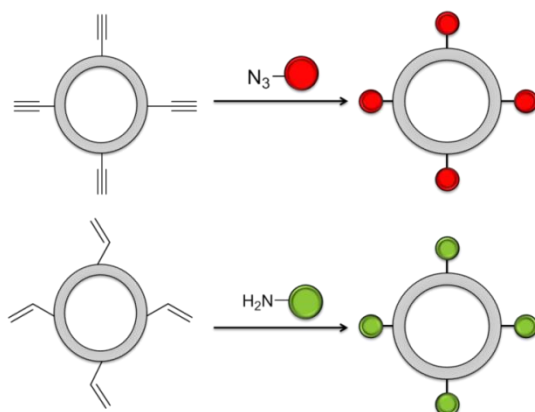
Figure 36. Schematic representation of vesicle functionalisation – alkyne functionalisation (top) and acrylate functionalisation (bottom).

Both reactions proceeded at room temperature. The Michael addition required the addition of a catalytic base, DMAP. Samples were characterised using FCS in cooperation with Jennifer Schultze (for an introduction to the technique see section 3.1.2.2). The results are summarised in Figure 37 and Table 11. Figure 37 shows the autocorrelation curves of the two dyes (black) and the dye-functionalised alkyne and acrylate vesicles (red). The vesicular samples show a higher diffusion time compared to the free dye. This is caused by the covalent linkage of the dye to the vesicle. The dye then diffuses with the vesicle and consequently takes longer to leave the observation volume.
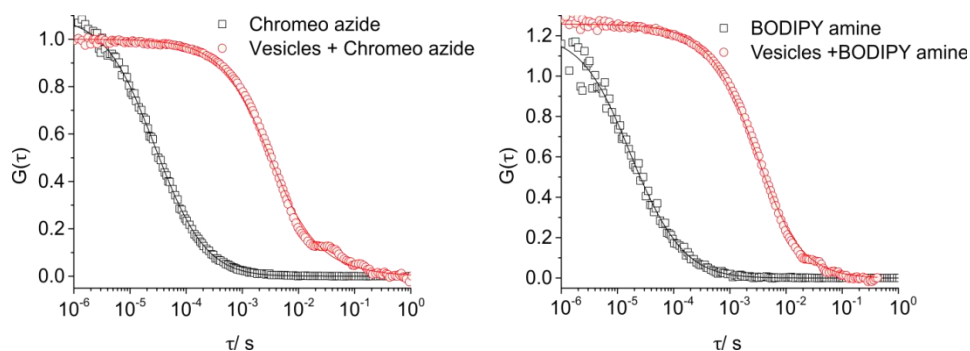
Figure 37. FCS autocorrelation curves of free chromeo azide (left, black circles) and the dye-functionalised vesicles (left, red circles) and free BODIPY amine (right, black circles) and the dye-functionalised vesicles (right, red circles).

Table 11 summarises the numerical data. The dyes show low diffusion times of 32 or 20 µs which is typical for low molecular weight molecules. R_H was calculated using the Stokes Einstein equation. The vesicular samples show diffusion times of about 2800 µs and corresponding R_H of circa 60 nm, which is in good accordance with the light scattering data

presented in section 3.2.5.1. Differences in size can be attributed to variations during the extrusion process.

Table 11. FCS data for functionalised PB$_{237}$-*b*-PEO$_{101}$ vesicles and the fluorescent dyes.

Sample	τ/ µs	R_H/ nm
Chromeo azide	32	0.6
Alkyne Vesicles + Chromeo azide	2790	63
BODIPY amine	20	0.5
Acrylate Vesicles + BODIPY amine	2850	64

3.2.6. Polymersomes via Microfluidics

The remaining chapters of section 3.2 deal with polymersomes produced using a microfluidic setup. Microfluidic offers a suitable platform for the production of polymersomes with diameters in the µm-range. Previous attempts using the cDICE technique failed in that regard (see 3.2.4). Large polymersomes are desirable for various reasons. Not only does the increased size allow for easier imaging, it also enables the embedding of a complex protein machinery, whose many parts would statistically not fit in a vesicle of only 100 nm diameter, resulting in vesicles that lack necessary components. Such a protein machinery might comprise several enzymes catalysing a cascade reaction or a translational machinery for protein production. One goal of this work was to supply a suitable container for such a system, therefore PB-*b*-PEO block copolymers were tested using a microfluidic setup. The functionalities introduced in section 3.2.3 may be used to produce functional polymersomes in a microfluidic environment. The microfluidic production of polymersomes was carried out by Dr. Julien Petit at the Max Planck Institute for Dynamics and Self-organisation. Further reactions and imaging were carried out at the Max Planck Institute for Polymer Research. It has been recently demonstrated that microfluidics offers a reliable platform for the on-demand high-throughput of polymersomes.[171] The structures are monodisperse (at least directly after production, diffusion processes later on increase the dispersity) and the technique offers a high encapsulation efficiency.[172] One drawback is the necessity to add compounds, such as a surfactant and others, which will be explained in detail later on. A schematic representation of the PDMS microfluidic chip used for polymersome production is shown in Figure 38. The setup consists of two consecutive cross-junctions in a flow-focusing configuration. The inner fluid (IF) is sheared at the first junction by the middle fluid (MF), generating a water-in-oil emulsion. At the second junction, those droplets are in turn sheared

by the outer fluid (OF), thereby forming a water-in-oil-in-water double emulsion. The double emulsion template serves as a precursor for the polymersomes.
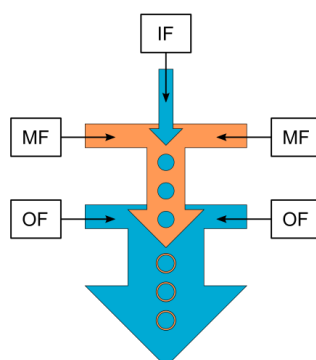
Figure 38. Schematic Microfluidic Setup. IF is the inner fluid (aqueous), MF the middle fluid (oil) and OF the outer fluid (aqueous).

The IF is an aqueous solution of F108, a non-ionic surfactant, and sucrose. The MF is a solution of the respective polymer in oleic acid. The OF is again an aqueous solution of F108, glycerol, poly(diallyldimethylammonium chloride) (PDADMAC), sucrose and ethanol. Glycerol serves to increase the viscosity of the OF, increasing the shear stress at the cross-junction, thereby improving the droplet formation. PDADMAC, a polyelectrolyte, is used as a channel treatment agent, enhancing the hydrophilicity of the PDMS channel, which is hydrophobic by nature. Furthermore, sucrose was added both in the IF and OF in order to balance the osmolarities and to prevent bursting of vesicles due to an osmotic shock. The purpose of ethanol is the extraction of the oleic acid from the double emulsion template. As the oleic acid is extracted, the volume of the oil phase of the double emulsion decreases. This induces the migration of the block copolymers, originally dissolved in the oil phase, towards the water-oil interface. At this point, the block copolymers will self-assemble, with the hydrophilic PEO reaching into the inner and outer aqueous solution, while the hydrophobic PB blocks remain at the centre of the membrane. As this extraction process is completed, the membrane becomes thinner and thinner, resulting in the formation of a polymersome (Figure 39).
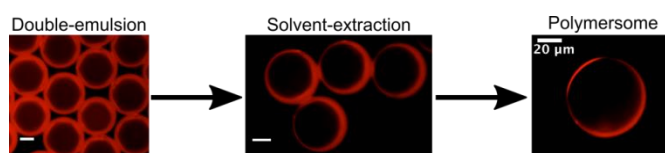
Figure 39. Illustration of the extraction process from the double emulsion.

3.2.6.1.   *Orthogonal Labeling*

All microfluidics experiments were performed using PB_{237}-*b*-PEO_{10}. In a normal microfluidics experiment, Nile Red is added to the MF for subsequent imaging of the polymersomes. Here that step was omitted. Instead, the functional PB-*b*-PEO block copolymers introduced in section 3.2.3 were mixed into the oil phase to generate functional polymersomes. These are brought to reaction with the specific dyes from section 3.2.5.2, i.e. chromeo azide for the alkyne functionality and BODIPY amine for the acrylate functionality. The results are summarised in Figure 40. The reaction conditions for the dyes were the same as in section 3.2.5.2. The samples were imaged using CLSM. Channels widths were set so that the crosstalk between them remained minimal. For additional verification, spectra were recorded over the relevant wavelengths. As a result, the two dyes could be unmistakably detected separately. Alkyne-functionalised polymersomes (first row in Figure 40) were stained using chromeo azide dye. The polymersomes are visible in red in the respective channel. The BODIPY amine channel remains dark, proving there is no crosstalk between the channels. The spectrum shows the maximum emission at 570 nm. Acrylate-functionalised polymersomes (middle row in Figure 40) were labelled using BODIPY amine dye. In this case, the polymersomes can be imaged in green in the BODIPY amine channel. The chromeo azide channel remains dark, there is no spill over from the green channel. The spectrum shows the maximum emission at 520 nm. In a last step, polymersomes bearing both an alkyne and an acrylate functionality were prepared and labelled with both dyes (bottom row in Figure 40). Accordingly, fluorescence can be detected in both channels and the emission spectrum reveals two peaks, one at 520 nm (BODIPY amine) and a second at 570 nm (chromeo azide). This proves that the two functionalities may be addressed separately and simultaneously, thereby establishing an orthogonal labelling system for bifunctional polymersomes.
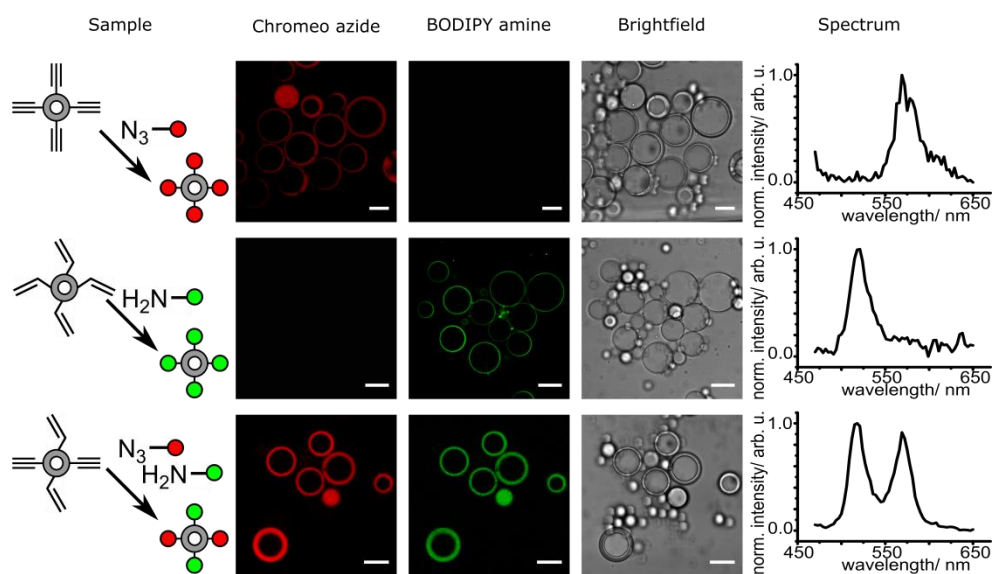
Figure 40. CLSM results for orthogonally labeled polymersomes. Shown are the chromeo azide channel (red), the BODIPY amine channel (green) and the brightfield channel. The scale bars are 30 µm. A spectrum of the fluorescent intensity was taken to identify the dyes.

3.2.6.2. Exchange

Previous chapters established a vesicle system with two orthogonally labelled functional groups – alkyne and acrylate. This system offers the possibility to investigate the diffusion of polymer chains between vesicles. Alkyne-functionalised vesicles, labelled with chromeo azide (red) and acrylate-functionalised vesicles, labelled with BODIPY amine (green) (Figure 41) were mixed to monitor the exchange of polymer chains between the two species of vesicles. Two theoretical outcome scenarios exist and are illustrated in Figure 41. If no diffusion of the polymer chains takes place, the coexistence of red and green vesicles is expected. Should the polymer chains diffuse and exchange between vesicles, or should the vesicles themselves fuse, colocalisation of red and green dye is expected in the form of colocalisation (yellow).
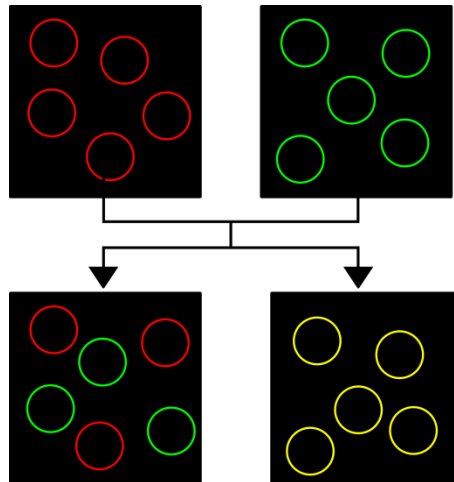
Figure 41. Principle of exchange study. Two separately labeled samples, one with chromeo azide and one with BODIPY amine, are mixed and investigated over time.

The data acquisition process is shown in Figure 42. After mixing, the sample was imaged over several weeks at defined time points in all relevant channels (Figure 42). Spectra were recorded to quantify the amount of chromeo azide and BODIPY amine by integration for several regions of interest (ROIs).
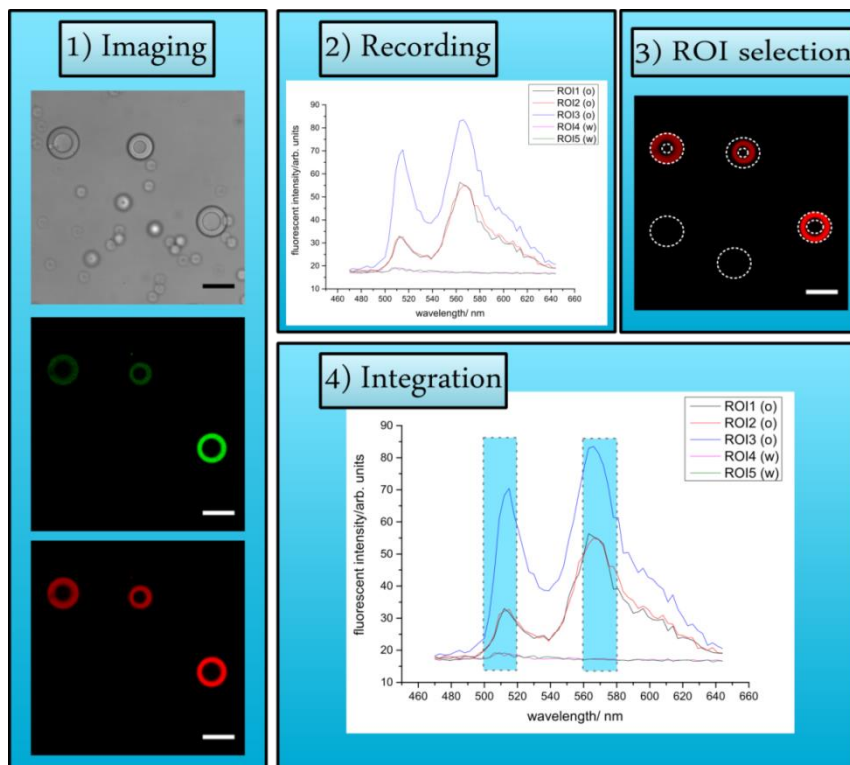
Figure 42. Processing steps for exchange measurements. First, all relevant channels were imaged. Secondly, a spectrum was recorded from 470-644 nm at the position of the image. Thirdly, regions of interest (ROIs) were selected at relevant objects and the background. Lastly, the emission peak of each dye was integrated.

Due to the well-known stability of polymersomes, which is caused in part by the low diffusion of polymer chains, colocalisation of the two dyes was not expected.[35] However, almost all objects imaged exhibited two emission peaks, i.e. both dyes were present. Furthermore, it was evident that the sample contained free BODIPY amine dye. In Figure 42-4, ROI4 and 5, which were recorded in the water phase, exhibit a small emission peak at 520 nm, i.e. the emission of BODIPY amine, the intensity of which differed from image to image. Therefore, there is an additional amount of free BODIPY amine in the hydrophobic polymer phase, which is not equal to the amount in the water, but related to it by the distribution coefficient of BODIPY amine in the two phases. The data was corrected for this using a control experiment, which determined the distribution of BODIPY amine between the water and oil phase in a polymer sample without acrylate functionalities. In order to relate this to the original data, the volume of water to organic phase has to be taken into account, since the concentration depends on the volume available. A correction factor x for the original data war calculated using the following equation:

$$x = \frac{I_{\text{oil, bg}}}{I_{\text{water, bg}}} * \frac{V_{\text{oil, bg}}}{V_{\text{water, bg}}} \tag{7}$$

With $I_{\text{oil, bg}}$ the integral of BODIPY amine in the oil phase, $I_{\text{water, bg}}$ the integral of BODIPY amine in the water phase, $V_{\text{oil, bg}}$ the volume of the oil phase and $V_{\text{water, bg}}$ the volume of the water phase. The index bg denotes properties of the sample measured for background correction. This factor x was used to correct the original data using the following equation:

$$I_{\text{oil, or}} = \frac{x * I_{\text{water, or}} * V_{\text{water, or}}}{V_{\text{oil, or}}} \tag{8}$$

With $I_{\text{oil, or}}$ the integral of BODIPY amine in the oil phase, $I_{\text{water, or}}$ the integral of BODIPY amine in the water phase and $V_{\text{water, or}}$ and $V_{\text{oil, or}}$ the volumes of the water and oil phase. The index or denotes properties of the original sample. This correction could only be carried out for BODIPY amine, because chromeo azide did not show an emission peak in the water. This does not mean that there is no free chromeo azide in the sample, simply that its concentration is too low to be detected.

The uncorrected and corrected data is shown in Figure 43. The relative amount of both dyes is plotted over the investigated time, crosses mark the average of each set of data points.
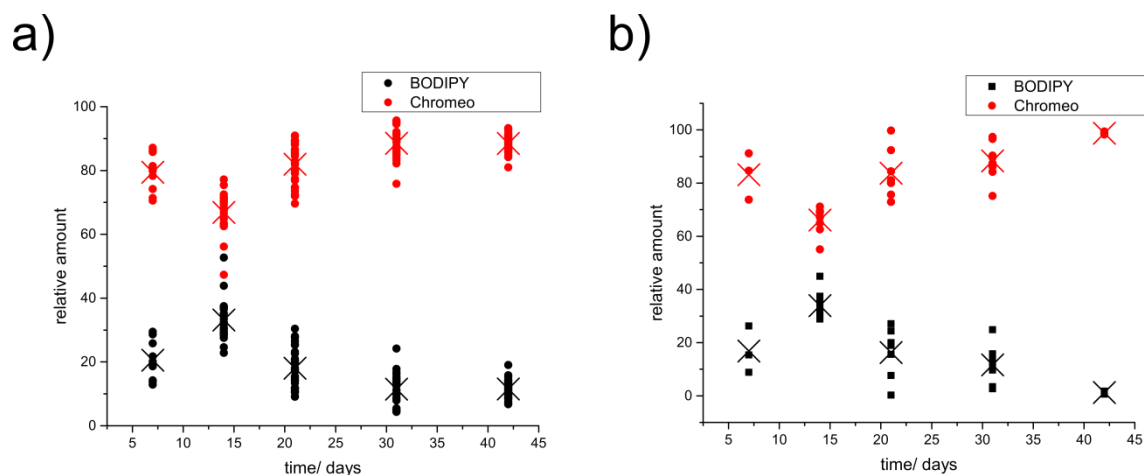
Figure 43. Exchange results of uncorrected (a) and corrected (b) data. The cross denotes the average of each set of data points (n≥3).

The data illustrates the impossibility to identify the original dye of an object. If that were possible, a larger variance of data points would be expected, i.e. data points with a high amount of BODIPY amine which were originally labeled with this and data points with a low amount of BODIPY amine which were originally labeled with chromeo azide and only had BODIPY amine diffuse inside. All objects imaged contained both dyes. Therefore, it can be concluded that an exchange takes place. The question remains, whether it is in exchange of labeled polymer chains or of free dye molecules that were not covalently attached. Though attempts were made to correct the data for free dye, there is no way to prove that this was entirely successful. The colocalisation of both dyes is therefore either caused by residual, freely diffusing dye in the system, by diffusion of labeled polymer chains or by vesicle fusion. The apparent increase of chromeo azide over time in expense of BODIPY amine over time is likely caused by bleaching of the latter, to which it was susceptible.

3.2.6.3. Biotin Functionalisation

In the previous chapters, the orthogonal functionalisation of vesicles was stablished using dyes as a model compound. In this chapter, the acrylate functionality will be addressed using biotin, a biomolecule well-known for its extraordinarily stable complexes with the proteins avidin, streptavidin and NeutrAvidin (dissociation constant, K_d=10^{-14}-10^{-16} M).[173] Therefore, the interaction of biotin-functionalised polymersomes with NeutrAvidin-coated surfaces will be investigated.

An excess of amine-functionalised biotin was reacted with vesicles containing PB-*b*-PEO-acrylate. The ^{1}H NMR spectra of the educt and product are shown in Figure 44. The acrylate's resonances of the starting material appear at 5.8-6.5 ppm and are no longer detectable after the reaction with biotin. In addition, the terminal methylene group, which was

visible at 4.3 ppm before the reaction, is no longer detectable as well. No resonances of biotin can be identified, due to its poor solubility in chloroform, which was used as a solvent. Micellisation occurs to minimise contact between biotin and the solvent, causing the resonances of biotin and the methylene group to be no longer detectable. A spectrum of the aminated biotin is shown in Figure 44 as well, to illustrate that biotin resonances should be identifiable among the signals of the polymer backbone, e.g. at 4.29-4.49 ppm.
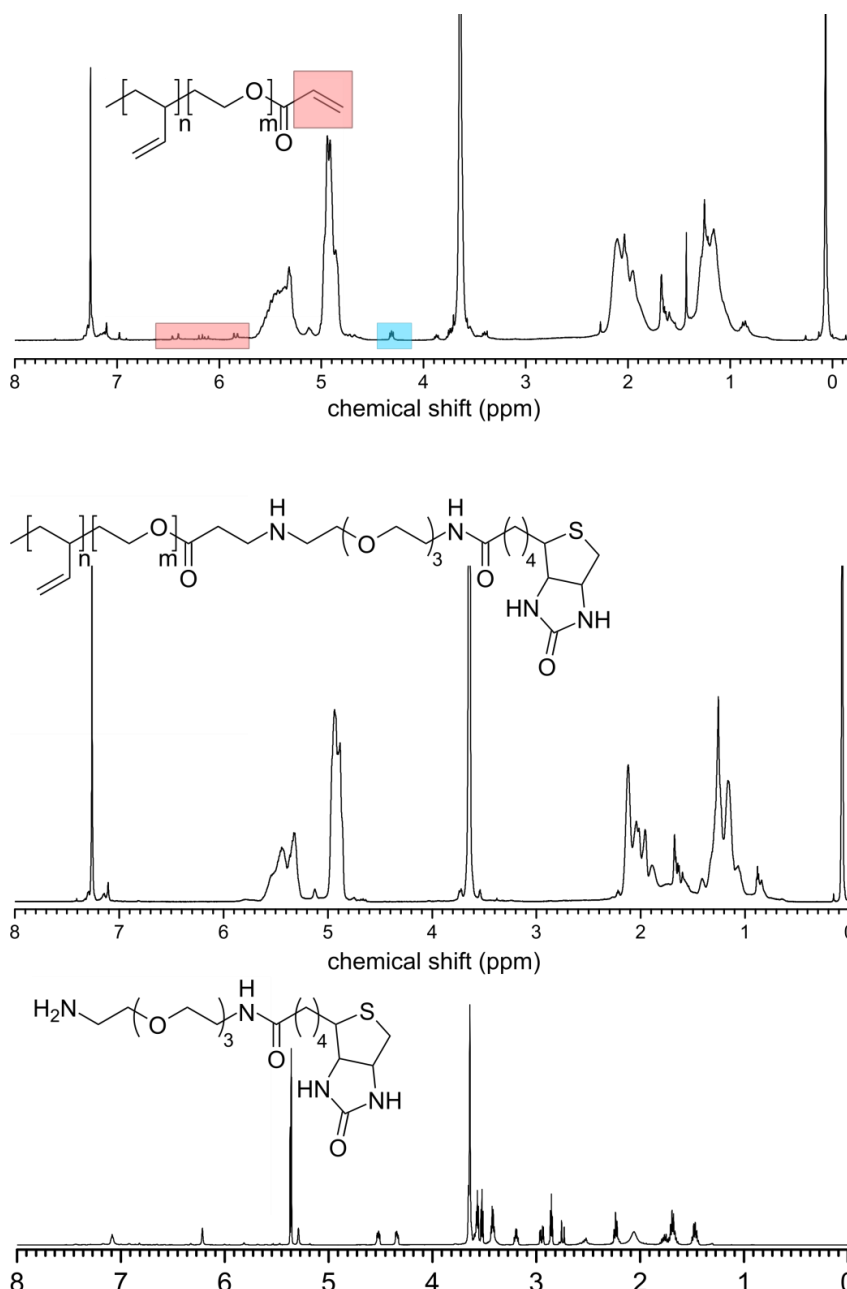
Figure 44. ^{1}H NMR (500 MHz, 298 K) spectra of PB-*b*-PEO-acrylate (top) and biotin-functionalised PB-*b*-PEO (middle) and amine-functionalised biotin (bottom) in CDCl$_3$.

Biotinylated vesicles were further used to study the adhesion with NeutrAvidin-coated surfaces. Using a micropipette force sensor device, we measured the adhesion force between polymersomes and dedicated substrates. Micropipette experiments were carried out by Dr. Julien Petit at the Max Planck Institute for Dynamics and Self-Organisation. This force sensor technique allows studying the membrane properties of single vesicles. A double-L shaped micropipette was used to grab a single polymersome and study its interactions with a defined substrate (Figure 45a). A polystyrene spike near the tip was tracked to measure the deflection of the pipette. Both substrates, uncoated glass and NeutrAvidin-coated glass, were placed side-by-side on the substrate holder, which allowed testing the adhesion of the same vesicle on both substrates. Multiple approach/retract cycles of the substrates on the polymersome were performed. The deflection over time curves are summarised in Figure 45b-e. As the glass is pressed against the vesicle, the pipette is pushed back and the deflection increases. Then, once the glass slide is retracted, the pipette can return to its original position, the deflection decreases to its original value. If there are adhesive interactions between the vesicle and the glass plate, the deflection will drop below its starting value, as the vesicle sticks to the glass, forcing the pipette to follow. Depending on the adhesion strength, at some point the vesicle is forced out of contact with the glass plate and the pipette returns to the original value. This process can be repeated until the vesicle ruptures or escapes. The deflection below the original value is directly linked to the adhesion between vesicle and glass slide. Experiments were carried out for biotinylated and non-biotinylated vesicles on NeutrAvidin-coated glass and uncoated glass respectively. It can be seen from Figure 45b-e, that the strongest adhesive forces are between biotinylated vesicles and NeutrAvidin-coated glass. All other combinations exhibit smaller deflections.
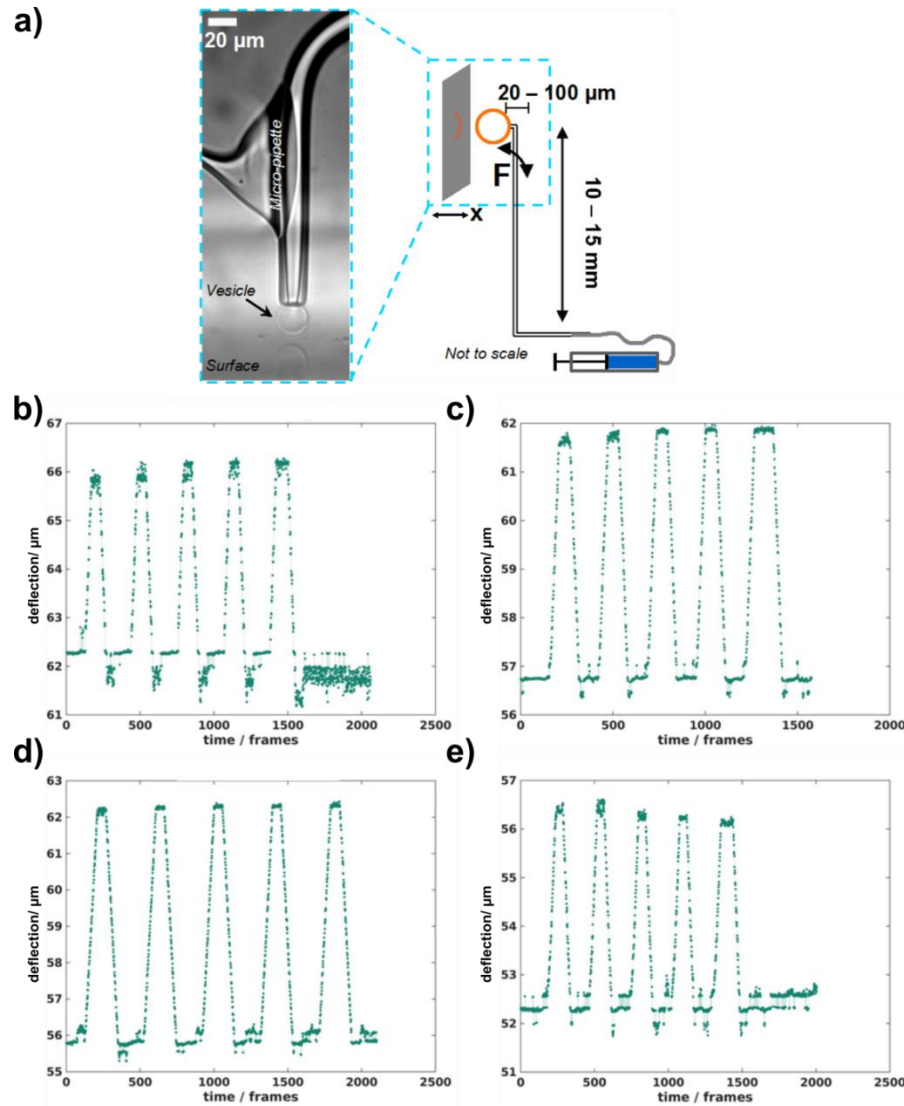
Figure 45. Schematic illustration of the micropipette setup (a). Deflection over time curves for biotin-functionalised vesicles on NeutrAvidin-coated glass (b) and uncoated glass (c). Deflection over time cuves for unfunctionalised vesicles on NeutrAvidin-coated glass (d) and uncoated glass (e).

From this data, force-distance curves were calculated knowing the spring constant of the pipette. The results are shown in Figure 46a. The approach of the glass surface is shown as a dashed line, the retraction as a solid line. Again, it can be seen that biotinylated vesicles on NeutrAvidin-coated glass have the highest adhesion force. The adhesion force of all samples is summarised in Figure 46b.
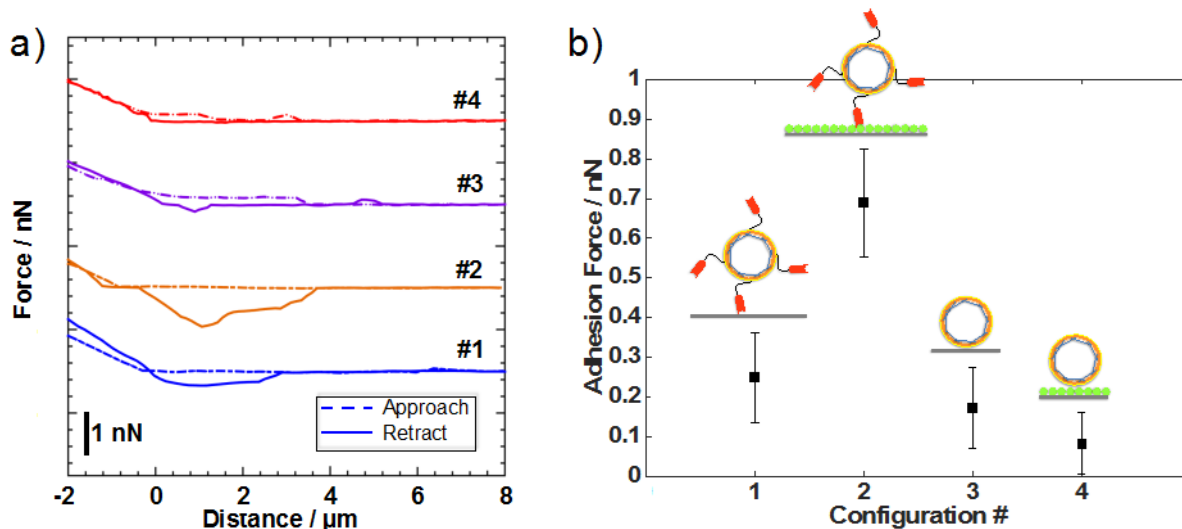
Figure 46. Force-distance curves of biotin-functionalised and non-functionalised vesicles on NeutrAvidin-coated glass and glass (a). Dashed lines are the approach, solid lines the retraction. Mean adhesion force of biotin-functionalised and non-functionalised vesicles on glass and NeutrAvidin-coated glass (b).

The results are summarised in Table 12. Biotinylated vesicles on NeutrAvidin-coated glass had a mean adhesion force of (0.689±0.135) nN, a significant difference to the other configurations, whose mean adhesion force ranged from (0.083±0.077) nN for non-biotinylated polymersomes on NeutrAvidin-coated glass to (0.249±0.114) nN for biotinylated polymersomes on glass. Thus, this difference in the adhesion properties is a clear proof that the polymersomes were successfully functionalised with biotin.

Table 12. Mean adhesion force, standard deviation and number of measurements *N* for micropipette experiments.

	Biotin(+)/ glass	Biotin(+)/ NAv	Biotin(-)/ glass	Biotin(-)/ NAv
Mean adhesion force/ nN	0.249	0.689	0.173	0.083
Std/ nN	0.114	0.135	0.101	0.077
N	21	25	20	29

In summary, vesicles made from PB-*b*-PEO-acrylate were successfully biotinylated, as proven by ^{1}H NMR spectroscopy and micropipette experiments. They showed an increased adhesion to NeutrAvidin-coated glass compared to non-functionalised vesicles.

3.2.7. Conclusion

This chapter presented the synthesis of three PB-*b*-PEO block copolymers with a molecular weight of 7600, 8600 and 17 200 g/mol. All three block copolymers were successfully functionalised at the hydroxyl end group with an alkyne, acrylate and succinic acid end groups, allowing the formation of multi-functional polymersomes by mixing different functionalities together for self-assembly. It was attempted to adapt a technique for the production of lipid GUVs, cDICE, for giant polymersomes. Due to difficulties regarding solubility and phase separation, no polymersomes could be obtained. Instead, small polymersomes ranging from 100-200 nm in diameter were produced using the solvent displacement method and investigated using DLS and SLS. Vesicles were obtained from all three PB-*b*-PEO block copolymers and all three functionalities. This offers the possibility to tailor the polymersome's surface to a specific purpose, which was shown with dyes as model molecules. Large polymersomes in the µm-range were successfully produced using a microfluidic platform. Simultaneous and orthogonal labelling of alkyne and acrylate vesicles with the fluorescent dyes was proven by CLSM. The exchange between differently labelled polymersomes was investigated. However, the system likely contained to much free dye to yield a definite answer. Vesicles from PB-*b*-PEO-acrylate were biotinylated using an amine-bearing biotin. Their interactions with NeutrAvidin-coated glass were investigated using the micropipette force sensor technique. These functional polymersomes present a versatile module for artificial cells. The succininc acid group offers the possibility to alter the surface charge of the membrane, while the alkyne and acrylate allow for chemical modifications with azides or amines respectively, using mild reaction conditions.

3.3. Hybrid Vesicles

Hybrid vesicles from the phospholipid DPPE and PB-*b*-PEO block copolymer were prepared using the film hydration technique. The hybrid structure was proven by fluorescence cross-correlation spectroscopy (FCCS). Radical crosslinking of the PB double bond enhanced the vesicles' stability, allowing extraction of the lipid from the membrane. This extraction did not disturb the vesicular structure and offers a platform for permeable polymersomes.

3.3.1. Motivation

Hybrid vesicles are formed when amphiphilic block copolymers - the building block of polymersomes - and lipids - the building block of liposomes –form a mixed vesicular structure. As liposomes are limited in their chemical versatility, due to the available lipids, the addition of polymers offers a high modularity; both the hydrophobic and the hydrophilic block can consist of different monomers and they are easily functionalised (see section 3.2.3).[174]

Due to their high molecular weight, polymersomes exhibit enhanced stability and lower permeability compared to liposomes.[35] However, whether these properties count as an advantage or a disadvantage depends on the application. In some cases a certain permeability across the membrane is desired. The goal of this chapter was to develop polymersomes with a permeable membrane. To this end, hybrid vesicles are manufactured from PB-*b*-PEO block copolymers and 1,2-dipalmitoyl-*sn*-glycero-3-phosphoethanolamine (DPPE). Crosslinking the PB double bonds leads to a densely connected polymer shell, from which the lipid can be extracted, generating permeable polymersomes in the process (Figure 47). [128]

Figure 47. Illustration of the hybrid vesicle strategy. The lipid is represented in pink, the polymer in orange. An exemplary diffusion process over the permeable membrane is shown in green.

3.3.2. Crosslinking Polymersomes

The radical crosslinking reaction in PB-*b*-PEO vesicles was investigated. PB_{85}-*b*-PEO_{68}, the smallest of the herein used PB-*b*-PEOs, was used for all experiments in this chapter, as its low molecular weight minimises the deformation the polymer has to undergo in order to mix with the smaller lipid (see section 2.2.3). A radical crosslinking reaction, initiated by a hydrophobic azo initiator, 2,2'-azobis(2,4-dimethylvaleronitrile) (V-65), was chosen. After heating, it generates two radicals, which will attack the PB double bond, initiating a radical chain reaction (Scheme 10).

R = PB-*b*-PEO   I =

V-65

Scheme 10. Radical crosslinking of PB-*b*-PEO double bonds.

Different initiator concentrations ranging from 1.4 to 11.1 mol% (relative to the PB double bond) were tested (Figure 48a) and investigated using TEM. At 2.8 mol% of the crosslinker, vesicles can be detected, after the crosslinking reaction by conventional TEM, i.e. crosslinking stabilises the PB layer in dry state TEM. The remaining V-65 concentrations show undefinable agglomerates. An investigation of crosslinker concentrations closer to 2.8 mol% (Figure 48b) confirmed 2.8 mol% as the suitable concentration for vesicle crosslinking. All further experiments were carried out using this initiator concentration.

a)

1.4 mol% 2.8 mol% 5.6 mol% 11.1 mol%

b)

2.1 mol% 2.8 mol% 3.5 mol%
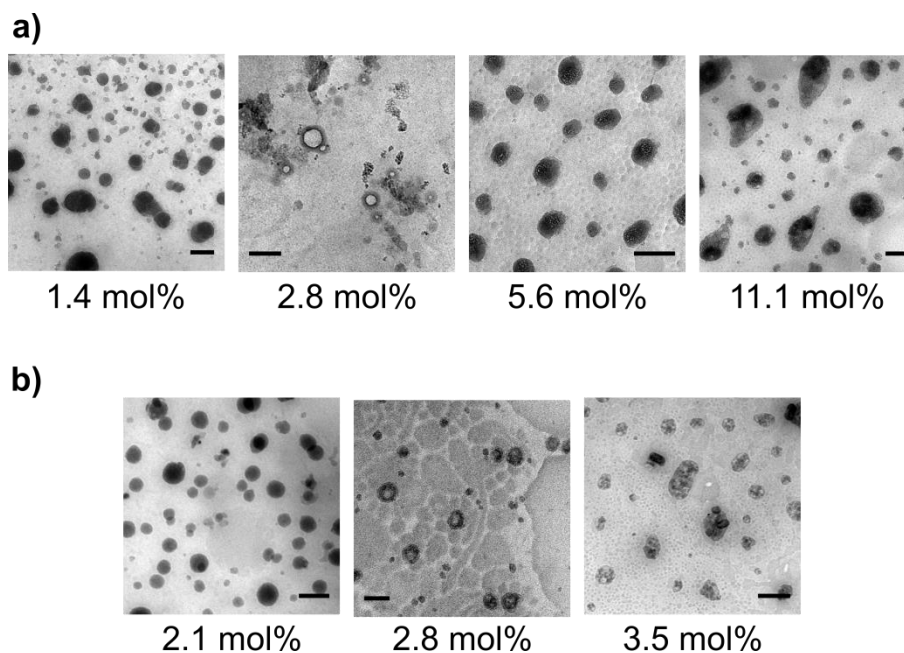
Figure 48. TEM micrographs of PB$_{85}$-*b*-PEO$_{68}$ samples crosslinked with V-65 (a and b). The amount of V-65 relative to the PB double bonds is given below each image. Scale bars are 200 nm, with the exception of both 2.8 mol% images (100 nm) and the 3.5 mol% image (400 nm).

3.3.3. Hybrid Vesicles

Having established a protocol for crosslinked PB-*b*-PEO vesicles, the next step was putting the lipid into the mix. The phospholipid DPPE was chosen as a model lipid (Scheme 11). As a saturated compound it will not be affected by the radical reaction taking place at the polymer.
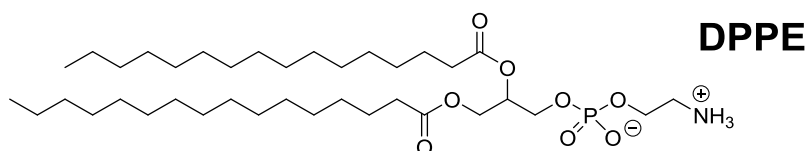
DPPE

Scheme 11. Chemical structure of 1,2-dipalmitoyl-*sn*-glycero-3-phosphoethanolamine (DPPE).

Samples with 5, 10 and 15 mol% lipid (relative to the polymer amount) were prepared. Of this amount, 1 mol% was always a fluorescently labelled derivative of DPPE - 1,2-dipalmitoyl-*sn*-glycero-3-phosphoethanolamine-*N*-(lissamine rhodamine B sulfonyl) (Liss Rhod DPPE), the purpose of which was enabling the monitoring of the extraction. Samples were no longer prepared using the solvent displacement technique, because the molecular weight of the lipid did not allow for dialysis. Instead the film hydration technique (4.3.4) was used. Samples were imaged using TEM (Figure 49), all three samples exhibited vesicular structures.
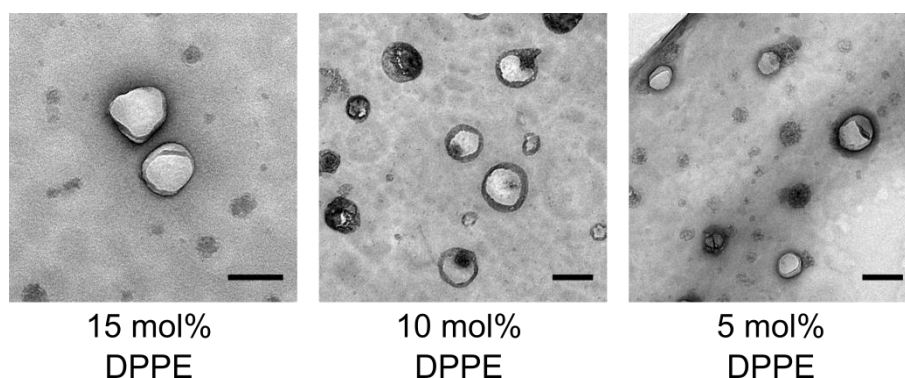

15 mol%
DPPE

10 mol%
DPPE

5 mol%
DPPE

Figure 49. TEM micrographs of hybrid vesicles. The lipid content is given below each image (1 mol% of which is Liss Rhod DPPE). Scale bars are 200 nm, except for the first image (100 nm).

Samples were further investigated using light scattering. To this end, sample without Liss Rhod DPPE were prepared, as its fluorescence would interfere with the measurement. Samples were extruded through a 200 nm membrane to reduce the dispersity and size, measurements were made before and after crosslinking. The results are summarised in Table 13. The ρ-ratio is used as an indicator for the sample morphology, with a value of 1.00 referring to vesicles. All samples show a R_H between 61.3 and 78.8 nm. Differences can be caused by differences during the extrusion. Furthermore, all samples exhibit a ρ-ratio very close to 1.00, indicating that vesicles were formed for all lipid concentrations, as confirmed by TEM. Interestingly, the crosslinked samples show smaller values for both R_g and R_H. Since the extrusion took place before the crosslinking, no differences could have taken place at this stage, i.e. the size differences are significant. The crosslinking seems to tighten the hydrophobic PB region of the vesicles, thereby shrinking the vesicle. The relative shrinkage of crosslinked sample to non-crosslinked sample (calculated from R_H) is given in Table 13. It could be expected to be more pronounced the lower the lipid content is, and while the 5 mol% sample does show the highest shrinkage, the overall trend does not support this hypothesis.

Table 13. Light scattering results for hybrid vesicles.

DPPE	condition	R_g/ nm	R_H/ nm	ρ-ratio	Shrinkage/ %
15 mol%	not crosslinked	61.4	67.0	0.92	6.27
	crosslinked	59.4	62.8	0.95	
10 mol%	not crosslinked	68.1	69.8	0.98	4.30
	crosslinked	64.5	66.8	0.97	
5 mol%	not crosslinked	77.1	78.8	0.98	22.21
	crosslinked	56.8	61.3	0.93	

FCCS was employed to investigate whether DPPE and PB-*b*-PEO do in fact form hybrid vesicles, rather than separate lipo- and polymersomes. The basic principle is identical with FCS, which has been explained in section 3.2.5.2. In contrast to FCS, in FCCS one is able measures two fluorescent species at the same time and determine the dependency of their diffusion. This is illustrated in Figure 50. Two independently-diffusing species will enter and leave the observation volume randomly and independently. Each will have its own autocorrelation curve and the cross correlation between them will be zero. This would be expected if the sample contained separate liposomes and polymersomes. If they form hybrid vesicles, their diffusion through the observation volume will coincide. Consequently, the cross correlation will be larger than zero.
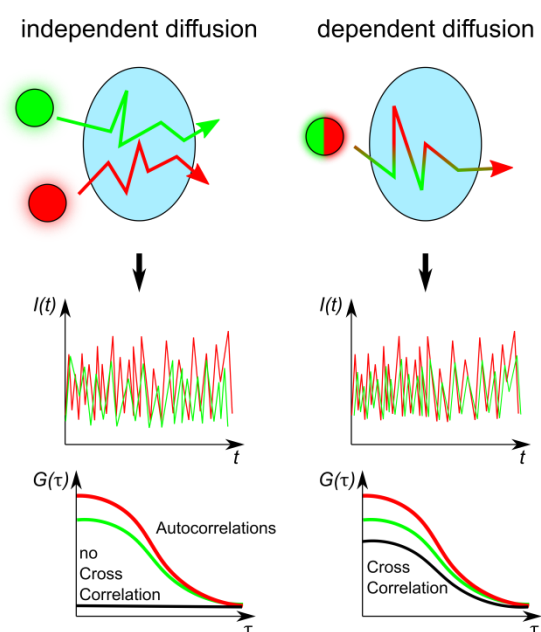

Figure 50. Principle of FCCS.

This method requires both the lipid and the polymer to be fluorescently labeled, therefore Liss Rhod PE and BODIPY amine-functionalised PB-*b*-PEO-acrylate were used. The results are shown in Figure 51. First, liposomes made from DPPE and Liss Rhod DPPE were measured together with free BODIPY amine dye to ensure that there is no unspecific interaction between the lipid and the dye (Figure 51a). The graph shows the autocorrelation curves of the liposomes (red) and the BODIPY amine dye (blue). The numerical results are summarised in Table 14. BODIPY amine shows a notably faster diffusion time of 18 µs compared to the liposomes at 1460 µs, as expected for single, small molecules. The cross correlation curve amplitude is close to zero, proving the independent diffusion of the two fluorescent species. In the hybrid vesicle samples (Figure 51b) both species – Liss Rhod DPPE (in red) and labelled PB-*b*-PEO (in blue) – show a slow decay of their respective autocorrelation curve, ergo both fluorescent species are assembled into larger structures made from many fluorophores. Liss Rhod DPPE shows a diffusion time of 2875 µs, labelled PB-*b*-PEO diffuses at 1633 µs. This difference is caused by the two fluorophores being excited by two separate lasers each of which has its own detection volume. The amplitude of the cross correlation curve is now strongly increased compared to the previous sample, proving that Liss Rhod DPPE and labelled PB-*b*-PEO diffuse dependently, i.e. hybrid vesicles were formed.
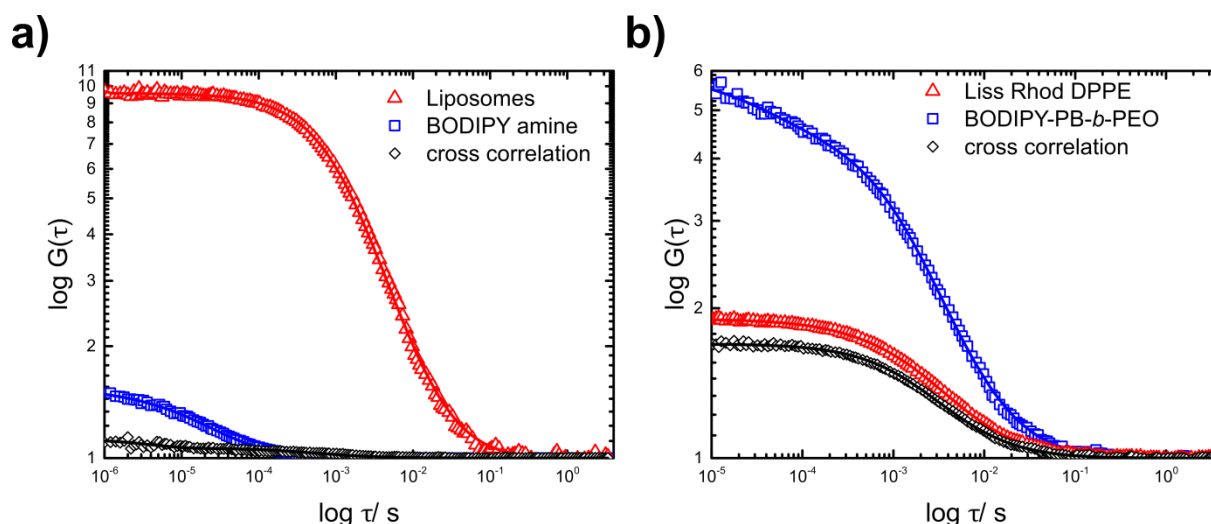
Figure 51. FCCS results for liposomes made from DPPE and Liss Rhod DPPE with free BODIPY amine dye (a) and hybrid vesicles made from DPPE, Liss Rhod DPPE- and BODIPY-labeled PB-*b*-PEO (b).

In an ideal FCCS measurement both types of fluorescent species should have similar concentrations and thus both autocorrelation curves should have similar amplitudes, with the one corresponding to the species with red shifted fluorescence being a bit lower due to the larger observation volume. Here, Liss Rhod DPPE has a lower amplitude than the labeled

polymer, i.e. an apparently higher concentration. There may be two reasons for this. Firstly, it was evident during the measurements that both fluorophores existed in two different states. Liss Rhod DPPE was in an equilibrium between micelles and hybrid vesicles. BODIPY amine was mostly covalently attached to the polymer and part of hybrid vesicles, but some remained freely diffusing in the sample. Consequently, a two component fit had to be used for both autocorrelations (Table 14 only shows the data of the relevant component, the second one is not shown). As a result, there was only limited control over the concentration of the fluorophores in the hybrid vesicles. The second reason could be that the sample contained two different species of vesicles. The experimentally observed higher concentration of Liss Rhod DPPE could stem from the existence of vesicles carrying only Liss Rhod DPPE as a fluorophore. That would mean that there were hybrid vesicles coexisting with liposomes or that an amount of hybrid vesicles were not sufficiently labeled with BODIPY amine to be detectable. This would be supported by the observation that the sample still contained free BODIPY amine dye, ergo the reaction was not quantitative.

In conclusion, FCCS proved the existence of hybrid vesicles and indicated the co-existence of liposomes.

Table 14. FCCS results for liposomes made from DPPE and Liss Rhod DPPE with free BODIPY amine dye and hybrid vesicles labeled with Liss Rhod DPPE and BODIPY-labeled PB-*b*-PEO.

Sample	Component	τ/ µs	R_H/ nm[a]	D/ m^2 s^{-1} [a]
Liposomes + BODIPY amine	Liss Rhod DPPE	1460	29.0	5.99E-10
	BODIPY amine	18	0.4	7.79E-12
Hybrid Vesicles	Liss Rhod DPPE	2875	60.3	2.89E-11
	BODIPY-PB-*b*-PEO	1633	38.2	5.90E-12

[a] calculated from τ obtained from FCS. Alexa 488 (τ = 22 µs) and Rhodamin 6G (τ = 26 µs) were used for calibration.

3.3.4. Permeable Polymersomes

To obtain permeable polymersomes, the lipid has to be extracted from the membrane. Hybrid vesicles with 15, 10 and 5 mol% DPPE (1 mol% of which was Liss Rhod DPPE) were prepared and dialysed against a 1:1 mixture of ethanol and water, which was changed twice. The mixture is able to dissolve DPPE, thereby continually extracting it from the hybrid vesicles. The progress was monitored by fluorescence intensity measurements of Liss Rhod DPPE (Figure 52). Aliquots were taken regularly from the outer water/ethanol phase, however, the concentration of Liss Rhod DPPE was below the detection limit and is therefore not shown. All three samples show a significantly reduced amount of Liss Rhod DPPE after the extraction, meaning that the extraction of DPPE from hybrid vesicles using a

water/ethanol mixture is possible. The fluorescent intensity did not approach zero in the timeframe of 1 week. The amount of DPPE could be further reduced by a longer dialysis or a more frequent change of the medium. However, the extraction will slow down over time, because there will always be an equilibrium between the amount of lipid in the vesicles and the amount in solution.
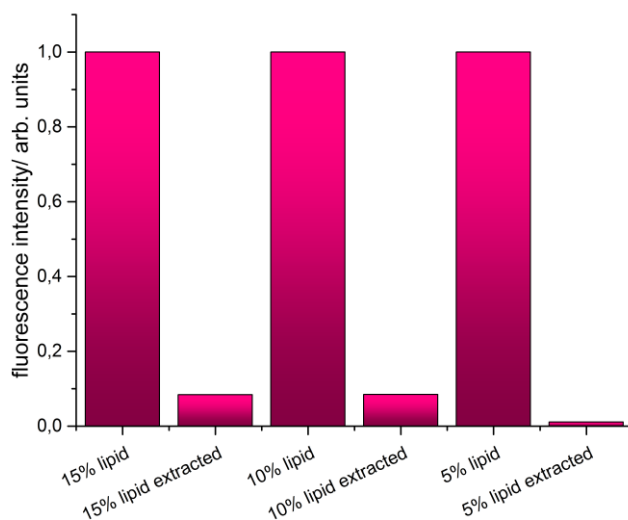
Figure 52. DPPE extraction from hybrid vesicles monitored by Liss Rhod DPPE fluorescence intensity.

Dynamic light scattering measurements after the extraction showed that the vesicles remained intact during the extraction. With a R_H between 65 and 77 nm, size distributions of all samples remain close to the initial values (see Table 13). In addition, these results further prove the extraction of Liss Rhod DPPE. DLS measurements of hybrid vesicles with Liss Rhod DPPE were impossible, because the fluorophore would have been excited by the laser.
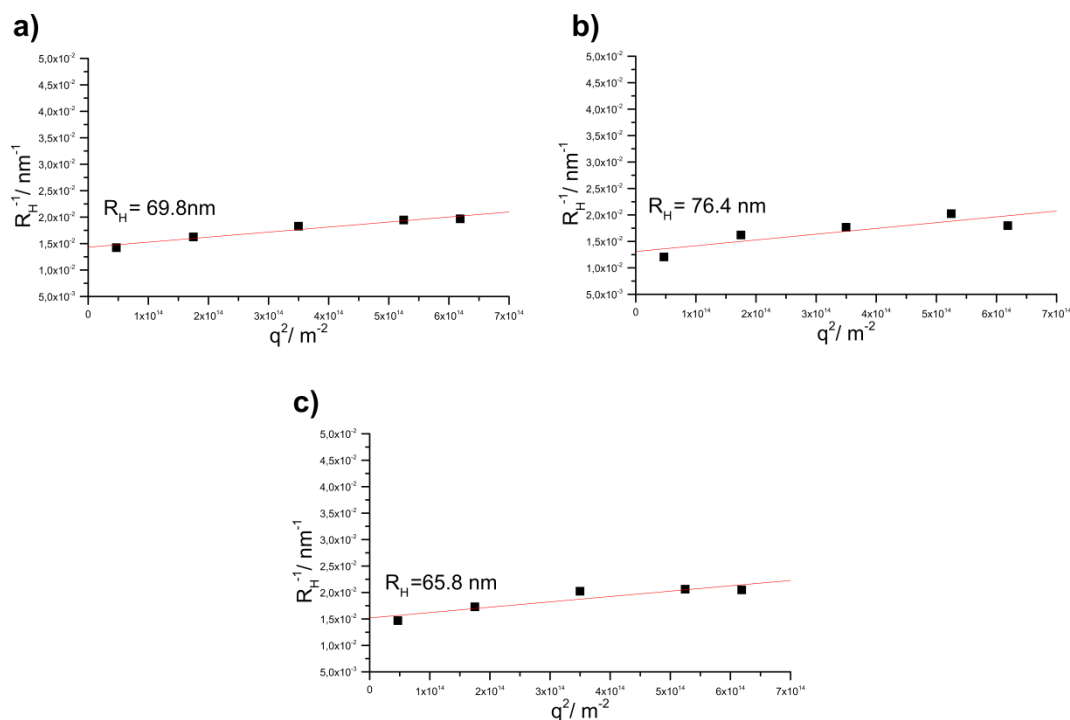
Figure 53. DLS data for hybrid vesicles after DPPE extraction. Samples contained either 15 mol% (a), 10 mol% (b) or 5 mol% (c) lipid.

3.3.5. Conclusion

In this chapter, a strategy for permeable polymersomes was developed. A similar system has been used to enhance the relaxivity of a magnetic resonance contrast agent by increased water diffusion.[128] Polymersomes from pH-responsive polymers have been reported to become permeable in a certain pH-range.[175, 176] Other works rely on complete dissociation of the polymersomes to achieve a release, hydrophilic modifications of the hydrophobic block or reconstitution of membrane proteins.[177-179] Here, hybrid vesicles were formed from the phospholipid DPPE and PB-*b*-PEO, as proven by FCCS. The PB block was crosslinked and the lipid was extracted to generate a stable, permeable membrane. Vesicles remained undisturbed by the extraction process, as proven by DLS. This system offers a versatile platform for further investigations. High molecular weight materials could be enclosed and protected within, while small molecules could diffuse through the permeable membrane. This is a system akin to a cell and it obvious that an interesting next step is loading the permeable polymersomes with enzymes, which would be trapped within due to their size. Of course, the size exclusion limit for a given lipid content needs to be investigated. It seems reasonable, that by increasing the lipid content before the extraction, the size exclusion limit could be pushed higher

3.4. Poly(butadiene)-*block*-poly(ethyl ethylenephosphate)-based Materials[4]

Poly(butadiene)-*block*-poly(ethyl ethylenephosphate) (PB-*b*-PEEP) polymers with varying hydrophilic block lengths were synthesised by ring-opening polymerisation of EEP from a PB-OH macroinitiator. The aqueous self-assembly in dependence of the hydrophilic block length was studied using light scattering and TEM. With increasing block length, polymersome formation was observed. A preparation method for biological TEM samples was established as a suitable method to image PB-*b*-PEEP polymersomes in their native state.

3.4.1. Motivation

One of the key aspects of life is the principle of compartmentalisation. As life is a non-equilibrium state, a barrier is needed to confine substances, create gradients and keep an organism out of stasis. This barrier is the cell membrane, a highly complex system, consisting of different lipids, proteins, and other molecules – the result of millions of years of evolution. A simpler system is offered by liposomes, vesicular structures from lipids, which have been investigated for their application in medicine, drug delivery, and other fields.[180-182] Polymersomes are an artificial analogue to liposomes, their building units are block copolymers instead of lipids. They benefit from the entire toolkit of polymer chemistry, e.g. variety of building blocks, molecular weights and, probably most importantly, enhanced stability compared to liposomes.[35] Since their discovery, polymersomes have been produced from a number of different amphiphilic copolymers. For mimicking the fluidity of a natural membrane, copolymeric materials with low glass transition temperature are of particular interest. Common materials include poly(ethyl ethylene)-*block*-poly(ethylene oxide), poly(butadiene)-*block*-poly(ethylene oxide) or poly(dimethylsiloxane)-*block*-poly(2-methyl-oxazoline).[12, 183, 184] The examples of polymersomes containing a phosphate building block are sparse, yet these materials bear an inherent similarity to the predominant species in cell membranes, the phospholipids, and impart biodegradable segments in polymersomes.[185, 186] In this chapter, polymersomes from a new amphiphilic block copolymer – poly(butadiene)-*block*-poly(ethyl ethylene phosphate) (PB-*b*-PEEP) – are presented.

3.4.2. Synthesis

PB-*b*-PEEP block copolymers were synthesised as shown in Scheme 12. First, 1,3-butadiene was polymerised anionically in cyclohexane (to achieve mainly 1,4-addition) with

---

[4] A publication based on this chapter is in preparation.

sec-butyllithium as an initiator and end-capped with ethylene oxide to yield a hydroxyl-functional poly(butadiene)-macroinitiator. Propagation with ethylene oxide, resulting in formation of a PB-b-PEO block copolymer, is prevented by the strong coordination of the lithium counterion to the oxyanion at the active chain-end.[187] The PB macroinitiator was used to subsequently polymerise ethyl ethylene phosphate (EEP) using 1,8-diazabicyclo[5.4.0]undec-7-ene (DBU) as a catalyst and a thiourea (TU) cocatalyst. This two-catalyst system has been shown to reduce side reaction such as transesterifications, which the ring-opening polymerisation of EEP is prone to.[188]
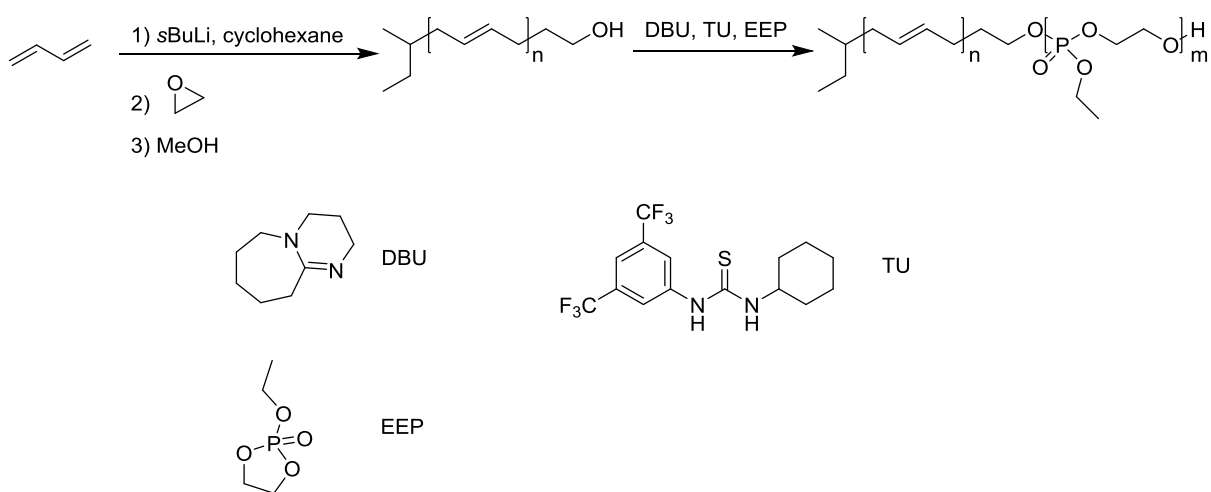
Scheme 12. Synthetic protocol for poly(butadiene)-*block*-poly(ethyl ethylene phosphate) block copolymers. For clarity only the 1,4-addition of 1,3-butadiene is shown.

The resulting PB-b-PEEP block copolymers were analysed by NMR spectroscopy and SEC. Figure 54 shows a ^{1}H NMR spectrum of a PB-*b*-PEEP block copolymer, the resonances of the PB block are detected at 0.9-2.3 ppm (alkyl signals) and 4.7-5.8 ppm (for the olefins). The resonances of the PEEP block are detected at 1.3-1.5 ppm and 3.7-4.5 ppm. The formation of a block copolymer is proven by additional ^{1}H DOSY NMR spectroscopy, as the signals of the PB and the PEEP exhibit the same diffusion signal (see Figure 54). This is further confirmed by Figure 54b, the SEC curves of the PB macroinitiator and a PB-*b*-PEEP block copolymer. The distribution of the PB-*b*-PEEP block copolymer shows a shift to higher elution volumes compared to the PB-macroinitiator. This indicates a decrease in the hydrodynamic radius of the polymer (not necessarily a decrease in molecular weight), i.e. addition of the PEEP block leads to a tighter polymer coil in the SEC eluent.[189]
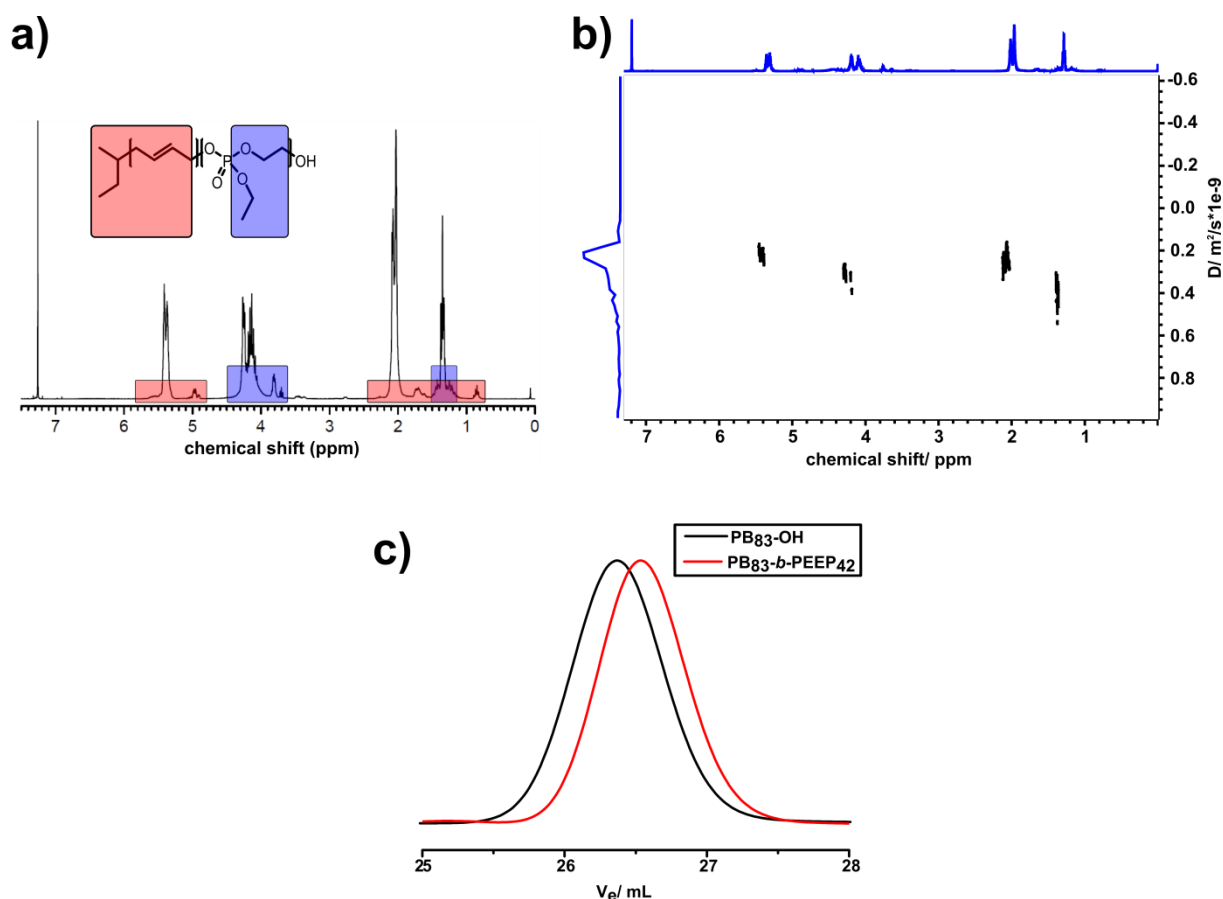
Figure 54. Exemplary characterisation data of PB$_{83}$-*b*-PEEP$_{42}$. ^{1}H NMR spectrum of PB$_{83}$-*b*-PEEP$_{42}$ in CDCl$_3$ (a). ^{1}H DOSY NMR (500 MHz, 298 K) spectrum of PB$_{83}$-*b*-PEEP$_{42}$ in CDCl$_3$.(b) and SEC traces of PB$_{83}$-OH (black) and PB$_{83}$-*b*-PEEP$_{42}$ (red) in THF (c).

The characterisation data of all PB-*b*-PEEP block copolymers is summarised in Table 15. From one PB-OH macroinitiator, block copolymers ranging from 3 to 125 PEEP units were synthesised. The degree of polymerisation was determined from NMR spectroscopy. All samples show a narrow size distribution with molecular weight dispersities Đ between 1.02 to 1.08. SEC measurements illustrate that there is no correlation between the number average molecular weight from SEC (M_n, SEC) and the number average molecular weight from NMR spectroscopy (M_n, NMR) on our set-up. Short PEEP blocks (entry 2 and 3 in Table 15) have no apparent effect on M_n, SEC, while medium PEEP blocks (entry 4 in Table 15) lead to an increase in M_n, SEC. Long PEEP blocks (entry 5 and 6 in Table 15) decrease M_n, SEC. These changes do not reflect on the molecular weight of the polymer, but rather on the coil behaviour in the eluent.

Table 15. Characterisation data of PB-*b*-PEEP block copolymers and the PB-OH precursor.

Entry	Sample[a]	DP_{PB}	DP_{PEEP}[a]	M_n[a]/ g/mol	M_n[b]/ g/mol	Đ
1	PB$_{83}$-OH	83	-	4 500	8 000	1.03
2	PB$_{83}$-*b*-PEEP$_3$	83	3	5 000	8 000	1.03
3	PB$_{83}$-*b*-PEEP$_7$	83	7	5 600	8 000	1.03
4	PB$_{83}$-*b*-PEEP$_{16}$	83	16	7 000	8 500	1.08
5	PB$_{83}$-*b*-PEEP$_{42}$	83	42	9 800	8 100	1.03
6	PB$_{83}$-*b*-PEEP$_{125}$	83	125	23 000	7 500	1.02

[a]determined by NMR
[b]determined by SEC

A targeted molecular weight is omitted in Table 15, because during EEP polymerisation, a surplus of EEP is used and quenched before total conversion. This reduces the side reactions shown in Scheme 13, but consequently means reaching a definite molecular weight is impossible without exact knowledge regarding the kinetics of the selected polymerisation parameters (temperature, solvent, etc.).
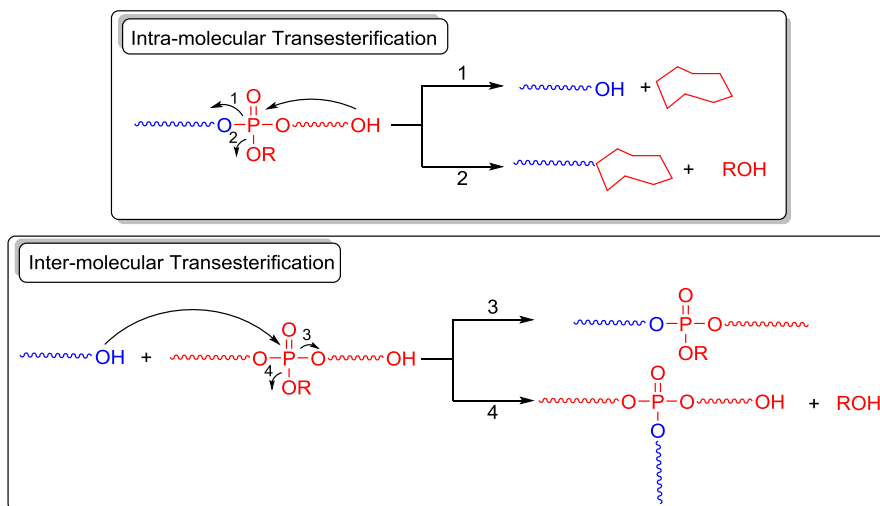
Scheme 13. Side reactions for the polymerisation of EEP.

Thermal characterisation revealed two glass transition temperatures, one at -98 °C for the PB block and a second at -71 C for the PEEP block, already indicating a strong phase separation between the two blocks (see Figure 55). Furthermore, both blocks have a glass transition temperature well below room temperature, making them ideal candidates to mimic the fluidity of a natural biomembrane.
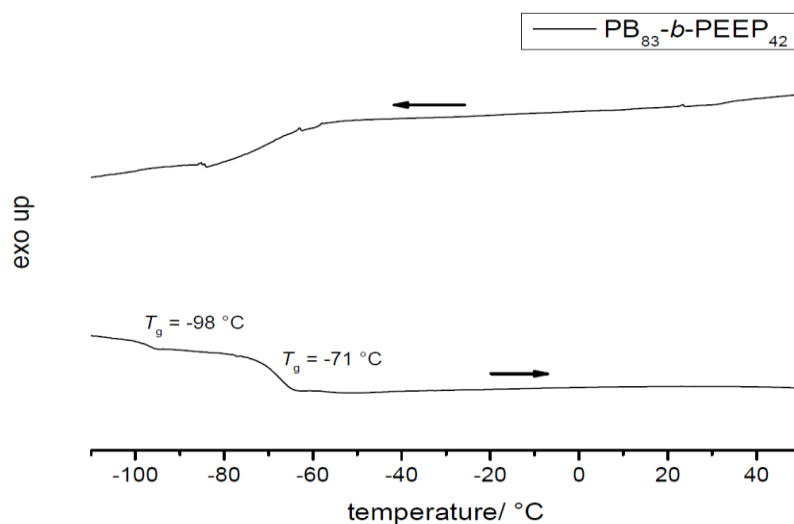
Figure 55. DSC curve of PB$_{83}$-*b*-PEEP$_{42}$ (cooling and 2nd heating curve, 10K·min^{-1}). T_g is the glass transition temperature.

3.4.3. Self-assembly

PB-*b*-PEEP block copolymers were investigated regarding their self-assembly behaviour in water. Starting from a solution in THF, a good solvent for both blocks, an excess of water is introduced to the system. This forces the block copolymers to self-assemble into stable structures, minimising the contact between the hydrophobic PB blocks and the aqueous environment. This solvent displacement method usually yields quite disperse structures, therefore the samples were extruded through a polycarbonate membrane with a pore size of 200 nm.[190] The self-assembly structure was assessed using static and dynamic light scattering (Figure 56). From dynamic light scattering, the hydrodynamic radius R_H was obtained. Static light scattering measurements yielded the radius of gyration R_g. From these two values, the ρ-ratio can be calculated (for details see 3.2.5.1). The ρ-ratio provides information on the morphology of the scattering species by comparing theoretically calculated ρ-ratio values to the experimental results. ρ-ratios of 1 are indicative of a hollow sphere with an infinitesimally thin membrane, i.e. values close to $\rho = 1$ indicate the formation of a polymersome. The decrease in the ρ-ratio is translated to a thicker membrane until at $\rho = 0.775$ a homogenous sphere is reached.[170] The ρ-ratios of PB-*b*-PEEP block copolymers investigated ranged from 0.81 to 1.12 with no clear trend regarding the PEEP

block length. Apart from the shortest hydrophilic block prepared, PB_{83}-b-$PEEP_3$, all samples show a ρ-ratio that indicates a vesicular structure. Differences in R_H are not discussed, because the sample preparation required extrusion and differences in size may easily stem from slight differences during the extrusion, such as speed and pressure and not the polymer structure.
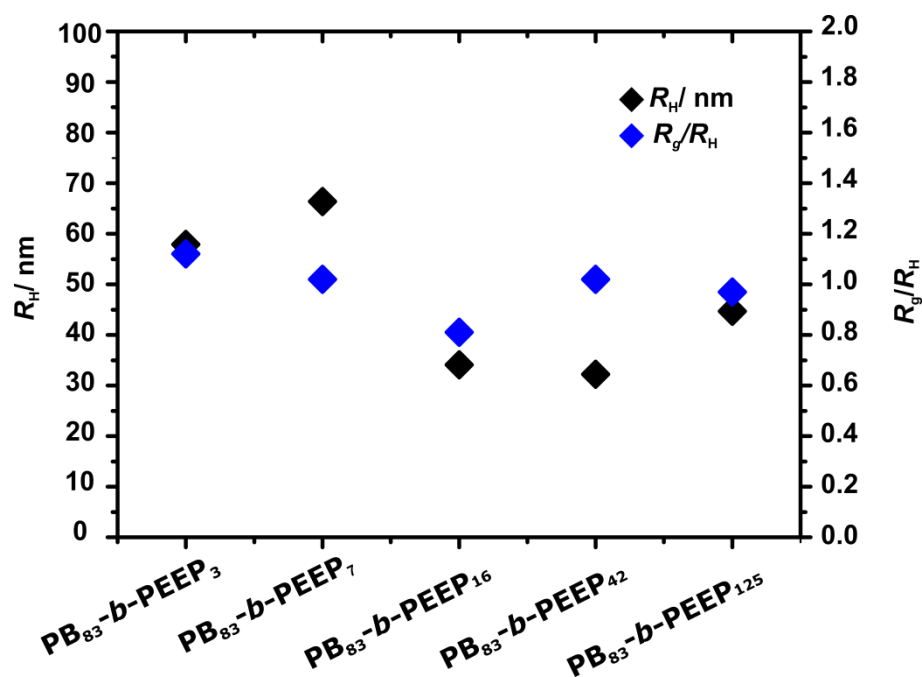
Figure 56. Light scattering results for PB-b-PEEP block copolymers.

For direct visualisation, the self-assembly structure was investigated using TEM (Figure 57). Cryo-TEM investigations failed, because the fragile polymersomes and micellar structures tend to disintegrate immediately upon contact with the charged holey carbon substrate prior to the vitrification. Therefore, samples were crosslinked using OsO_4 before drop-casting the aqueous solution on a grid. Non-crosslinked samples cannot be imaged in TEM, as the self-assembled structures of the two low T_g segments are only stable in solution and would be destroyed during the drying process. Additionally, OsO_4 serves as a contrast agent during the imaging. PB-b-PEEP block copolymers with a short hydrophilic PEEP block of 3 or 7 repeating units (entry 2 and 3 in Table 15) form compound micelles as observed in TEM (Figure 57a and b). These consist of several inverse micelles with hydrophilic PEEP at their surface. With an increasingly longer hydrophilic block (entry 4 and 5 in Table 15), the morphology changes to coexisting compound micelles and polymersomes (Figure 57c and d). The longer PEEP blocks can no longer be sufficiently incorporated into compound micelles. For PB_{83}-b-$PEEP_{125}$ (entry 6 in Table 15) only polymersomes are detected from TEM (Figure 57e). This shift from compound micelles to polymersomes with an increasing hydrophilic block length is well-known in literature.[191]

Figure 57. TEM micrographs of PB-*b*-PEEP block copolymers. Samples were crosslinked with OsO$_4$ for stability and to enhance contrast. PB$_{83}$-*b*-PEEP$_3$ (a), PB$_{83}$-*b*-PEEP$_7$ (b), PB$_{83}$-*b*-PEEP16 (c), PB$_{83}$-*b*-PEEP$_{42}$ (d) and PB$_{83}$-*b*-PEEP$_{125}$ (e).

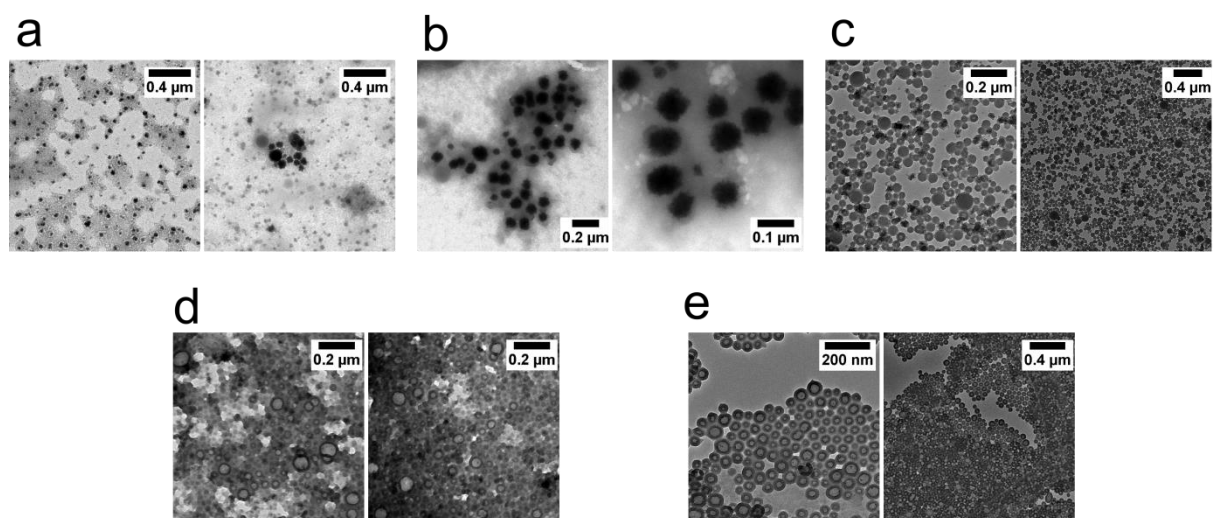In addition to TEM imaging in the dry state, we implemented embedding in trehalose, which is a technique established for biological samples.[192] Sugar embedding was developed in 1975 by Unwin and Henderson as a way to protect biological samples against the vacuum conditions of electron microscopy without introducing artefacts. Since then, trehalose (Figure 58a), a non-reducing disaccharide, has become the most popular choice in sugar embedding, owing to its ability to stabilise proteins and protect the samples from beam damage.[193] The exact mechanism how trehalose stabilises and protects the specimen is unclear. However, there are three prevalent theories (Figure 58b). The first, the 'vitrification theory', states that trehalose forms an amorphous, glass-like structure around the specimen. Because trehalose has the highest glass transition temperature among the disaccharides (values between 73 and 115 °C have been reported), it is able to form such a film under ambient conditions.[194, 195] The 'water replacement theory' defines the substitution of the hydration shell by trehalose as the crucial factor. The multiple hydroxyl groups of trehalose stabilise the specimen. Since trehalose preferentially form hydrogen bonds not with itself but with other molecules, it is the ideal candidate compared to other disaccharides. In the 'preferential exclusion theory' the focus lies on the interaction between trehalose and water, rather than on that between trehalose and the specimen. Here, trehalose decreases the hydration shell of the specimen by drawing water molecules away and into its own water shell. This stabilises the specimen as it reduces its flexibility. Here, trehalose outshines the other disaccharides because its hydration shell is the largest out of all of them.[196] The truth, at it is often the case, most likely lies between the different theories. The 'preferential

exclusion theory' offers an explanation why water is drawn away from the specimen, while the 'water replacement theory' explains why the interaction between trehalose and specimen are favourable. Lastly, the 'vitrification theory' elucidates the stability of the trehalose film.

a)

b)
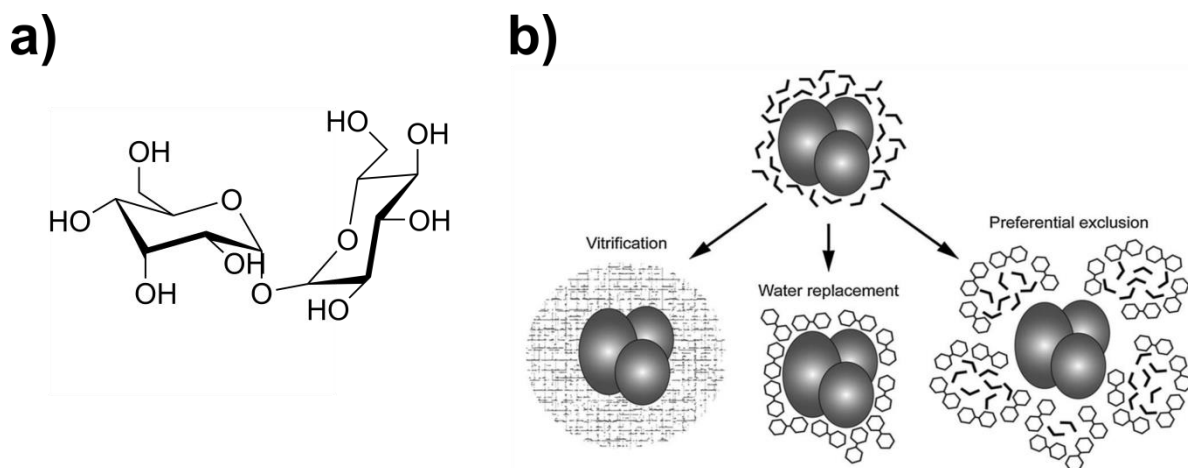
Figure 58. Chemical structure of trehalose (a) and proposed mechanisms for trehalose embedding (b). b is reprinted from [192]), with permission from Elsevier.

Herein, we show that the morphologies obtained from trehalose TEM imaging are in good accordance with TEM imaging in the dry state. The results for polymersome forming PB-*b*-PEEP block copolymers (entry 4, 5 and 6 in Table 15) are shown in Figure 59. The vesicular structure is well preserved in the trehalose film, enabling imaging of the samples in their native state, compared to the dry state. Consequently, trehalose embedding can be a suitable method to image non-biological samples as well. Compared to cryoTEM, trehalose embedding does neither require specialised equipment nor prolonged preparation times and allows storing the samples at ambient temperature, which makes it faster and more convenient to handle. On the other hand, low contrast materials might be difficult to visualise using trehalose embedding, owing to the increased contrast of the surrounding medium compared to cryoTEM (sugar vs. water). This can be circumvented using additional staining materials. Interestingly, it was not possible to achieve imaging of the block copolymers with short EEP blocks (entry 2 and 3 in Table 15). This is most likely caused by the mechanism of stabilisation by the trehalose embedding. In samples with a short PEEP block, it is likely that there are not enough hydrogen bonding sites available to sufficiently stabilise the sample.
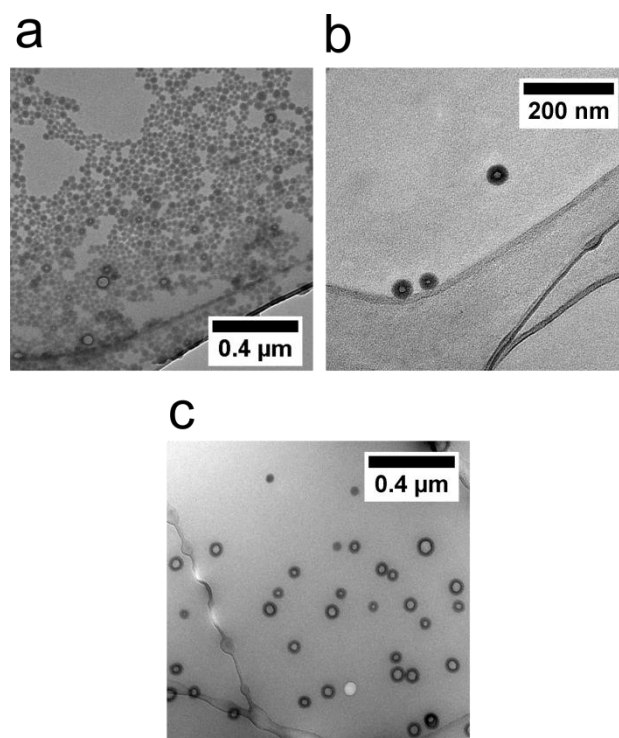
Figure 59. TEM micrographs of PB-*b*-PEEP block copolymers forming vesicles embedded in trehalose. Samples were crosslinked with OsO$_4$ for enhanced contrast. PB$_{83}$-*b*-PEEP$_{16}$ (a), PB$_{83}$-*b*-PEEP$_{42}$ (b) and PB$_{83}$-*b*-PEEP$_{125}$ (c).

CryoTEM investigations of PB-*b*-PEEP block copolymers failed, because the fragile polymersomes tend to disintegrate immediately upon contact with the charged holey carbon substrate prior to the vitrification (Figure 60).
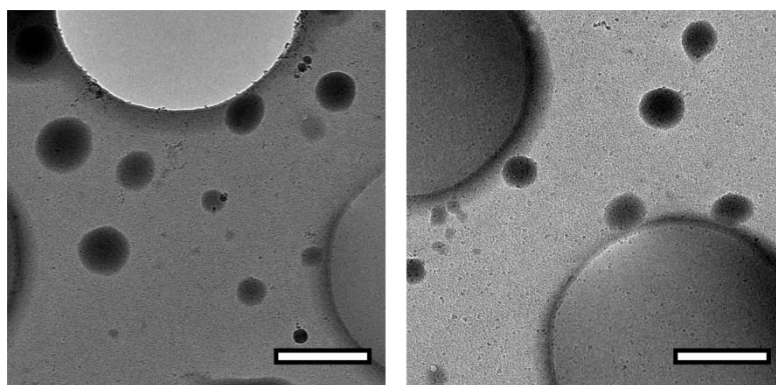
Figure 60. cryoTEM micrographs of PB-*b*-PEEP block copolymers. Scale bars are 1000 nm.

3.4.4. Conclusion

In summary, this chapter presented the first amphiphilic poly(phosphoester)-based block copolymers. This was achieved using a PB-OH macroinitiator and subsequent ring-opening polymerisation of EEP. These block copolymers self-assembled into polymersomes in water, as determined by light scattering and TEM imaging. It was shown that trehalose embedding

is a fast and convenient method to image these polymersomes via TEM in their native state, avoiding laborious cryo-TEM procedures. Similar to cell membranes build out of phospholipids, these polymersomes contain phosphate groups, making them a promising synthetic analogue to biological membranes.

4.   Experimental Part

4.1.   Ferrocene-based Materials

4.1.1. Materials and Instrumentation

All materials and solvents, unless stated otherwise, were purchased from Sigma Aldrich. Nile Red was obtained from Acros Organics. SDS was supplied by Fluka. Glucose and hydrochloric acid (0.1 M) were purchased from Carl Roth. All experiments were conducted in MilliQ water.

Dynamic light scattering (DLS) was measured with a Nicomp™ 380 Submicron Particle Sizer (PSS-Nicomp) at an angle of 90° or on an ALV spectrometer consisting of a goniometer and an ALV-5004 multiple-tau fulldigital correlator (320 channels) which allows measurements over an angular range from 20° to 150. A He–Ne Laser (wavelength of 632.8 nm) is used as light source. TEM measurements were carried out on a JEOL 1400 at a voltage of 120 kV, images were recorded with a GATAN Ultrascan 1000 CCD-camera. SEM measurements were carried out using a Zeiss Gemini 1530. Ultrasonication was carried out using a Branson W450-D sonifier at 69% amplitude with a 1/8 inch tip. Cyclic voltammetry and electrolysis experiments were conducted using a Solartron SI1286 potentiostat. Cyclic voltammetry measurements were carried out under guidance of Philipp Schäfer at the Max Planck Institute for Polymer Research in Mainz. CLSM measurements were performed on a TCS SP5 (Leica) using a 488 nm Argon laser at 15% power and a HCX PL APO CS 63x oil objective (numerical aperture 1.40). Fluorescence intensity was measured on a Tecan Plate Reader Infinite M1000 at an excitation wavelength of 520 nm. UV/Vis spectra were recorded on a Perkin Elmer Lambda 25 spectrometer. ^{1}H NMR spectra were recorded on a Bruker Avance 300 MHz spectrometer at room temperature. All spectra were recorded at room temperature in $CDCl_3$. DSC measurements were performed using a Mettler-Toledo DSC 823 at a scan rate of 10 K/min under nitrogen atmosphere. SEC measurements were carried out in THF. The sample concentration was 1 g L^{-1}. Three SDV columns (PSS) with a particle size of 10 µm and pore sizes of 106, 104 and 500 Å and a 1260 RID Shodex RI-101 detector (ERC) were employed. Calibration was achieved using PS standards provided by Polymer Standards Service. The eluent was used at 30 °C and a flow rate of 1 mL min^{-1}. FCS measurements were carried out by Andreas Best on a commercial setup (Zeiss, Germany) consisting of the module ConfoCor 2 and an inverted microscope model Axiovert 200 with a Zeiss C-Apochromat 40x/1.2W water immersion objective FITC dextran was excited using an argon-ion laser (488 nm) and the emission detected in the range 505-550 nm. The size of the

observation volumes was calibrated using reference dyes with known diffusion coefficients, Alexa 488.

4.1.2. Stimulus-responsive Release from Poly(ferrocenylsilane) Nanocontainers[5]

PFS synthesis

PFS was synthesized according to literature.[156] In a glovebox under argon atmosphere, a flamed out Schlenk tube was charged with dimethyl[1]silaferrocenophane in THF. A solution of sodium cyclopentadienide in THF (1 M) was added in the dark. The solution was polymerized at 5 °C for 4 hours under light irradiation, after which time dimethyl[1]silaferrocenophane was consumed. The Schlenk tube was transferred to a glovebox and charged with methylvinyl[1]ferrocenophane in the absence of light. The reaction was continued for 2 h under light irradiation and quenched with a few drops of freshly distilled trimethylsilyl chloride. After evaporation of the solvents, the obtained film was redissolved in THF and precipitated using methanol. The obtained orange powder was vacuum dried.
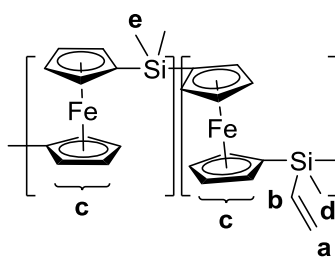
Figure 61. Poly(dimethyl ferrocenylsilane)$_{0.87}$-block-poly(methyl vinyl ferrocenylsilane)$_{0.13}$

^{1}H NMR (300 MHz, CDCl$_3$): δ 6.62-6.49 (m, 0.13, **a**), 6.13-5.84 (m, 0.26, **b**), 4.29-4.11 (m, 8, **c**), 0.63 (s, 0.40, **d**), 0.56 (s, 5.20, **e**).

Procedure for PFS nanocontainers preparation

In a screw cap vial PFS (8 mg) was dissolved in DCM (0.5 g) and hexadecane (8 mg). 4 g of 0.01 wt% SDS in MilliQ water was added. The mixture was stirred at 1000 rpm for 30 min. For emulsification the sample was subjected to ultrasonication for 2 min (alternating between 30 s pulse and 10 s pause) using a Branson W450-D sonifier at 69% amplitude with a 1/8 inch tip and ice-cooling. DCM was evaporated at 40 °C while stirring at 500 rpm

---

[5] This chapter (with the exception of 3.1.1.5) is based on the publication 'Stimulus-Responsive Release from Poly(ferrocenyl silane) Nanocontainers' by Laura Thomi, Philipp Schaefer, Katharina Landfester, and Frederik R. Wurm, published 2016 in Macromolecules, volume 49 on page 105-109 (http://pubs.acs.org/doi/full/10.1021/acs.macromol.5b02367). Reprinted with permission.

overnight. The obtained orange dispersions were purified by centrifugation at 1163 rzb for 20 minutes. The supernatant was removed and an equivalent amount of MilliQ water was added. The purification steps were repeated twice. The final dispersion was analyzed using DLS and electron microscopy.

For nanocontainers loaded with 2-propylpyridine, 8 mg of a 10 wt% solution of propylpyridine in hexadecane was used instead of pure hexadecane. For nanocontainers loaded with Nile Red, 0.5 g of a 0.04 wt% solution of Nile Red in DCM was used instead of pure DCM.

Cyclic voltammetry and electrolysis of PFS nanocontainers

Cyclic voltammetry measurements were carried out in degassed PBS buffer (without the addition of Ca^{2+} and Mg^{2+}) with a platinum wire counter electrode, a glassy carbon working electrode and an Ag/AgCl/3 M KCl reference electrode.

Scan rates were either 10 or 20 mV s^{-1}. Polymer film samples were prepared by drop casting a solution of PFS in DCM onto the working electrode and evaporation. The samples of the dispersions were prepared either by drop casting the aqueous dispersion onto the working electrode or measured directly from the diluted dispersion with a final solid content of 0.02%. For electrolysis a constant potential of 0.75 V was applied until an electric charge of 0.34 C had flown, which was equivalent to complete oxidation of the ferrocene groups in the sample (0.0035 mmol fc in 400 µL dispersion) For faster conversion a platinum plate working electrode with a surface of 3.9 cm^2 was used and the solution was stirred. Aliquots were taken at 0%, 50% and 100% conversion and visualized by TEM.

Chemical oxidation of PFS nanocontainers

For CLSM imaging 200 µL PFS nanocontainer dispersion (containing 475 µg PFS or 1.96 µmol ferrocene) were mixed with 40 µL of an aqueous 50 mg L^{-1} FITC-dextran solution and 3 µL 0.1 M HCl. For the oxidation 16.5 µmol H_2O_2 or 16.5 units Glucose Oxidase (250000 units g^{-1}) and 2.97 mg glucose (16.5 µmol) were added. The total volume was brought up tp 400 µL by addition of water.

Solvatochromism of Nile Red in PFS nanocontainers

For nanocontainers loaded with Nile Red, 0.5 g of a 0.04 wt% solution of Nile Red in DCM was used instead of pure DCM. To remove any Nile Red from the continuous phase, the dispersion was dialyzed for 36 h against 3x 200 mL 0.01% SDS solution in water. The fluorescence intensity of loaded and empty PFS nanocontainers was measured from 550 to 630 nm at an excitation wavelength of 520 nm.

For oxidized samples, 200 µL PFS nanocontainer dispersion (520 µg PFS or 2.15 µmol ferrocene) were mixed with 22 µL 0.1 M HCl and 39.6 µmol H_2O_2. Unoxidized samples were brought to an equivalent volume using water.

Release of 2-propylpyridine

For nanocontainers loaded with 2-propylpyridine, 8 mg of a 10 wt% solution of 2-propylpyridine in hexadecane was used instead of pure hexadecane. PFS nanocontainers (0.03 mmol fc) and glucose oxidase (3675 units) were dialyzed (1000 MWCO, regenerated cellulose) against aqueous 0.01% SDS solution as a control or against an aqueous solution containing 0.01wt% SDS, 1.32 wt% glucose and 0.56 wt% 0.1 M HCl for several days. The total volume was 50 mL. Aliquots were taken from the outer phase at set intervals. 2-propylpyridine was quantified using UV spectroscopy.

4.1.3. PFS Nanocontainers via Double Emulsion

Final procedure for double emulsion formation

The composition of the three phases can be found in Table 16. Water was used as a solvent for the inner and outer water phase (w_i and w_o respectively), dichlormethane was used for the oil phase (*o*). w_i and *o* were stirred for 30 min at 900 rpm. The volume ratio was 1:5 (w_i to *o*). For emulsification the sample was subjected to ultrasonication for 1 min (alternating between 20 s pulse and 10 s pause) using a Branson W450-D sonifier at 69% amplitude with a 1/8 inch tip and ice-cooling. w_o was stirred separately at 375 rpm. Using a syringe pump, the preformed water in oil emulsion was added to w_o at a speed of 2.4 mL/h. The final ratio of *w*/*o* to w_o was 1:4. The dichlormethane was evaporated over night at 40 °C and 375 rpm.

Table 16. Composition of the different phases used for double emulsion formation, inner water phase (w_i), oil phase (*o*) and outer water phase (w_o).

Phase	composition
w_i	1.2 wt% NaCl 9.52×10^{-5} mol/L FITC-dextrane
o	7.5 wt% oleic acid in DCM 16 mg/mL PFS
w_o	3 wt% SDS

4.2. Poly(butadiene)-*block*-poly(ethylene oxide)-based Materials

4.2.1. Materials and Instrumentation

All materials and solvents, unless stated otherwise, were purchased from Sigma Aldrich. Butadiene and ethylene oxide were supplied by GHC Gerling. Borosilicate glass capillaries were supplied by Hilgenberg. Dialysis tubes were obtained from Spectrumlabs. The LiposoFast Basic setup as well as the polycarbonate membranes were purchased from Avestin. Chromeo 546 azide was purchased from SantaCruz Biotechnology. 4,4-Difluoro-5,7-dimethyl-4-bora-3A, 4A-diaza-s-indacene-3-propionyl ethylenediamine hydrochloride (BODIPY Amine dye) was supplied by ThermoFisher Scientific. FCS measurements were carried out by Jennifer Schultze and Inka Negwer on a commercial setup (Zeiss, Germany) consisting of the module ConfoCor 2 and an inverted microscope model Axiovert 200 with a Zeiss C-Apochromat 40×/1.2W water immersion objectiveZeiss Mikroskop (Axiovert 200, ConfoCor2). BODIPY amine was excited using an argon-ion laser (488 nm) and its emission was detected in the range 505-550 nm. Chromeo azide was excited using a helium-neon laser (543 nm) and the emission detected in the range 560-615 nm. The size of the observation volumes was calibrated using reference dyes with known diffusion coefficients, Alexa 488 and Rh6G respectively. CLSM measurements were performed on a TCS SP5 (Leica) using a 458 nm Argon laser, a 561 nm DPSS laser and a HCX PL APO CS 63x water objective. ^{1}H NMR spectra were recorded on a Bruker Avance 300 MHz spectrometer. ^{1}H DOSY (Diffusion ordered spectroscopy) spectra were measured on a Bruker 500 AMX NMR. All spectra were recorded at room temperature in CDCl$_3$. ^{1}H spectra were processed with MestReNova 10.1. ^{1}H DOSY spectra were processed with TopSpin 3.0. SEC measurements were carried out in THF. The sample concentration was 1 g L^{-1}. Three SDV columns (PSS) with a particle size of 10 μm and pore sizes of 106, 104 and 500 Å and a 1260 RID Shodex RI-101 detector (ERC) were employed. Calibration was achieved using PI standards provided by Polymer Standards Service. The eluent was used at 30 °C and a flow rate of 1 mL min^{-1}. Light scattering measurements were performed on an ALV spectrometer consisting of a goniometer and an ALV-5004 multiple-tau full-digital correlator (320 channels) which allows measurements over an angular range from 30° to 150. A He-Ne Laser (wavelength of 632.8 nm) is used as light source. For temperature controlled measurements the light scattering instrument is equipped with a thermostat from Julabo. Diluted dispersions were filtered through low protein binding hydrophilic PTFE membrane filters with a pore size of 0.45 μm (LCR Millipore). Measurements were performed at 20°C at 9 (dynamic) resp. 25 (static) angles ranging from 30° to 150.

4.2.2. PB-*b*-PEO Synthesis

In this work, three different PB-*b*-PEO polymers were used. At this point, an exemplary synthesis procedure will be given as well as the characterisation data. Reactions were carried out in flamed out glassware under argon atmosphere. Freshly prepared cumylpotassium was used as an initiator. For that, potassium (2.5 g) was washed with THF and petroleum ether and dried under vacuum. To that, THF (120 mL) and cumyl methyl ether (5.2 mL) was added (ratio potassium to cumyl methyl ether 2:1). The reaction was allowed to take place for 48 h, after which the mixture was filtered. The concentration of cumyl potassium in the filtrate was determined by an exemplary polymerisation of 1,3-butadiene and determination of the molecular weight. 1,3-butadiene was polymerised anionically in THF at -65 °C in THF to yield primarily 1,2-addition. Cumyl potassium was added to 1,3-butadiene (10 g). The polymerisation proceeded for 72 h in THF (200 mL). After that, ethylene oxide (4.3 g) was added while cooling and polymerised for 72 h. The reaction was quenched by addition of degassed methanol. The polymer was obtained by precipitation in cold acetone and dried under vacuum.
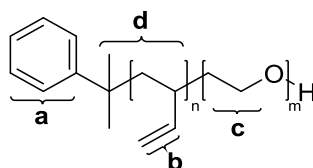
Figure 62. Poly(butadiene)-*block*-poly(ethylene oxide)

[1]**H NMR** (300 MHz, CDCl3): δ 7.24-7.07 (m, superimposed by solvent, **a**), 5.58-4.84 (m, 3nH, **b**), 3.64 (s, 4mH, **c**). 2.27-0.77 (m, 3n+6H, **d**).

4.2.3. PB-*b*-PEO Functionalisation

The hydroxyl end group of the PB-*b*-PEO polymers was functionalised to an alkyne, acrylate or succinic acid. Functionalisation of all three groups was carried out on all three PB-*b*-PEO polymers. Again only an exemplary synthesis procedure is shown together with the characterisation data. The degree of functionalisation is summarised at the end of this section in Table 8.

Alkyne Functionalisation

The procedure was adapted from literature.[197] The reaction was carried out in flamed out glassware. DCM was freshly distilled and PB-*b*-PEO was dried from benzene prior to the reaction. PB-*b*-PEO (0.2 g, 26.32 µmol) and propiolic acid (0.42 g, 6.03 mmol) were dissolved in DCM (10 mL, dry). The solution was stirred and cooled to -20 °C. A solution of

DCC (5.40 mg, 26.21 µmol) and DMAP (1.8 mg, 14.73 µmol) in DCM (3 mL, dry) was added dropwise over a period of 20 min. The cooling bath was removed and the reaction mixture was stirred for an additional 24 h at room temperature. The crude reaction mixture was washed twice with HCl (1 M, 5 mL) and brine (5 mL). The combined aqueous phase was extracted with DCM (3 mL). The combined organic phase was dried using $MgSO_4$, concentrated under reduced pressure and dialysed overnight against DCM (200 mL, 1000 MWCO dialysis tube). The product was dried under vacuum. The yield was at least 47%. The degree of functionalisation was determined from the ^{1}H NMR spectrum by the deviation of the integral of **e** from the ideal value of 2.

Figure 63. Poly(butadiene)-*block*-poly(ethylene oxide) with an alkyne end group functionalisation

^{1}**H NMR** (300 MHz, CDCl$_3$): δ 7.24-7.07 (m, superimposed by solvent, **a**), 5.58-4.84 (m, 3nH, **b**), 4.34 (t, 2H, **e**), 3.64 (s, 4(m-1)H, **c**). 3.72 (t, 2H, **f**), 2.92 (s, 1H, **g**), 2.27-0.77 (m, 3n+6H, **d**).

Acrylate Functionalisation

The procedure was adapted from literature.[198] The reaction was carried out in flamed out glassware. DCM was freshly distilled and PB-*b*-PEO was dried from benzene prior to the reaction. PB-*b*-PEO (0.2 g, 26.32 µmol) and triethyl amine (1.34 mg, 13.24 µmol, dry) were dissolved in DCM (10 mL, dry). The solution was stirred and cooled to 0 °C. Acryoyl chloride (54.5 mg, 0.60 mmol) was added dropwise. After 30 min the cooling bath was removed and the reaction mixture was stirred for an additional 72 h at room temperature. The crude reaction mixture was washed thrice with $NaHCO_3$ (saturated, 5 mL). The combined aqueous phase was extracted with DCM (5 mL). The combined organic phase was washed with water until the aqueous phase was neutral (thrice, 5 mL) and the combined organic phase was extracted again with DCM (5mL). The organic phase was dried using $MgSO_4$ and concentrated under reduced pressure. The obtained solution was dialysed overnight against DCM (200 mL, 1000 MWCO dialysis tube). The product was dried under vacuum. The yield was at least 97%.
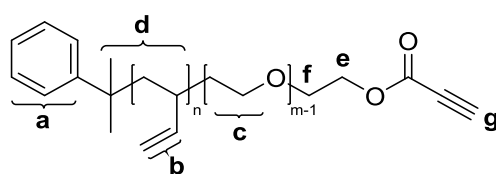
Figure 64. Poly(butadiene)-*block*-poly(ethylene oxide) with an acrylate end group functionalisation

¹H NMR (300 MHz, CDCl₃): δ 7.24-7.07 (m, superimposed by solvent, **a**), 6.47-5.84 (m, 3H, **g**), 5.58-4.84 (m, 3nH, **b**), 4.32 (t, 2H, **e**), 3.64 (s, 4(m-1)H, **c**). 3.74 (t, 2H, **f**), 2.27-0.77 (m, 3n+6H, **d**).

Succinic Acid Functionalisation

The procedure was adapted from literature.[199] The reaction was carried out in flamed out glassware. DCM was freshly distilled and PB-*b*-PEO was dried from benzene prior to the reaction. PB-*b*-PEO (0.2 g, 26.32 µmol) was dissolved in DCM (10 mL, dry). Succinic anhydride (0.12 g, 1.21 mmol) and DMAP (3.2 mg, 26.19 µmol) were added to the solution. The reaction mixture was stirred for 72 h at room temperature. The crude reaction mixture was washed with KH₂PO₄ (saturated, 5 mL). The combined aqueous phase was extracted thrice with DCM (5 mL). The combined organic phase was washed thrice with NaHCO₃ (saturated, 5 mL). The aqueous NaHCO₃ phase was extracted with DCM (5 mL). The combined organic phases were dried using Na₂SO₄ and concentrated under reduced pressure. The obtained solution was dialysed overnight against DCM (200 mL, 1000 MWCO dialysis tube). The product was dried under vacuum. The yield was at least 76%.
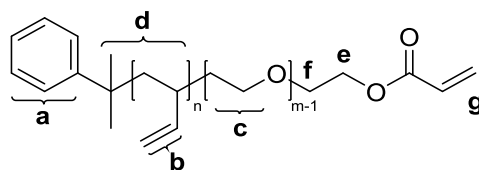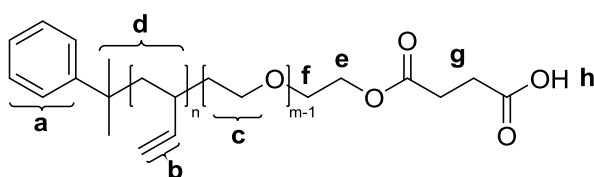

Figure 65. Poly(butadiene)-*block*-poly(ethylene oxide) with an acrylate end group functionalisation

¹H NMR (300 MHz, CDCl₃): δ 11.05 (s, 1H, **h**), 7.24-7.07 (m, superimposed by solvent, **a**), 5.58-4.84 (m, 3nH, **b**), 4.26 (t, 2H, **e**), 3.64 (s, 4(m-1)H, **c**). 3.72 (t, 2H, **f**), 2.64, (dt, 4H, **g**), 2.27-0.77 (m, 3n+6H, **d**).

4.2.4. Giant Unilamellar Vesicles via cDICE

Setup

The setup consisted of a specially manufactured chamber, consisting of two petri dishes glued together to form a closed cylinder (35 mm diameter) with an aperture (10 mm diameter) at the top. This chamber was fixed on a rotating motor. The motor was operated from 1000-1800 rpm.
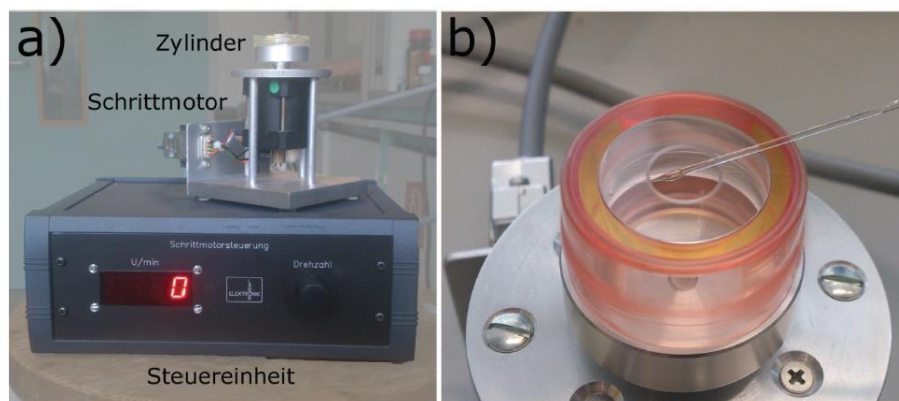
Figure 66. Setup for cDICE (a) and close up on capillary and chamber (b). Image reproduced with permission by Dr. Max Bernhardt.

Capillary preparation

Borosilicate glass capillaries (purchased from Hilgenberg) with a diameter of 5 µm were glued to the opening of a 1 mL syringe using a two component epoxy glue (UHU Plus sofortfest) in a dust free environment to prevent clogging of the capillary. After drying, the capillaries were hydrophobised by silane coating. For this, capillaries were immersed in a solution of 3-mercaptopropyltrimethoxysilane (0.1 wt%) in water/methanol (1:9). To prevent clogging, nitrogen pressure (0.8 bar) was applied to the capillary. Capillaries were dried for 1 h at 100 °C.

Polymer in oil solution

For the polymer in oil solution (POS) PB_{85}-*b*-PEO_{68} (PB-b-PEO 1) (89 mg) were dissolved in methanol/chloroform (1:9). The solvent was slowly removed under reduced pressure to form a thin polymer film at the bottom of the flask. Ethylbenzene (10 mL) and low molecular weight mineral oil (5 mL) were added and the POS was kept at 500 rpm until dissolution.

GUV production

To the rotating chamber, water (dispersing aqueous solution (DAS)), POS and decane were added in this sequence. The respective amounts are summarised in Table 17. Due to the

different densities of the liquids and the rotation of the chamber, perpendicular layers are formed (see Figure 66b). A water-filled (encapsulated aquoues solution (EAS)) capillary with an applied nitrogen pressure (see Table 17) was immersed in the decane layer. The resulting droplets were continuously sheared of by the rotation of the decane layer and transported to the DAS because of the higher density of the EAS and the rotation. EAS-droplets passed into the POS layer, leading to a coating with the amphiphilic block copolymer (coating). When the EAS-droplet passed the second interface into the DAS layer, a second coat of polymer was added (zipping), forming a GUV. Produced GUVs were collected from the DAS phase, after the rotation was gradually stopped. GUVs were labeled by addition of CellMask Deep Red. MilliQ grade water was used for all steps.

Table 17. Experimental details for cDICE runs.

Run	U/min	Pressure/ bar	DAS/ mL	POS/ mL	Decane/ mL
1	1 500	1.0	3	3	2
2	1 500	1.8	2	3	2
3	1 000	1.8	3	3	2
4	1 800	1.8	3	2	2
5	1 800	1.8	3	2	2
6	1 800	1.0	3	2	2

4.2.5. Polymersomes via Solvent Displacement

4.2.5.1. Self-assembly

Self-assembly was achieved by different techniques, the solvent displacement and the film hydration method. Generally, solvent displacement was employed, as it is more facile. Only in cases where solvent displacement was not feasible, the film hydration method was used instead. After self-assembly samples were typically extruded to reduce their polydispersity and/or size. MilliQ grade water was used for all steps.

Self-assembly via solvent displacement

About 5 mg of polymer were dissolved in THF (2 mL) and placed in a dialysis tube (1000 MWCO) and dialysed against water (400 mL) overnight. The formerly clear solution had turned opaque, indicating self-assembly. The final mass of the sample was determined.

Extrusion

The LiposoFast setup was cleaned using ethanol, THF and water. Polycarbonate

membranes were purged with water. Samples were extruded 11 times in volumes of up to 1 mL starting with a 1000 nm membrane, then a 400 nm membrane and finally a 200 nm membrane. Between different membranes, the setup was cleaned using water.

4.2.5.2.   *Dye Functionalisation*

All dye functionalisations were carried out on vesicles in aqueous solution using the functional polymers from section 4.2.3.

Chromeo 546 azide

A stock solution of Chromeo 546 azide in MilliQ grade water was prepared (5.66E-7 mol/mL) and diluted further if necessary. 0.5 eq dye (respective to the amount of alkyines) were added and allowed to react overnight. The functionalisation was proven by FCS measurements.

BODIPY Amine

A stock solution of BODIPY Amine dye in MilliQ grade water was prepared (7.42E-7 mol/mL) and diluted further if necessary. 0.5 eq dye (respective to the amount of acrylates), 0.5 eq NaOH and 0.25 eq DMAP were added to the sample and allowed to react overnight. The functionalisation was proven by FCS measurements.

4.2.6. Polymersomes via Microfluidics

Microfluidic experiments were carried out by Dr. Julien Petit at the Max Planck Institute for Dynamics and Self-organisation using the functional polymers from section 4.2.3. Labeling and Imaging was done at the Max Planck Institute for Polymer Research. All microfluidic experiments were carried out using PB_{237}-*b*-PEO_{101} and its derivatives. The solutions used in the microfluidic experiments are characterised in Table 18. The different middle fluids are listed in Table 19. A new solution (entry 4 in Table 19) containing only the alkyne functionality was prepared after a period of 10 months as the first one (entry 1 in Table 19) no longer yielded good results. The experimental details on all microfluidic samples are summarised in Table 20.

Table 18. Solutions used in microfluidic experiments.

	solvent	components	concentration
inner fluid (IF)	water	F108	1 wt%
		sucrose	0.4 M
middle fluid (MF)	oleic acid	polymer	1 wt%
outer fluid (OF)	water	F108	1 wt%
		glycerol	15 wt%
		PDADMAC	2 wt%
		ethanol	14 wt%
		sucrose	0.2 M

Table 19. Middle fluid solutions in chronological order.

Middle fuid	$m_{PB\text{-}b\text{-}PEO}$/ mg	n_{alkyne}/ nmol	$n_{acrylate}$/ nmol	$m_{oleic\ acid}$/ g
1	72.8	37	-	7.35
2	72.7	-	180	7.35
3	72.5	64	116	7.25
4	64.1	33	-	6.41

Table 20. List of experimental conditions for all microfluidics samples.

Sample	Date	MF used	IF flow rate/ µL/h	MF flow rate/ µL/h	OF flow rate/ µL/h	Run time/ h
1-10	July 2015	1	50	120	750	0.05
11-20	July 2015	1	65	85	375	0.05
1-5	August 2015	1	50	100	750	0.05
1-5	August 2015	2	50	100	700	0.05
6-8	August 2015	2	50	100	800	0.05
6-10	August 2015	3	50	100	800	0.05
1-5	October 2015	3	50	100	500	0.17
1-5	18/11/15	2	50	90	490	0.08

6-10	18/11/15	1	40	90	500	0.08
1-5	19/11/15	2	80	80	420	0.08
6-10	19/11/15	1	80	80	420	0.08
3-7	17/02/16	2	50	120	550	0.08
8-12	17/02/16	1	50	100	575	0.08
6-10	15/03/16	4	50	120	600	0.08
1-2	17/03/16	4	100	80	350	0.08
3-5	17/03/16	4	50	150	1100	0.08
6-8	17/03/16	4	50	100	450	0.08

4.2.6.1.   *Orthogonal Labeling*

Depending on whether samples contained an alkyne or acrylate functionality (or both), they were labeled using Chromeo 546 azide or BODIPY Amine (or both). The reactions were carried out as described in section 4.2.5.2. Sample aliquots of 5 or 10 µL were used for labeling. The amount of functional groups was calculated using the following equation

$$n_{\text{fg}} = \frac{M_{\text{MF, aliquot}}}{M_{\text{MF, total}}} * m_{\text{fg, total}} * FD * \frac{1}{M_{\text{n}}} \tag{9}$$

with n_{fg} the amount of functional groups, $M_{MF, aliquot}$ and $M_{MF, total}$ the mass of the middle fluid in the aliquot and the prepared solution, respectively. $m_{fg,total}$ is the amount of functional polymer in the prepared OF. *FD* is the degree of functionalisation and M_n is the molecular weight of the polymer. $M_{MF, aliquot}$ is calculated from the flow rates and the run time in Table 20, $M_{MF, total}$ and $m_{fg,total}$ are taken from Table 19. *FD* and M_n are taken from Table 8.

4.2.6.2.   *Exchange*

Sample preparation and imaging

Vesicles from PB_{237}-*b*-PEO_{101} and PB_{237}-*b*-PEO_{101}-alkyne were stained with chromeo azide. To this end, 20 µL vesicle sample (1.46E-11 mol alkyne) were mixed with 2.46 µL chromeo azide stock solution (2.95E-9 mol/mL. 0.5 eq) and left to react overnight. Vesicles from PB_{237}-*b*-PEO_{101} and PB_{237}-*b*-PEO_{101}-acrylate were stained with BODIPY amine. The vesicle sample (20 µL, 6.98E-11 mol acrylate) were mixed with BODIPY amine (4.71 µL, 7.42E-9 mol/mL, 0.5 eq), NaOH (3.49 µL, 0.1E-4 M, 0.5 eq) and DMAP (2.44 µL, 8.19E-9 mol/mL, 0.25 eq).

The reaction took place overnight. To minimise bleaching of the dyes, samples were covered in aluminium foil at all times. Samples were first measured separately, then they were mixed and aliquots were measured at certain points in time. For imaging, 2-5 µL sample were placed in an ibidi µ-Slide. Images with at least three relevant regions of interest were measured at different points in the sample. A spectrum was recorded over the same area. Regions of interest were selected over the relevant objects and the water phase for background information. Some samples drifted while recording the spectrum, in this case the ROIs were shifted accordingly for the emission maximum of each dye.

For data correction, a vesicle sample made from PB_{237}-b-PEO_{101} and PB_{237}-b-PEO_{101}-alkyne (5 µL) was mixed with different amounts of BODIPY amine (0.25 eq, 0.5 eq, 1 eq and 2 eq) and measured the same way.

Data processing and correction

Spectra were integrated from 500-520 nm (region of BODIPY amine) and 560-580 nm (region of chromeo azide). The correction factor x and the corrected integral $I_{oil, or}$ was calculated using the equations introduced in section 3.2.6.2. From the sum of the two dye's integral, the relative amount of each dye was calculated.

4.2.6.3. Functionalisation

Proof of concept by ^1H NMR spectroscopy

PB-b-PEO-acrylate (11.1 mg, 1.46E-6 mol acrylate) was dissolved in THF (4 mL) and dialysed against MilliQ grade water (600 mL) overnight using a 1000 MWCO dialysis tube. The resulting vesicle dispersion was mixed with amine-functionalised biotin (15.28 mg, 3.65E-5 mol, 25 eq) and DMAP (4.46 mg, 3.65E-5 mol, 25 eq) and stirred at 800 rpm for 5 days. Unreacted biotin and DMAP was removed by dialysis against MilliQ grade water (2 L, 2x changed over 5 days) using a 1000 MWCO dialysis tube. The purified sample was obtained after freeze-drying (8.0 mg).

Micropipette experiments

Vesicles from PB_{237}-b-PEO_{101} and PB_{237}-b-PEO_{101}-acrylate (30 µL, 9.94E*11 mol acrylate) were mixed with amine-functioanlised biotin (4.84 µL, 4.97E-11 mol, 0.5 eq) and DMAP (3.04 µL, 2.49E*11 mol, 0.25 eq). Micropipette experiments were carried out by Dr. Julien Petit at the Max Planck Institute for Dynamics and Self-organisation.

4.3. Hybrid Vesicles

Hybrid vesicles consisted of PB_{85}-b-PEO_{68} (see section 4.2.2 for synthetic details) and a saturated phospholipid - 1.2-Dipalmitoyl-sn-glycero-3-phosphoethanolamine – as well as a

corresponding fluorescent lipid - 1,2-dipalmitoyl-sn-glycero-3-phosphoethanolamine-N-(lissamine rhodamine B sulfonyl).

4.3.1. Materials and Instrumentation

All materials and solvents, unless stated otherwise, were purchased from Sigma Aldrich. The LiposoFast Basic setup, as well as the polycarbonate membranes were purchased from Avestin. 1.2-Dipalmitoyl-*sn*-glycero-3-phosphoethanolamine and 1,2-dipalmitoyl-sn-glycero-3-phosphoethanolamine-N-(lissamine rhodamine B sulfonyl) (ammonium salt) were purchased from Avanti Polar Lipids, Inc. V65 was supplied by Wako. TEM measurements were carried out on a JEOL 1400 at a voltage of 120 kV, images were recorded with a GATAN Ultrascan 1000 CCD-camera. FCCS measurements were carried out by Inka Negwer at the Max Planck Institute for Polymer Research in Mainz using an inverted Zeiss LSM880 microscope and simultaneous excitation with an argon-ion laser (488 nm) and a helium-neon laser (543 nm). The emissions were detected in the range of 500-526 nm and 598-651 nm. The sizes of the observation volumes were calibrated using reference dyes with known diffusion coefficients, Alexa 488 and Rh6G respectively. A Zeiss C-Apochromat 40x/1.2 W Autocorr M27 water immersion objective was used for the experiments. A Zeiss C-Apochromat 40x/1.2 W Autocorr M27 water immersion objective was used for the experiments. Fluorescence intensity measurements were performed on an Infinite M1000 platereader by Tecan, Austria using 96-well plates. Light scattering measurements were performed on an ALV spectrometer consisting of a goniometer and an ALV-5004 multiple-tau full-digital correlator (320 channels) which allows measurements over an angular range from 30° to 150. A He-Ne Laser (wavelength of 632.8 nm) is used as light source. For temperature controlled measurements the light scattering instrument is equipped with a thermostat from Julabo. Diluted dispersions were filtered through low protein binding hydrophilic PTFE membrane filters with a pore size of 0.45 µm (LCR Millipore). Measurements were performed at 20°C at 9 (dynamic) resp. 25 (static) angles ranging from 30° to 150. MilliqQ grade water was used at all steps.

4.3.2. Crosslinking Polymersomes

Crosslinking with a V-65

Samples were prepared using the solvent displacement method as described in section 4.2.5.1 and different amounts of the radical initiator V-65 were added to the polymer solution in THF. For that a stock solution of V65 in THF was prepared and 1.38 mol%, 2.76 mol%, 5.52 mol% and 11.04 mol% (relative to the PB double bond) were added. Self-assembly took place overnight, the extrusion steps were omitted. Crosslinking was performed on stirred

aliquots (2 mL) at 65 ^C for 4 h. Samples were imaged using TEM, 2.76 mol% V65 showed the best result.

4.3.3. Hybrid Vesicles

Self-assembly and Crosslinking

Self-assembly was achieved using the film hydration technique (see section 4.2.5.1). Solvent displacement was not feasible as the molecular weight of DPPE (692 g/mol) might result in loss of lipid during the dialysis step of the solvent displacement method. Samples were prepared as described in section 4.2.5.1, with the exception that V65 (2.76 mol% relative to PB double bond), DPPE (either 14, 9 or 4 mol% relative to PB-*b*-PEO) and Liss-Rhod DPPE (1 mol% relative to PB-*b*-PEO) were added to the polymer in THF. Depending on the use, samples were extruded or the step was omitted. Crosslinking was performed as described in section 4.3.2)

FCCS measurements

For FCCS measurements, a pure polymer sample was with PB_{85}-*b*-PEO_{68} (4.7 mg, 0.62 µmol) and acrylate-functionalised PB_{85}-*b*-PEO_{68} (1.2 mg, 0.16 µmol) was prepared using the solvent displacement method (see section 4.2.5.1). After self-assembly, BODIPY amine (0.5 eq relative to acrylate functionality, 0.08 µmol), NaOH (0.5 eq, 0.08 µmol) and DMAP (0.25 eq, 0.04 µmol) were added. The reaction took place for 72 h, after which time the BODIPY-labeled polymer was obtained by freeze-drying (5.9 mg yield). The labeled polymer was used to prepare a hybrid vesicle sample as described in section 4.3.3. Since there was no necessity for crosslinking, V65 was not added. The sample was dialysed against water (1000 mL, changed twice) using a 1000 MWCO dialysis tube to remove free BODIPY amine dye for 5 days.

4.3.4. Porous Polymersomes

Self-assembly via film hydration

 A 10 mL round bottom flask was cleaned with ethanol, THF and acetone. About 5 mg of polymer were weigthed into the flask and dissolved in THF (2 mL). The solvent was gently removed using a rotary evaporator to yield a thin polymer film at the bottom of the flask. The film was dried under vacuum (ca. 1 mbar) for 1 h. Then, a clean stirring bar and water (5 mL) were added without breaking the film. The clear sample was stirred at 500 rpm overnight, after which the self-assembly was evident by disappearance of the film and opaqueness of the sample. The final mass of the sample was determined.

DPPE extraction

DPPE extraction was monitored by fluorescent intensity of Liss Rhod DPPE. Hybrid vesicle samples were dialysed against water:ethanol (1:1, 1000 mL, 2x changed) using a 50K MWCO dialysis tube for 7 days. Aliquots (1 mL) were taken from the outer solution to be measured regarding the fluorescent intensity. The fluorescent intensity before and after the dialysis was measured with a Liss Rhod DPPE serial dilution for calibration purposes.

4.4. Poly(butadiene)-*block*-poly(ethyl ethylenephosphate)-based Materials

4.4.1. Materials and Instrumentation

TEM measurements were carried out on a JEOL 1400 at a voltage of 120 kV, images were recorded with a GATAN Ultrascan 1000 CCD-camera. ^{1}H NMR spectra were recorded on a Bruker Avance 300 MHz spectrometer. ^{1}H DOSY (Diffusion ordered spectroscopy) spectra were measured on a Bruker 500 AMX NMR. All spectra were recorded at room temperature in CDCl$_3$. ^{1}H spectra were processed with MestReNova 10.1. ^{1}H DOSY spectra were processed with TopSpin 3.0. DSC measurements were performed using a Mettler-Toledo DSC 823 at a scan rate of 10 K/min under nitrogen atmosphere. SEC measurements were carried out in THF. The sample concentration was 1 g L^{-1}. Three SDV columns (PSS) with a particle size of 10 µm and pore sizes of 106, 104 and 500 Å and a 1260 RID Shodex RI-101 detector (ERC) were employed. Calibration was achieved using PI standards provided by Polymer Standards Service. The eluent was used at 30 °C and a flow rate of 1 mL min^{-1}. Light scattering measurements were performed on an ALV spectrometer consisting of a goniometer and an ALV-5004 multiple-tau full-digital correlator (320 channels) which allows measurements over an angular range from 30° to 150. A He-Ne Laser (wavelength of 632.8 nm) is used as light source. For temperature controlled measurements the light scattering instrument is equipped with a thermostat from Julabo. Diluted dispersions were filtered through low protein binding hydrophilic PTFE membrane filters with a pore size of 0.45 µm (LCR Millipore). Measurements were performed at 20°C at 9 (dynamic) resp. 25 (static) angles ranging from 30° to 150. Extrusion was done using a LiposoFast setup and polycarbonate membranes by Avestin.

All chemicals and solvents were supplied by Sigma Aldrich unless stated otherwise. Butadiene and ethylene oxide were purchased from GHC Gerling. Cyclohexane was supplied by Fisher Chemicals. All experiments were conducted in flamed-out glassware under argon atmosphere or vacuum.

4.4.2. Synthesis

Synthesis of poly(butadiene) macroinitiator (PB-OH)

Butadiene (10 g, 0.19 mol) was added to cyclohexane (200 mL, dry) while cooling using a mixture of isopropanol and dry ice. *sec*Butyllithium (1.4 M, 1.9 mL) was added while still cooling. The polymerisation took place overnight at room temperature. Hydroxylation was achieved by adding an excess ethylene oxide (4 mL) while cooling. After 30 minutes, the cooling was removed at the mixture was left for 4 h at room temperature. The polymer was terminated using methanol.
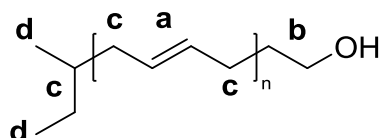

Figure 67. Poly(butadiene) macroinitator. For clarity, only the 1-4 addition is shown.

^{1}H NMR (CDCl$_3$): δ 5.59-5.48 (m, 6H, -C*H*=CH$_2$), 5.44-5.32 (m, 154H, **a**), 5.04-4.90 (m, 12H, -CH=C*H$_2$*), 3.68-3.64 (m, 4H, **b**), 2.27-1.09 (m, 329H, **c**), 0.90-0.83 (m, 6H, **d**)

Synthesis of ethyl ethylene phosphate (EEP)

A solution of ethanol (6.32 g, 137 mmol, dry) and triethylamine (13.88 g, 137 mmol, dry) in THF (15 mL, dry) was added dropwise to a stirred solution of 2-chloro-1,3,2-dioxaphospholan 2-oxide (19.55 g, 137 mmol) in THF (80 mL, dry). The reaction was stirred for two hours. The solution was filtrated under inert atmosphere and the filtrate was left overnight at -20 °C for complete precipitation of the triethylammonium chloride. The solution was concentrated in vacuo and distilled under reduced pressure to yield the product (12.26 g, 83 mmol, 61% yield, b.p. 160 °C at $8.0*10^{-1}$ mbar).
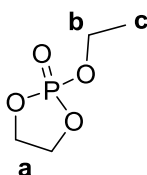

Figure 68. Ethyl ethylene phosphate

^{1}H NMR (CDCl$_3$): δ 4.42-4.24 (m, 4H, **a**), 4.17-4.06 (m, 2H, **b**), 1.28 (t, 3H, **c**, J 7.1 Hz)
^{31}P NMR (CDCl$_3$): δ 17.39.

Synthesis of N-[3,5-bis(trifluoromethyl)phenyl]-N'-cyclohexyl-thiourea (TU)

N-[3,5-bis(trifluoromethyl)phenyl]-*N'*-cyclohexyl-thiourea was synthesised according to

literature.[200] Cyclohexylamine (0.91 g, 9.19 mmol) as added dropwise to a stirred solution of 3,5-bis(trifluoromethyl)phenyl isothiocyanate (2.57 g, 9.48 mmol) in THF (10 mL, dry). After stirring the solution for five hours at room temperature, the solvent was evaporated. The crude product was recrystallized from chloroform (3.5 mL). The product was obtained from filtration of the hot solution. The product was washed with chloroform and dried in vacuum (1.63 g, 4.40 mmol, 48% yield).
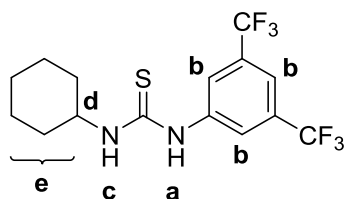
Figure 69. *N-[3,5-bis(trifluoromethyl)phenyl]-N'-cyclohexyl-thiourea*

^{1}H NMR (DMSO-d$_6$): δ 9.81 (s, 1H, **a**) 8.23-8.16 (m, 3H, **b**), 7.71 (s, 1H, **c**), 4.11 (s, 1H, **d**), 1.94-1.24 (m, 10H, **e**).

Polymerisation of ethyl ethylene phosphate (EEP)

The protocol was adapted from literature.[188] Ethyl ethylene phosphate was polymerised at 0 °C in THF using PB-OH as an initiator and 1,8-diazabicyclo[5.4.0]undec-7-ene (DBU) as a catalyst and a thiourea cocatalyst. The ratios of initiator to catalyst to cocatalyst were 1:5:5. All reactants were dried under vacuum from toluene. To a solution of PB-OH (0.25 g, 0.054 mmol) and TU (0.10 g, 0.270 mmol) in THF (0.7 mL) a solution of EEP in THF (4.0 M, 1.1 mL, 4.40 mmol) was added. The solution was cooled to 0 °C and a solution of DBU in THF (2.7 M, 0.1 mL, 0.270 mmol) was added. Polymerisation was carried out for 30 min and terminated using acetic acid in THF: The mixture was dialysed against THF in a 1000 MWCO dialysis tube for 72 h (solvent change every 24 h). The product was dried under vacuum.
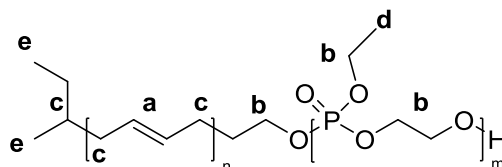
Figure 70. Poly(butadiene)-*b*-poly(ethyl ethylene phosphate).

^{1}H NMR (CDCl$_3$): δ 5.59-5.48 (m, 6H, -C*H*=CH$_2$), 5.44-5.32 (m, 154H, **a**), 5.04-4.90 (m, 12H, -CH=C*H$_2$*), 4.53--3.64 (m, 256H, **b**), 2.27-1.09 (m, 329H, **c**), 1.54-1.33 (m, 126H, **d**), 0.90-0.83 (m, 6H, **e**).

4.4.3. Self-assembly

Self-assembly by solvent displacement

PB-*b*-PEEP (5 mg) was dissolved in THF (2 mL) and dialysed against MilliQ water (400 mL) in a 1000 MWCO dialysis tube overnight. Samples were successively extruded through polycarbonate membranes of decreasing pore size (1000 nm, 400 nm and 200 nm).

TEM preparation

For TEM imaging, 8 µL sample were mixed with 2 µL OsO_4 solution (4%) and placed on a C-coated copper grid. For trehalose embedding, 8 µL sample were mixed with 2 µL OsO_4 solution and 8µL trehalose solution (1 wt% in water), placed on a lacey copper grid and blotted using filter paper.

5. Summary and Conclusion

This work presents an exploratory study towards a functional compartment usable for bottom up approach of a minimal cell. Two projects deal with permeable nanocontainers, either redox-responsive nanocapsules or permeable polymersomes. The two remaining projects deal with functional nanocontainers, i.e. polymersomes with different surface functionalisations and polymersomes from biodegradable poly(phosphoesters).

In chapter 3.1, nanocontainers from ferrocene-based materials were presented. Their functionality lies in the redox-responsive properties of the ferrocene-containing polymers. These first redox-responsive poly(ferrocenylsilane) nanocontainers were prepared in a miniemulsion approach through solvent evaporation. The redox-responsive behaviour was studied using CV, which revealed that the oxidation is hindered in dispersion. Complete oxidation of PFS nanocontainers was achieved through electrolysis, during which the nanocontainer morphology changed. Chemical or enzymatically coupled oxidation of PFS nanocontainers led to cargo release. The PFS nanocontainers add a new tool to the kit of responsive nanocarriers, enriching the field of smart materials and their application in drug delivery, self-healing applications and synthetic biology. A double emulsion/solvent evaporation protocol was found to be an unsuitable method to produce PFS nanocontainers with a hydrophilic core. An optically stable double emulsion was obtained, but the fluorophore was not retained in the inner water core. Several techniques remain to be tested, e.g. membrane emulsification, Shirasu Porous Glass (SPG) membranes or a mixromixer setup.

Chapter 3.2 deals with polymersomes made from poly(butadiene)-*block*-poly(ethylene oxide) block copolymers. Three PB-*b*-PEOs of different molecular weights and block ratios were synthesised by anionic polymersiation from a cumyl initator. In post-polymerisation reactions, the hydroxyl end group was functionalised with alkyne, acrylate or succinic acid end groups, allowing the formation of multi-functional polymersomes by mixing different functionalities together for self-assembly. Small polymersomes ranging from 100-200 nm in diameter were produced using the solvent displacement method. Vesicles were obtained from all three PB-*b*-PEO block copolymers and all three functionalities. This offers the possibility to tailor the polymersome's surface to a specific purpose, which was shown with dyes as model molecules. The cDICE technique, which was developed for lipid-based GUVs, was found to be unusable for the production of giant polymersomes. Instead, large, functional polymersomes in the µm-range were successfully produced using a microfluidic platform. Simultaneous and orthogonal labelling with the fluorescent dyes was shown. The exchange between differently labelled polymersomes was investigated. However, the system contained

to much free dye to yield a definite answer. Vesicles from PB-*b*-PEO-acrylate were biotinylated using an amine-bearing biotin. Their interactions with NeutrAvidin-coated glass was investigated using the micropipette technique. Biotinylated vesicles showed a higher adhesion force to NeutrAvidin-coated glass compared to non-biotinylated vesicles. These functional polymersomes present a versatile module for artificial cells. The succininc acid group offers the possibility to alter the surface charge of the membrane, while the alkyne and acrylate allow for chemical modifications with azides or amines respectively, using mild reaction conditions.

Chapter 3.3 introduces a hybrid vesicle system, which was modified to obtain permeable polymersomes. Hybrid vesicles were formed from DPPE and PB-*b*-PEO. After crosslinking the PB block, DPPE was extracted to form a stable, permeable vesicle. Polymersomes remained undisturbed by the extraction process. This system offers a versatile platform for further investigations. High molecular weight materials could be enclosed and protected within, while small molecules could diffuse through the permeable membrane. The size exclusion limit for a given lipid content remains to be investigated. It seems reasonable, that by increasing the lipid content before the extraction, the size exclusion limit could be pushed higher.

In chapter 3.4, polymersomes made from amphiphilic poly(phosphoester)s, an emerging class of biodegradable polymers, are presented. PB-*b*-PEEP block copolymers were prepared via ring-opening polymerisation from a PB-OH macroinitiator. Depending on the amphiphilic proportions, polymers self-assemble into polymersomes in water. Trehalose embedding, a TEM preparation method established for biological specimen, was shown to be a fast and convenient method to image these polymersomes via TEM in their native state, avoiding laborious cryo-TEM procedures. Similar to cell membranes build out of phospholipids, these polymersomes contain phosphate groups, making them a promising synthetic analogue to biological membranes.

In conclusion, different nanocarriers bearing either chemical functionalities or responsiveness were developed. In synthetic biology, such containers are needed to separate and protect their cargo and mimic certain cell functions. The functionality introduces a communication path to the outside, e.g. through redox-responsiveness or adhesion. Functional nanocarriers serve as a platform to develop interacting systems of increasing complexity until at some point, those complex systems resemble a minimal cell.

6. Zusammenfassung

Diese Arbeit präsentiert verschiedene Nanoträger, die als Baustein für eine minimale Zelle nutzbar sind. Zwei Projekte beschäftigen sich mit permeablen Nanoträgern, entweder redox-responsive Nanokapseln oder permeable Polymersome. Zwei weitere Projekte behandeln funktionelle Nanoträger, d.h. Polymersome mit verschiedenen Oberflächenfunktionalitäten und Polymersome aus bioabbaubaren Poly(phosophoestern). Es wurde besonderer Wert auf eine Funktionalität der Nanoträger, die über die Barrierefunktion hinausgeht, gelegt.

Im ersten Projekt, wurden Nanocontainer basierend auf ferrocen-haltigen Materialien entwickelt. Hier liegt die Funktionalität in den redox-responsiven Eigenschaften der ferrocen-haltigen Polymere. Zunächst wurden redox-responsive Nanocontainer basieren auf Poly(ferrocenylsilan) durch ein Miniemulsions-Lösemittelverdampfungsverfahren hergestellt. Die erhaltenen Hohlkugeln bestehen aus einer festen PFS Hülle und einem flüssigen Hexadecankern und konnten mit hydrophober Ladung versehen werden. Das redox-responsive Verhalten wurde mittels CV untersucht, wobei festgestellt wurde, dass die Oxidation in Dispersion gehindert ist. Vollständige Oxidation der PFS Nanocontainer wurde durch Elektrolyse erreicht, wodurch sich die Morphologie der Nanocontainer änderte, was durch TEM Aufnahmen veranschaulicht wurde. Chemische oder enzymatisch gekoppelte Oxidation der PFS Nanocontainer führte zur Freisetzung der hydrophoben Ladung. Weiterhin wurde versucht PFS Nanocontainer mit einem hydrophilen Inneren zu produzieren. Hierzu wurde eine Doppelemulsion mit anschließender Lösungsmittelverdampfung verwendet, allerdings konnten keine Nanocontainer nachgewiesen werden. Obwohl eine optisch stabile Dispersion durch Zugabe von Natriumchlorid als osmotisches Agens und Verwendung von Ölsäure und SDS als Tenside erreicht wurde, zeigten DLS Messungen zwei verschiedene Spezies, der Größe nach zu urteilen vermutlich feste Partikel und Hohlkugeln. FCS Messungen zeigten, dass die Hohlkugeln allerdings kein fluoreszierendes FITC-dextran enthielten, was als Marker der inneren Wasserphase zugesetzt wurde. Weiterhin waren die so hergestellten Proben recht instabil und fielen bald nach der Zugabe der Primäremulsion aus, was die inhärente Fragilität dieses Protokolls zeigt. Alternative Möglichkeiten, um PFS Nanocontainer mit hydrophilen Inneren zu generieren, sind Membranemulsifikation, SPG membranen oder ein Mikromixer.

Das zweite Projekt behandelt aus Poly(butadien)-*block*-poly(ethylenoxid) bestehende Polymersome. Drei PB-*b*-PEO Blockcopolymere wurden mittels anionischer Polymerisation mit einem Cumylinitiator hergestellt. Der hydrophile Anteil aller drei Polymere lag im oder

nahe am Bereich, in dem Polymersombildung zu erwarten wäre. Durch Postpolymerisationsreaktionen wurde die Hydroxy Endgruppe mit Alkin, Acrylat oder Bernsteinsäure Endgruppen versehen, wodurch multifunktionelle Polymersome geformt werden konnten. Weiterhin wurde versucht, eine Technik zur Produktion von GUVs aus Lipiden, cDICE, für die Herstellung von Polymersomen im μm-Bereich zu adaptieren. Allerdings war dies, aufgrund von Problemen bezüglich der Polymerlöslichkeit und Phasenseparation, nicht möglich. Stattdessen wurden kleine Polymersome im Bereich von 100-200 nm Durchmesser durch Lösungsmittelverdrängung hergestellt und mittels DLS und SLS charakterisiert. So wurde ermittelt, dass alle drei Blockcopolymere mit allen drei Funktionalitäten Vesikel bilden. Vesikel mit Alkinfunktionalität wurden mit dem funktionellen Farbstoff Chromeo Azid zur Reaktion gebracht, Vesikel mit Acrylatfunktionalität wiederum mit dem funktionellen Farbstoff BODIPY Amin. Die kovalente Anbindung der Farbstoffe wurde durch FCS nachgewiesen. Polymersome im μm-Bereich wurden über Mikrofluidik hergestellt. Die funktionellen Alkin- und Acrylatgruppen konnten simultan und orthogonal mit Farbstoffen markiert werden. Der Austausch der fluoreszenzmarkierten Polymerketten wurde untersucht, allerdings enthielt das System vermutlich zu viel freien Farbstoff, um definitive Rückschlüsse auf die Diffusion der Polymerketten ziehen zu können. Polymersome mit Acrylatgruppen wurden biotinyliert, indem sie mit amin-funktionalisiertem Biotin zur Reaktion gebracht wurden. Die Interaktion der biotinylierten Vesikel mit NeutrAvidin-beschichtetem Glas wurde mittels einer Mikropipette untersucht. Biotinylierte Polymersome zeigten eine sehr viel höhere Adhäsion an das beschichtete Glas als unfunktionalisierte Polymersome.

Das dritte Projekt etabliert Hybridvesikel als PB-*b*-PEO Blockcopolymeren und Lipiden. Diese Hybridvesikel wurden modifiziert, um so permeable Polymersome zu erhalten. Hierzu wurden Vesikel aus PB-*b*-PEO radikalisch an der Doppelbindung vernetzt, wodurch sie ihre vesikuläre Form auch außerhalb von Lösungsmittel behielten, was TEM Messungen im Trockenen erlaubte. Hybridvesikel wurden durch Mischen des Lipids DPPE mit Blockcopolymer über die Filmhydratationsmethode hergestellt. Vesikelbildung wurde durch Lichtstreuung bestätigt. Erneut wurde die Doppelbindung radikalisch vernetzt, wodurch die Vesikelbildung auch mittels TEM bestätigt werden konnte. Die Existenz von Hybridvesikeln wurde durch FCCS Messungen nachgewiesen. Das Lipid wurde aus den vernetzten Vesikeln extrahiert, was durch Fluoreszenzintensität verfolgt und quantifiziert wurde. Nach abgeschlossener Extraktion behielten die Vesikel ihre Struktur, was durch Lichtstreuung gezeigt wurde. Dieses System stellt eine Plattform für weitere Anwendungen dar. Hochmolekulare Materialien können sicher eingeschlossen werden, während

niedermolekulare Substanzen frei über die Membran diffundieren können. Die Ausschlussgrenze bezüglich des Molekulargewichts muss hier noch näher untersucht werden, doch es liegt nahe, dass diese durch die initiale Lipidmenge moduliert werden kann.

Das vierte Projekt zeigt Polymersome aus einem neuartigen, amphiphilen Poly(phosphoester), eine Klasse von potentiell bioabbaubaren Polymeren. Poly(butadien)-*block*-poly(ethyl ethylenpohsphat) Blockcopolymere wurden durch ringöffnende Polymerisation von EEP an einen PB-OH Makroinitiator hergestellt. Die Selbstanordnung zu Polymersomen in Wasser wurde anhand von Lichtstreuung und TEM gezeigt. Weiterhin wurde eine für biologische Proben etablierte TEM-Präparationsmethode, die Trehaloseeinbettung, erfolgreich für die hier gezeigten Polymersome verwendet. Dies ist eine einfache und effiziente Möglichkeit, um aufwändige cryoTEM Messungen zu umgehen. Die entwickelten Polymersome tragen, wie die Phospholipide der Zellmembran, eine Phosphatgruppe in ihrem hydrophilen Block, was sie zu einem vielversprechenden, synthetischen Analogon zu biologischen Membranen macht.

Diese Arbeit präsentiert eine Auswahl verschiedener Nanocarrier, die unterschiedliche Funktionalitäten tragen. Sie bieten eine Ausgangsplattform, um komplexere Systeme mit interagierenden Bausteinen zusammenzustellen, um so letztendlich ein komplexes System, das einer minimalen Zelle gleicht, zu erreichen.

Literature

[1] A. Marmur, *Langmuir* **2004**, *20*, 3517.

[2] A. R. Parker, H. E. Townley, *Nat Nano* **2007**, *2*, 347.

[3] D. Porter, F. Vollrath, *Adv. Mater.* **2009**, *21*, 487.

[4] S. Rasmussen, L. Chen, M. Nilsson, S. Abe, *Artificial Life* **2003**, *9*, 269.

[5] Z. Deng, Y. Qian, Y. Yu, G. Liu, J. Hu, G. Zhang, S. Liu, *J. Am. Chem. Soc.* **2016**, *138*, 10452.

[6] K. Piradashvili, E. M. Alexandrino, F. R. Wurm, K. Landfester, *Chem. Rev.* **2016**, *116*, 2141.

[7] N. Eslahi, M. Abdorahim, A. Simchi, *Biomacromolecules* **2016**, *17*, 3441.

[8] A.-M. Caminade, D. Yan, D. K. Smith, *Chem. Soc. Rev.* **2015**, *44*, 3870.

[9] Y. Li, K. Xiao, W. Zhu, W. Deng, K. S. Lam, *Advanced Drug Delivery Reviews* **2014**, *66*, 58.

[10] T. Y. Dora Tang, C. Rohaida Che Hak, A. J. Thompson, M. K. Kuimova, D. S. Williams, A. W. Perriman, S. Mann, *Nat Chem* **2014**, *6*, 527.

[11] A. Jesorka, O. Orwar, *Annual Review of Analytical Chemistry* **2008**, *1*, 801.

[12] B. M. Discher, Y.-Y. Won, D. S. Ege, J. C.-M. Lee, F. S. Bates, D. E. Discher, D. A. Hammer, *Science* **1999**, *284*, 1143.

[13] X. Liu, P. Zhou, Y. Huang, M. Li, X. Huang, S. Mann, *Angew. Chem. Int. Ed.* **2016**, *55*, 7095.

[14] M. Li, X. Huang, T. Y. D. Tang, S. Mann, *Curr. Opin. Chem. Biol.* **2014**, *22*, 1.

[15] E. Amstad, S.-H. Kim, D. A. Weitz, *Angew. Chem. Int. Ed.* **2012**, *51*, 12499.

[16] B. Iyisan, A. Janke, P. Reichenbach, L. M. Eng, D. Appelhans, B. Voit, *ACS Applied Materials & Interfaces* **2016**, *8*, 15788.

[17] N. P. Kamat, S. J. Henry, D. Lee, D. A. Hammer, *Small* **2013**, *9*, 2272.

[18] C. K. Weiss, K. Landfester, "Miniemulsion Polymerization as a Means to Encapsulate Organic and Inorganic Materials", in *Hybrid Latex Particles: Preparation with (Mini)emulsion Polymerization*, A.M. van Herk and K. Landfester, Eds., Springer Berlin Heidelberg, Berlin, Heidelberg, **2010**, p. 198.

[19] F. Z. Eram Sharmin, "*Polyurethane: An Introduction"*, InTech, **2012**, p. 9.

[20] D. F. O'Brien, B. Armitage, A. Benedicto, D. E. Bennett, H. G. Lamparski, Y.-S. Lee, W. Srisiri, T. M. Sisson, *Acc. Chem. Res.* **1998**, *31*, 861.

[21] J. Ding, G. Liu, *The Journal of Physical Chemistry B* **1998**, *102*, 6107.

[22] C. Nardin, T. Hirt, J. Leukel, W. Meier, *Langmuir* **2000**, *16*, 1035.

[23] E. V. Skorb, H. Möhwald, *Advanced Materials Interfaces* **2014**, *1*, 1400237.

[24] B. Kang, P. Okwieka, S. Schöttler, S. Winzen, J. Langhanki, K. Mohr, T. Opatz, V. Mailänder, K. Landfester, F. R. Wurm, *Angew. Chem. Int. Ed.* **2015**, *54*, 7436.

[25] X. Yan, M. Delgado, A. Fu, P. Alcouffe, S. G. Gouin, E. Fleury, J. L. Katz, F. Ganachaud, J. Bernard, *Angew. Chem. Int. Ed.* **2014**, *53*, 6910.

[26] G. Baier, D. Baumann, J. M. Siebert, A. Musyanovych, V. Mailänder, K. Landfester, *Biomacromolecules* **2012**, *13*, 2704.

[27] W. Li, J. A. Yoon, K. Matyjaszewski, *J. Am. Chem. Soc.* **2010**, *132*, 7823.

[28] R. H. Staff, M. Gallei, K. Landfester, D. Crespy, *Macromolecules* **2014**, *47*, 4876.

[29] H. Iatrou, K. Dimas, M. Gkikas, C. Tsimblouli, S. Sofianopoulou, *Macromolecular Bioscience* **2014**, *14*, 1222.

[30] W. Y. Ayen, B. Chintankumar, J. P. Jain, N. Kumar, *Polym. Adv. Technol.* **2011**, *22*, 158.

[31] H.-Y. Chang, Y.-L. Lin, Y.-J. Sheng, H.-K. Tsao, *Macromolecules* **2013**, *46*, 5644.

[32] H. Bermudez, A. K. Brannan, D. A. Hammer, F. S. Bates, D. E. Discher, *Macromolecules* **2002**, *35*, 8203.

[33] F. Itel, M. Chami, A. Najer, S. Lörcher, D. Wu, I. A. Dinu, W. Meier, *Macromolecules* **2014**, *47*, 7588.

[34] F. Ahmed, P. J. Photos, D. E. Discher, *Drug Dev. Res.* **2006**, *67*, 4.

[35] D. E. Discher, F. Ahmed, *Annual Review of Biomedical Engineering* **2006**, *8*, 323.

[36] H.-Y. Chang, Y.-J. Sheng, H.-K. Tsao, *Soft Matter* **2014**, *10*, 6373.

[37] J. N. Israelachvili, D. J. Mitchell, B. W. Ninham, *Journal of the Chemical Society, Faraday Transactions 2: Molecular and Chemical Physics* **1976**, *72*, 1525.

[38] R. Bleul, R. Thiermann, M. Maskos, *Macromolecules* **2015**, *48*, 7396.

[39] S. Jain, F. S. Bates, *Macromolecules* **2004**, *37*, 1511.

[40] D. E. Discher, A. Eisenberg, *Science* **2002**, *297*, 967.

[41] Y. Mai, A. Eisenberg, *Chem. Soc. Rev.* **2012**, *41*, 5969.

[42] C. Kirby, G. Gregoriadis, *Nat Biotech* **1984**, *2*, 979.

[43] H. Kukuchi, H. Yamauchi, S. Hirota, *CHEMICAL & PHARMACEUTICAL BULLETIN* **1991**, *39*, 1522.

[44] K. Kita-Tokarczyk, J. Grumelard, T. Haefele, W. Meier, *Polymer* **2005**, *46*, 3540.

[45] N. Berger, A. Sachse, J. Bender, R. Schubert, M. Brandl, *Int. J. Pharm.* **2001**, *223*, 55.

[46] B. Mui, L. Chow, M. J. Hope, *Methods Enzymol.* **2003**, *367*, 3.

[47] H. R. Marsden, C. B. Quer, E. Y. Sanchez, L. Gabrielli, W. Jiskoot, A. Kros, *Biomacromolecules* **2010**, *11*, 833.

[48] M. E. Yildiz, R. K. Prud'homme, I. Robb, D. H. Adamson, *Polym. Adv. Technol.* **2007**, *18*, 427.

[49] M. Pons, M. Foradada, J. Estelrich, *Int. J. Pharm.* **1993**, *95*, 51.

[50] A. Jahn, J. E. Reiner, W. N. Vreeland, D. L. DeVoe, L. E. Locascio, M. Gaitan, *J. Nanopart. Res.* **2008**, *10*, 925.

[51] K. Kuribayashi, G. Tresset, C. Ph, H. Fujita, S. Takeuchi, *Meas. Sci. Technol.* **2006**, *17*, 3121.

[52] A. Jahn, S. M. Stavis, J. S. Hong, W. N. Vreeland, D. L. DeVoe, M. Gaitan, *ACS Nano* **2010**, *4*, 2077.

[53] E. Lorenceau, A. S. Utada, D. R. Link, G. Cristobal, M. Joanicot, D. A. Weitz, *Langmuir* **2005**, *21*, 9183.

[54] C. Martino, S.-H. Kim, L. Horsfall, A. Abbaspourrad, S. J. Rosser, J. Cooper, D. A. Weitz, *Angew. Chem. Int. Ed.* **2012**, *51*, 6416.

[55] H. C. Shum, Y.-j. Zhao, S.-H. Kim, D. A. Weitz, *Angew. Chem. Int. Ed.* **2011**, *50*, 1648.

[56] L. Brown, S. L. McArthur, P. C. Wright, A. Lewis, G. Battaglia, *Lab on a Chip* **2010**, *10*, 1922.

[57] M. Sauer, T. Haefele, A. Graff, C. Nardin, W. Meier, *Chem. Commun.* **2001**, 2452.

[58] M. I. Angelova, D. S. Dimitrov, *Faraday Discussions of the Chemical Society* **1986**, *81*, 303.

[59] D. J. Estes, M. Mayer, *Colloids and Surfaces B: Biointerfaces* **2005**, *42*, 115.

[60] J. Lasch, *Biochimica et Biophysica Acta (BBA) - Reviews on Biomembranes* **1995**, *1241*, 269.

[61] R. L. Hamilton, J. Goerke, L. S. Guo, M. C. Williams, R. J. Havel, *J. Lipid Res.* **1980**, *21*, 981.

[62] S. Hauschild, U. Lipprandt, A. Rumplecker, U. Borchert, A. Rank, R. Schubert, S. Förster, *Small* **2005**, *1*, 1177.

[63] S. Pautot, B. J. Frisken, D. A. Weitz, *Proceedings of the National Academy of Sciences* **2003**, *100*, 10718.

[64] J. R. Howse, R. A. L. Jones, G. Battaglia, R. E. Ducker, G. J. Leggett, A. J. Ryan, *Nat Mater* **2009**, *8*, 507.

[65] R. Bleul, R. Thiermann, G. U. Marten, M. J. House, T. G. S. Pierre, U. O. Hafeli, M. Maskos, *Nanoscale* **2013**, *5*, 11385.

[66] M. Marguet, L. Edembe, S. Lecommandoux, *Angew. Chem. Int. Ed.* **2012**, *51*, 1173.

[67] L. Hosta-Rigau, P. Schattling, B. M. Teo, M. E. Lynge, B. Stadler, *Journal of Materials Chemistry B* **2014**, *2*, 6686.

[68] F. Perche, V. P. Torchilin, *Journal of Drug Delivery* **2013**, *2013*, 32.

[69] Y. Maitani, A. Nakamura, T. Tanaka, Y. Aso, *Int. J. Pharm.* **2012**, *427*, 372.

[70] G. Blume, G. Cevc, *Biochimica et Biophysica Acta (BBA) - Biomembranes* **1990**, *1029*, 91.

[71] J.-i. Yokoe, S. Sakuragi, K. Yamamoto, T. Teragaki, K.-i. Ogawara, K. Higaki, N. Katayama, T. Kai, M. Sato, T. Kimura, *Int. J. Pharm.* **2008**, *353*, 28.

[72] Z. Cao, L. Zhang, S. Jiang, *Langmuir* **2012**, *28*, 11625.

[73] L. Ren, S. Chen, H. Li, Z. Zhang, J. Zhong, M. Liu, X. Zhou, *Acta Biomaterialia* **2016**, *35*, 260.

[74] R. Wang, Cao, H., Tian, Z., Jin, B., Wang, Q., Ma, H., Wu, J., *Oncology Reports* **2015**, *33*, 783.

[75] L. Jiang, L. Li, X. He, Q. Yi, B. He, J. Cao, W. Pan, Z. Gu, *Biomaterials* **2015**, *52*, 126.

[76] P. Vabbilisetty, X.-L. Sun, *Organic & Biomolecular Chemistry* **2014**, *12*, 1237.

[77] M. Köhn, R. Breinbauer, *Angew. Chem.* **2004**, *116*, 3168.

[78] A. M. Bayer, S. Alam, S. I. Mattern-Schain, M. D. Best, *Chemistry – A European Journal* **2014**, *20*, 3350.

[79] S. Alam, D. S. Alves, S. A. Whitehead, A. M. Bayer, C. D. McNitt, V. V. Popik, F. N. Barrera, M. D. Best, *Bioconjugate Chem.* **2015**, *26*, 1021.

[80] P. P. Karmali, A. Chaudhuri, *Medicinal Research Reviews* **2007**, *27*, 696.

[81] Y. Obata, D. Suzuki, S. Takeoka, *Bioconjugate Chem.* **2008**, *19*, 1055.

[82] Z. Yuan, T. W. Hanks, *Polymer* **2008**, *49*, 5023.

[83] T. Peng, Q. Cheng, R. C. Stevens, *Anal. Chem.* **2000**, *72*, 1611.

[84] P. Brož, S. M. Benito, C. Saw, P. Burger, H. Heider, M. Pfisterer, S. Marsch, W. Meier, P. Hunziker, *J. Controlled Release* **2005**, *102*, 475.

[85] J. J. Lin, P. P. Ghoroghchian, Y. Zhang, D. A. Hammer, *Langmuir* **2006**, *22*, 3975.

[86] R. Nehring, C. G. Palivan, S. Moreno-Flores, A. Mantion, P. Tanner, J. L. Toca-Herrera, A. Thunemann, W. Meier, *Soft Matter* **2010**, *6*, 2815.

[87] M. Felici, M. Marzá-Pérez, N. S. Hatzakis, R. J. M. Nolte, M. C. Feiters, *Chemistry – A European Journal* **2008**, *14*, 9914.

[88] J. A. Opsteen, R. P. Brinkhuis, R. L. M. Teeuwen, D. W. P. M. Lowik, J. C. M. v. Hest, *Chem. Commun.* **2007**, 3136.

[89] S. F. M. van Dongen, M. Nallani, S. Schoffelen, J. J. L. M. Cornelissen, R. J. M. Nolte, J. C. M. van Hest, *Macromol. Rapid Commun.* **2008**, *29*, 321.

[90] S. F. M. van Dongen, W. P. R. Verdurmen, R. J. R. W. Peters, R. J. M. Nolte, R. Brock, J. C. M. van Hest, *Angew. Chem. Int. Ed.* **2010**, *49*, 7213.

[91] Z. Pang, W. Lu, H. Gao, K. Hu, J. Chen, C. Zhang, X. Gao, X. Jiang, C. Zhu, *J. Controlled Release* **2008**, *128*, 120.

[92] X. Yang, J. J. Grailer, I. J. Rowland, A. Javadi, S. A. Hurley, V. Z. Matson, D. A. Steeber, S. Gong, *ACS Nano* **2010**, *4*, 6805.

[93] M. A. Petersen, L. Yin, E. Kokkoli, M. A. Hillmyer, *Polymer Chemistry* **2010**, *1*, 1281.

[94] S. Egli, M. G. Nussbaumer, V. Balasubramanian, M. Chami, N. Bruns, C. Palivan, W. Meier, *J. Am. Chem. Soc.* **2011**, *133*, 4476.

[95] S. Domes, V. Filiz, J. Nitsche, A. Frömsdorf, S. Förster, *Langmuir* **2010**, *26*, 6927.

[96] D. Demirgoz, T. O. Pangburn, K. P. Davis, S. Lee, F. S. Bates, E. Kokkoli, *Soft Matter* **2009**, *5*, 2011.

[97] H. R. Marsden, J.-W. Handgraaf, F. Nudelman, N. A. J. M. Sommerdijk, A. Kros, *J. Am. Chem. Soc.* **2010**, *132*, 2370.

[98] Z. Hordyjewicz-Baran, L. You, B. Smarsly, R. Sigel, H. Schlaad, *Macromolecules* **2007**, *40*, 3901.

[99] S. F. M. van Dongen, H.-P. M. de Hoog, R. J. R. W. Peters, M. Nallani, R. J. M. Nolte, J. C. M. van Hest, *Chem. Rev.* **2009**, *109*, 6212.

[100] B. Le Droumaguet, K. Velonia, *Angew. Chem. Int. Ed.* **2008**, *47*, 6263.

[101] N. Cottenye, F. Teixeira, A. Ponche, G. Reiter, K. Anselme, W. Meier, L. Ploux, C. Vebert-Nardin, *Macromolecular Bioscience* **2008**, *8*, 1161.

[102] F. Liu, A. Eisenberg, *J. Am. Chem. Soc.* **2003**, *125*, 15059.

[103] S. Yu, T. Azzam, I. Rouiller, A. Eisenberg, *J. Am. Chem. Soc.* **2009**, *131*, 10557.

[104] X. Xiao, S. He, M. Dan, F. Huo, W. Zhang, *Chem. Commun.* **2014**, *50*, 3969.

[105] R. T. Pearson, N. J. Warren, A. L. Lewis, S. P. Armes, G. Battaglia, *Macromolecules* **2013**, *46*, 1400.

[106] S. Qin, Y. Geng, D. E. Discher, S. Yang, *Adv. Mater.* **2006**, *18*, 2905.

[107] F. Liu, V. Kozlovskaya, S. Medipelli, B. Xue, F. Ahmad, M. Saeed, D. Cropek, E. Kharlampieva, *Chem. Mater.* **2015**, *27*, 7945.

[108] H. Yoshimitsu, E. Korchagina, A. Kanazawa, S. Kanaoka, F. M. Winnik, S. Aoshima, *Polymer Chemistry* **2016**, *7*, 2062.

[109] Z.-Y. Qiao, R. Ji, X.-N. Huang, F.-S. Du, R. Zhang, D.-H. Liang, Z.-C. Li, *Biomacromolecules* **2013**, *14*, 1555.

[110] X. Chi, X. Ji, D. Xia, F. Huang, *J. Am. Chem. Soc.* **2015**, *137*, 1440.

[111] S. Cerritelli, D. Velluto, J. A. Hubbell, *Biomacromolecules* **2007**, *8*, 1966.

[112] A. Kumar, S. V. Lale, S. Mahajan, V. Choudhary, V. Koul, *ACS Applied Materials & Interfaces* **2015**, *7*, 9211.

[113] W.-F. Dong, A. Kishimura, Y. Anraku, S. Chuanoi, K. Kataoka, *J. Am. Chem. Soc.* **2009**, *131*, 3804.

[114] A. Napoli, M. Valentini, N. Tirelli, M. Muller, J. A. Hubbell, *Nat Mater* **2004**, *3*, 183.

[115] Q. Yan, J. Yuan, Z. Cai, Y. Xin, Y. Kang, Y. Yin, *J. Am. Chem. Soc.* **2010**, *132*, 9268.

[116] E. Blasco, J. L. Serrano, M. Piñol, L. Oriol, *Macromolecules* **2013**, *46*, 5951.

[117] G. Liu, X. Wang, J. Hu, G. Zhang, S. Liu, *J. Am. Chem. Soc.* **2014**, *136*, 7492.

[118] X. Wang, G. Liu, J. Hu, G. Zhang, S. Liu, *Angew. Chem. Int. Ed.* **2014**, *53*, 3138.

[119] Q. Yan, R. Zhou, C. Fu, H. Zhang, Y. Yin, J. Yuan, *Angew. Chem.* **2011**, *123*, 5025.

[120] Q. Yan, H. Zhang, Y. Zhao, *ACS Macro Letters* **2014**, *3*, 472.

[121] Q. Yan, W. Sang, *Chemical Science* **2016**, *7*, 2100.

[122] T. Ruysschaert, A. F. P. Sonnen, T. Haefele, W. Meier, M. Winterhalter, D. Fournier, *J. Am. Chem. Soc.* **2005**, *127*, 6242.

[123] M. Chemin, P.-M. Brun, S. Lecommandoux, O. Sandre, J.-F. Le Meins, *Soft Matter* **2012**, *8*, 2867.

[124] J. Nam, P. A. Beales, T. K. Vanderlick, *Langmuir* **2011**, *27*, 1.

[125] J. F. Le Meins, C. Schatz, S. Lecommandoux, O. Sandre, *Mater. Today* **2013**, *16*, 397.

[126] J. Chen, H.-N. Son, J. J. Hill, S. Srinivasan, F.-Y. Su, P. S. Stayton, A. J. Convertine, D. M. Ratner, *Nanomedicine: Nanotechnology, Biology and Medicine* **2016**, *12*, 2031.

[127] T. Kaiden, E. Yuba, A. Harada, Y. Sakanishi, K. Kono, *Bioconjugate Chem.* **2011**, *22*, 1909.

[128] Z. Cheng, A. Tsourkas, *Langmuir* **2008**, *24*, 8169.

[129] X. Gao, Y. Cui, R. M. Levenson, L. W. K. Chung, S. Nie, *Nat Biotech* **2004**, *22*, 969.

[130] R. Savić, L. Luo, A. Eisenberg, D. Maysinger, *Science* **2003**, *300*, 615.

[131] H. B. Na, I. C. Song, T. Hyeon, *Adv. Mater.* **2009**, *21*, 2133.

[132] L.-P. Lv, Y. Zhao, N. Vilbrandt, M. Gallei, A. Vimalanandan, M. Rohwerder, K. Landfester, D. Crespy, *J. Am. Chem. Soc.* **2013**, *135*, 14198.

[133] Q. Chen, H. Schönherr, G. J. Vancso, *Small* **2009**, *5*, 1436.

[134] G. Chen, A. S. Hoffman, *Nature* **1995**, *373*, 49.

[135] T. Tanaka, *Phys. Rev. Lett.* **1978**, *40*, 820.

[136] M. Irie, "Stimuli-responsive poly(N-isopropylacrylamide). Photo- and chemical-induced phase transitions", in *Responsive Gels: Volume Transitions II*, K. Dušek, Ed., Springer Berlin Heidelberg, **1993**, p. 49.

[137] J. S. Stamler, *Cell* **1994**, *78*, 931.

[138] P. N. Ciesielski, C. J. Faulkner, M. T. Irwin, J. M. Gregory, N. H. Tolk, D. E. Cliffel, G. K. Jennings, *Adv. Funct. Mater.* **2010**, *20*, 4048.

[139] K. Liang, G. K. Such, Z. Zhu, Y. Yan, H. Lomas, F. Caruso, *Adv. Mater.* **2011**, *23*, H273.

[140] S. Bian, J. Zheng, X. Tang, D. Yi, Y. Wang, W. Yang, *Chem. Mater.* **2015**, *27*, 1262.

[141] N. Ma, Y. Li, H. Xu, Z. Wang, X. Zhang, *J. Am. Chem. Soc.* **2010**, *132*, 442.

[142] A. F. Cunningham, *J. Am. Chem. Soc.* **1991**, *113*, 4864.

[143] R. H. Staff, M. Gallei, M. Mazurowski, M. Rehahn, R. Berger, K. Landfester, D. Crespy, *ACS Nano* **2012**, *6*, 9042.

[144] J. Elbert, F. Krohm, C. Rüttiger, S. Kienle, H. Didzoleit, B. N. Balzer, T. Hugel, B. Stühn, M. Gallei, A. Brunsen, *Adv. Funct. Mater.* **2014**, *24*, 1591.

[145] J. Galloro, M. Ginzburg, H. Míguez, S. M. Yang, N. Coombs, A. Safa-Sefat, J. E. Greedan, I. Manners, G. A. Ozin, *Adv. Funct. Mater.* **2002**, *12*, 382.

[146] A. Natalello, A. Alkan, A. Friedel, I. Lieberwirth, H. Frey, F. R. Wurm, *ACS Macro Letters* **2013**, *2*, 313.

[147] L. Cao, J. A. Massey, M. A. Winnik, I. Manners, S. Riethmüller, F. Banhart, J. P. Spatz, M. Möller, *Adv. Funct. Mater.* **2003**, *13*, 271.

[148] Y. Ma, W.-F. Dong, M. A. Hempenius, H. Mohwald, G. Julius Vancso, *Nat Mater* **2006**, *5*, 724.

[149] K. Kulbaba, A. Cheng, A. Bartole, S. Greenberg, R. Resendes, N. Coombs, A. Safa-Sefat, J. E. Greedan, H. D. H. Stöver, G. A. Ozin, I. Manners, *J. Am. Chem. Soc.* **2002**, *124*, 12522.

[150] A. C. Arsenault, D. A. Rider, N. Tétreault, J. I. L. Chen, N. Coombs, G. A. Ozin, I. Manners, *J. Am. Chem. Soc.* **2005**, *127*, 9954.

[151] S. B. Barrios, J. F. Petry, C. K. Weiss, C. L. Petzhold, K. Landfester, *J. Appl. Polym. Sci.* **2014**, *131*, n/a.

[152] D. Wu, V. Hornof, *Chem. Eng. Commun.* **1999**, *172*, 85.

[153] K. Kulbaba, I. Manners, *Macromol. Rapid Commun.* **2001**, *22*, 711.

[154] J.-F. Gohy, B. G. G. Lohmeijer, A. Alexeev, X.-S. Wang, I. Manners, M. A. Winnik, U. S. Schubert, *Chemistry – A European Journal* **2004**, *10*, 4315.

[155] J. B. Gilroy, S. K. Patra, J. M. Mitchels, M. A. Winnik, I. Manners, *Angew. Chem. Int. Ed.* **2011**, *50*, 5851.

[156] F. Wurm, S. Hilf, H. Frey, *Chemistry – A European Journal* **2009**, *15*, 9068.

[157] X.-J. Wang, L. Wang, J.-J. Wang, T. Chen, *Electrochim. Acta* **2007**, *52*, 3941.

[158] P. J. Peerce, A. J. Bard, *Journal of Electroanalytical Chemistry and Interfacial Electrochemistry* **1980**, *114*, 89.

[159] F. M. Fomin, K. S. Zaitseva, *Russ. J. Phys. Chem.* **2014**, *88*, 466.

[160] P. Greenspan, E. P. Mayer, S. D. Fowler, *The Journal of Cell Biology* **1985**, *100*, 965.

[161] W. Chen, C. Zhang, L. Song, M. Sommerfeld, Q. Hu, *J. Microbiol. Methods* **2009**, *77*, 41.

[162] K. N. Power-Billard, R. J. Spontak, I. Manners, *Angew. Chem. Int. Ed.* **2004**, *43*, 1260.

[163] R. Atkin, P. Davies, J. Hardy, B. Vincent, *Macromolecules* **2004**, *37*, 7979.

[164] C. Rocker, M. Potzl, F. Zhang, W. J. Parak, G. U. Nienhaus, *Nat Nano* **2009**, *4*, 577.

[165] K. Koynov, H.-J. Butt, *Current Opinion in Colloid & Interface Science* **2012**, *17*, 377.

[166] S. van der Graaf, C. G. P. H. Schroën, R. M. Boom, *Journal of Membrane Science* **2005**, *251*, 7.

[167] C. Charcosset, *J. Food Eng.* **2009**, *92*, 241.

[168] W. Ehrfeld, K. Golbig, V. Hessel, H. Löwe, T. Richter, *Industrial & Engineering Chemistry Research* **1999**, *38*, 1075.

[169] M. Abkarian, E. Loiseau, G. Massiera, *Soft Matter* **2011**, *7*, 4610.

[170] W. Schärtl, "*Light Scattering from Polymer Solutions and Nanoparticle Dispersions"*, Springer Laboratory, **2007**, p. 24.

[171] J. Petit, I. Polenz, J.-C. Baret, S. Herminghaus, O. Bäumchen, *The European Physical Journal E* **2016**, *39*, 1.

[172] H. C. Shum, D. Lee, I. Yoon, T. Kodger, D. A. Weitz, *Langmuir* **2008**, *24*, 7651.

[173] O. H. Laitinen, V. P. Hytönen, H. R. Nordlund, M. S. Kulomaa, *Cellular and Molecular Life Sciences CMLS* **2006**, *63*, 2992.

[174] B. M. Discher, D. A. Hammer, F. S. Bates, D. E. Discher, *Current Opinion in Colloid & Interface Science* **2000**, *5*, 125.

[175] M. S. Kim, D. S. Lee, *Chem. Commun.* **2010**, *46*, 4481.

[176] J. Gaitzsch, D. Appelhans, L. Wang, G. Battaglia, B. Voit, *Angew. Chem. Int. Ed.* **2012**, *51*, 4448.

[177] R. Cheng, F. Meng, S. Ma, H. Xu, H. Liu, X. Jing, Z. Zhong, *J. Mater. Chem.* **2011**, *21*, 19013.

[178] M. Spulber, A. Najer, K. Winkelbach, O. Glaied, M. Waser, U. Pieles, W. Meier, N. Bruns, *J. Am. Chem. Soc.* **2013**, *135*, 9204.

[179] W. Siti, H.-P. M. de Hoog, O. Fischer, W. Y. Shan, N. Tomczak, M. Nallani, B. Liedberg, *Journal of Materials Chemistry B* **2014**, *2*, 2733.

[180] L. K. Müller, K. Landfester, *Biochem. Biophys. Res. Commun.* **2015**, *468*, 411.

[181] Z. Cheng, A. Al Zaki, I. W. Jones, H. K. Hall, C. A. Aspinwall, A. Tsourkas, *Chem. Commun.* **2014**, *50*, 2502.

[182] J. Liu, H. Ma, T. Wei, X.-J. Liang, *Chem. Commun.* **2012**, *48*, 4869.

[183] W. Mueller, K. Koynov, K. Fischer, S. Hartmann, S. Pierrat, T. Basché, M. Maskos, *Macromolecules* **2009**, *42*, 357.

[184] K. Jaskiewicz, A. Larsen, I. Lieberwirth, K. Koynov, W. Meier, G. Fytas, A. Kroeger, K. Landfester, *Angew. Chem.* **2012**, *124*, 4691.

[185] F. Wang, Y.-C. Wang, L.-F. Yan, J. Wang, *Polymer* **2009**, *50*, 5048.

[186] T. Steinbach, F. R. Wurm, *Angew. Chem. Int. Ed.* **2015**, *54*, 6098.

[187] R. P. Quirk, J.-J. Ma, *J. Polym. Sci., Part A: Polym. Chem.* **1988**, *26*, 2031.

[188] B. Clément, B. Grignard, L. Koole, C. Jérôme, P. Lecomte, *Macromolecules* **2012**, *45*, 4476.

[189] B. J. Hunt, S. R. Holding, "*Size Exclusion Chromatography"*, Springer Science+Business Media Dordrecht, **1989**.

[190] S. So, T. P. Lodge, *Langmuir* **2016**, *32*, 4959.

[191] H. Deng, Y. Zhong, M. Du, Q. Liu, Z. Fan, F. Dai, X. Zhang, *Theranostics* **2014**, *4*, 904.

[192] P.-L. Chiu, D. F. Kelly, T. Walz, *Micron* **2011**, *42*, 762.

[193] J. R. Harris, D. Scheffler, *Micron* **2002**, *33*, 461.

[194] T. Chen, A. Fowler, M. Toner, *Cryobiology* **2000**, *40*, 277.

[195] J. L. Green, C. A. Angell, *The Journal of Physical Chemistry* **1989**, *93*, 2880.

[196] M. Sola-Penna, J. R. Meyer-Fernandes, *Arch. Biochem. Biophys.* **1998**, *360*, 10.

[197] L. Balas, B. Jousseaume, B. Langwost, *Tetrahedron Lett.* **1989**, *30*, 4525.

[198] K. Van Durme, S. Verbrugghe, F. E. Du Prez, B. Van Mele, *Macromolecules* **2004**, *37*, 1054.

[199] A. Pasternak, E. Kierzek, K. Pasternak, A. Fratczak, D. H. Turner, R. Kierzek, *Biochemistry* **2008**, *47*, 1249.

[200] R. C. Pratt, B. G. G. Lohmeijer, D. A. Long, P. N. P. Lundberg, A. P. Dove, H. Li, C. G. Wade, R. M. Waymouth, J. L. Hedrick, *Macromolecules* **2006**, *39*, 7863.

Appendix

List of Abbreviations

ATRP	Atom transfer radical polymerisation
Bis-MPA	2,2-Di(hydroxymethyl)propionic acid
BSA	Bovine serum albumin
BTC	Benzotriazole carbonate
CalB	Candida Antarctica lipase B
CD	Cyclodextrin
cDICE	Continuous droplet interface crossing encapsulation
CLSM	Confocal laser scanning microscopy
c(RGDyK)	Targeting peptide for the $\alpha_v\beta_3$ integrin receptor
CV	Cyclic voltammetry
DAS	Dispersing aqueous solution
DBU	1,8-Diazabicyclo[5.4.0]undec-7-ene
DCC	*N*,*N*'-Dicyclohexylcarbodiimide
DCM	Dichlormethane
DLS	Dynamic light scattering
DMAP	4-(Dimethylamino)-pyridine
DOPE	1,2-Dioleoyl-*sn*-glycero-3-phosphoethanolamine
DPPE	1,2-Dipalmitoyl-*sn*-glycero-3-phosphoethanolamine
DSC	Differential scanning calorimetry
DSPC	1,2-Distearoyl-*sn*-glycero-3-phosphocholine
DSPE	1,2-Distearoyl-*sn*-glycero-3-phosphoethanolamine

DSPG	1,2-Distearoyl-*sn*-glycero-3-phosphorylglycerol
EAS	Encapsulated aqueous solution
EDC	1-Ethyl-3-(3-dimethylaminopropyl)carbodiimide
EGFP	Enhanced green fluorescent protein
EYPC	Egg yolk phosphatidylcholine
Fc	Ferrocene
FCCS	Fluorescence cross-correlation spectroscopy
FCS	Fluorescence correlation spectroscopy
FITC	Fluorescin isothiocyanate
GOx	Glucose oxidase
GUV	Giant unilamellar vesicles
HHH	Hexagonally packed hollow hoops
hbPG	Hyperbranched poly(glycerols)s
IF	Inner fluid
IgG	Immunoglobulin G
KLA	A mitochondria-targeting peptide
LCM	Large compound micelle
LCST	Lower critical solution temperature
Liss Rhod DPPE	1,2-Dipalmitoyl-*sn*-glycero-3-phosphoethanolamine-*N*-(lissamine rhodamine B sulfonyl)
LOS	Lipid in oil solution
LUV	Large unilamellar vesicles
MF	Middle fluid
NEt$_3$	Triethylamine

NHS	*N*-Hydroxysuccinimide
NR	Nile Red
NTA-metal complex	Lysine-nitrilotriacetic acid-metal complexes
OA	Oleic acid
OF	Outer fluid
PAA-*b*-PS-*b*-P4VP	Poly(acrylic acid)-*block*-poly(styrene)-*block*-poly(4-vinyl pyridine)
PB-*b*-PEO	Poly(butadiene)-*block*-poly(ethylene oxide)
PBA-b-PAA	Poly(butyl acrylate)-*block*-poly(acrylic acid)
PBC-*b*-PDMA	Poly(benzyl carbamate)-*block*-poly(*N*,*N*-dimethyl acrylamide)
PBLG	Poly(γ-benzyl-L-glutamate)
PB-*b*-PEEP	Poly(butadiene)-*block*-poly(ethyl ethylenephosphate)
PBS	Phosphate buffered saline
PC	Phosphatidylcholine
PCL-*b*-PEO	Poly(caprolactone)-*block*-poly(ethylene oxide)
PDA	Polydiacetylene
PDADMAC	Poly(diallyldimethylammonium chloride)
PDMA-*b*-PS-*b*-PVBA	Poly(*N*,*N*-dimethylacrylamide)-*block*-poly(styrene)-*block*-poly[*N*-(4-vinylbenzyl)-*N*,*N*-dibutylamine]
PDPA	Poly[2-(diisopropylamino)ethyl methacrylate]
PEG/PEO	Poly(ethyleneglycol)/poly(ethylene oxide)
PEO-*b*-PAD	Poly(ethylene oxide)-*block*-poly[(*N*-amidino)dodecyl acrylamide]

PEO-*b*-PAGMA	Poly(ethylene oxide)-*block*-poly(azidomethyl benzoyl glycerol methacrylate)
PEO-*b*-PMCL	Poly(ethylene oxide)-*block*-poly(γ-methyl-ε-caprolactone)
PEO-*b*-PNBOC	Poly(ethylene oxide)-*block*-poly(2-nitrobenzyloxycarbonylaminoethylmethacrylate)
PEO-*b*-PPS-*b*-PEO	Poly(ethylene oxide)-*block*-poly(propylene sulfide)-*block*-poly(ethylene oxide
PEO-*b*-PS-*b*-PDEAEMA	Poly(ethylene oxide)-*block*-poly(styrene)-*block*-poly(2-diethylamino ethyl methacrylate)
PEO-*b*-PtNEA	Poly(ethylene oxide)-*block*-poly[*trans*-*N*-(2-ethoxyl-1,3-dioxan-5yl) acrylamide]
PFS	Poly(ferrocenyl silane)
PI-*b*-PCEMA	Poly(isoprene)-*block*-poly(2-cinnamoyl methacrylate)
PLA-*b*-PEO	Poly(lactide)-block-poly(ethylene oxide)
PMOXA-*b*-PDMS-*b*-PMOXA	Poly(2-methyl-oxazoline)-*block*-poly(dimethylsiloxane)-*block*-poly(2-methyl-oxazoline)
PNIPAM	Poly(*N*-isopropylacrylamide)
POPC	1-Palmitoyl-2-oleoyl-*sn*-glycero-3-phosphocholine
POS	Polymer in oil solution
PR_b	A targeting peptide for the $\alpha_5\beta_1$ integrin receptor
PS-*b*-PAA	Poly(styrene)-*block*-poly(acrylic acid)
PVCL	Poly(*N*-vinylcaprolactam)
RFP	Red fluorescent protein
SDS	Sodium dodecylsulfate
SEM	Scanning electron microscopy

SLS	Static light scattering
SUV	Small unilamellar vesicles
T7	A targeting peptide for the transferrin receptor
TAT	A cell-penetrating peptide
TEM	Transmission electron microscopy
THF	Tetrahydrofuran
TU	Thiourea
UCST	Upper critical solution temperature
V-65	2,2'-Azobis(2,4-dimethylvaleronitrile)
VfcGE	Vinyl ferrocenyl glycidyl ether

List of Symbols

Γ	Surface coverage of electrode
ΔE_{p}	Peak separation
η	Viscosity of the solvent
τ_{D}	Lateral diffusion
ω	rotation speed
A	Electrode surface
a_{0}	Area of the hydrophilic head group
$Đ$	Polydispersity index
D	Diffusion coefficient
DP	Degree of polymerisation
E_{pa}	Anodic peak potential
E_{pc}	Cathodic peak potential
F	Faraday constant
$f_{hydrophilic}$	Hydrophilic fraction
I	Intensity
l_{c}	Length of the amphiphile
I_{pa}	Anodic peak current
I_{pc}	Cathodic peak current
k_{B}	Boltzmann constant
K_{D}	Dissociation constant
M	Molecular weight
n	Number of transferred electrons

N	Average number of fluorescent species in V_{obs}
P_c	Critical packing parameter
Q_a	Transferred charge during oxidation
Q_c	Transferred charge during reduction
R_g	Radius of gyration
R_H	Hydrodynamic radius
S	Ratio of axial to lateral dimension of V_{obs}
T	Temperature
T_g	Glass transition temperature
T_m	Transition temperature of lipids/ melting temperature of polymers
v	Volume of the hydrophobic chain
V	Volume
V_{obs}	Observation volume
w_{xy}	Lateral radius of the ellipsoidal V_{obs}

Acknowledgement